Amalia M. de Juana Fabra

Local analysis of biomechanical arterial wall factors in atherosclerotic coronary arteries

MSc. Thesis in Biomedical Engineering

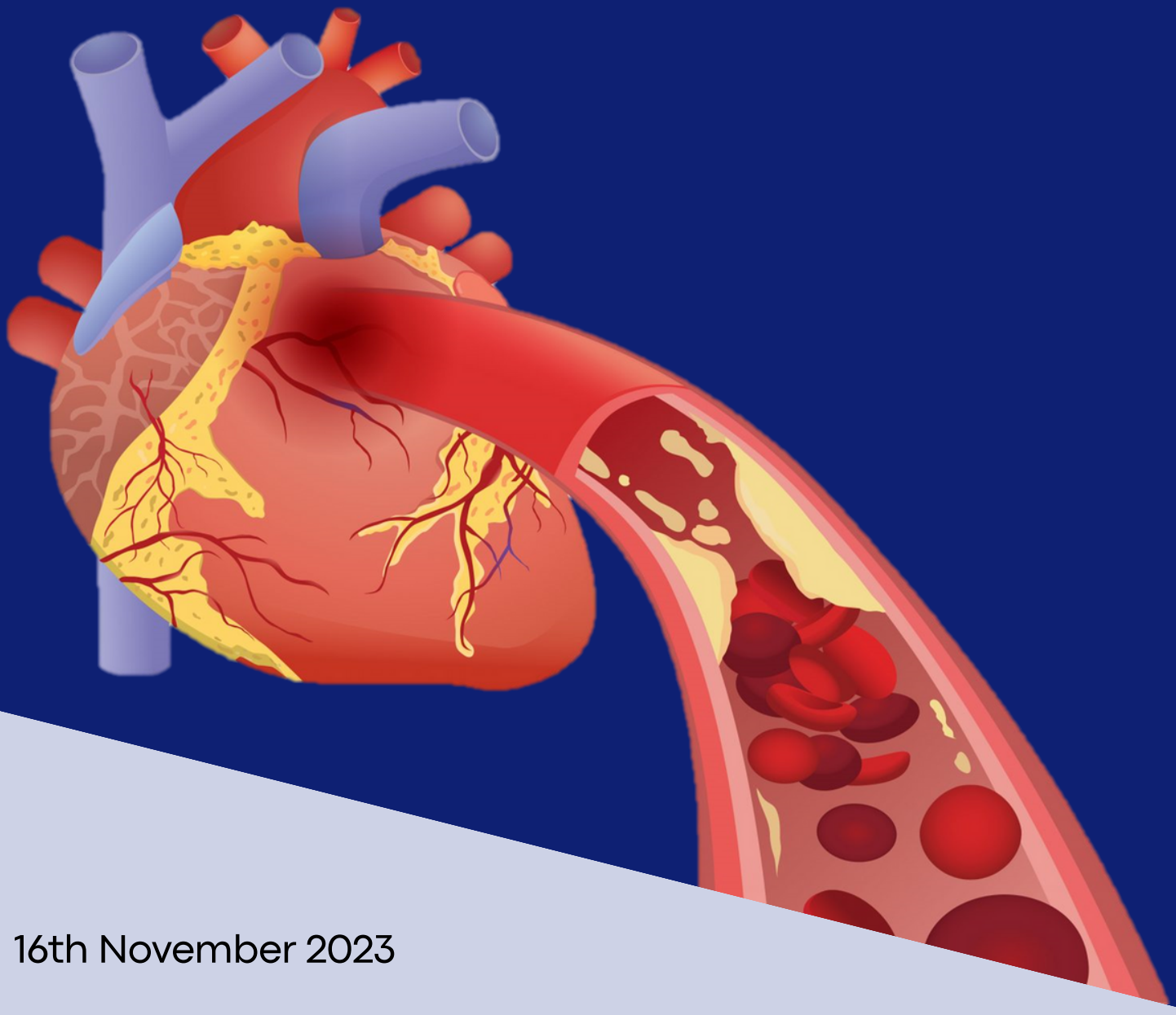

16th November 2023

MSc Thesis Project
BM51035

Local analysis of biomechanical arterial wall factors in atherosclerotic coronary arteries

BIOCCORA Pig Study

Amalia M. de Juana Fabra
5562511

Main supervisor: ***Dr. ir. A. Akyildiz***
Daily supervisor: ***Ir. A. Tziotziou***

November, 2023

Abstract

Atherosclerosis is an arterial condition characterized by the accumulation mainly of lipid tissue, resulting in the narrowing and stiffening of arteries. It is the leading cause of death among cardiovascular diseases and its development has been associated with wall shear (WSS) and wall mechanical stress (WMS). This study aimed to analyse WSS and WMS with two morphometric measurements, serving as indicators of the initiation and progression of atherosclerosis. 30 coronary arteries from 10 adult familial hypercholesterolaemic pigs fed a hig-fat diet were imaged at 3 time points, using intravascular ultrasound and optical coherence tomography. Two-dimensional geometries of the arteries and their lipid components, in combiation with their arterial pressure, were used to calculate WMS both at T1 and T2. WSS data was obtained at T1 and T2 by combining the 3D geometry of the arterial lumen and local flow velocity measurements. Arteries were segmented into 3 mm length and 45° sectors for analysis. It was observed that atherosclerosis developed in response to a high-fat diet, evidenced by a gradual increase in wall thickness over time even in the absence of lipidic components. Areas with thicker walls were predominantly found in regions exposed to low WSS and low WMS. Additionally, low WSS was found to promote atherosclerosis initiation and progression whereas high WMS appeared to support atherosclerosis progression. Throughout all time points, it was observed that WSS had a higher contribution to the development of atherosclerosis compared to WMS.

Index Terms– Atherosclerosis, Wall shear stress, Wall mechanical stress, Lipid-pool, Morphometrical measurements.

Acknowledgements

In August of 2021, I arrived to Delft without knowing what to expect and now, two and a half years later, I can say that not even in my best dreams I could have imagined it. These years have been amazing thanks to the people I have met along the way and to those that were already there. I will try to thank you, but I know that words will fall short.

First and foremost, I am deeply thankful to my family for their unconditional support, love and understanding during this challenging period. Without you, none of this could have been possible. Thank you, Aita y Ama, for giving me the opportunity to come to Delft and for supporting and helping me in every possible way and in every single situation. Thanks also to my sibling for always being there despite being each at different parts of the world, may the distance that separates us never be a problem.

I would also like to thank the Biomedical Engineering Department at Erasmus MC for providing me with the opportunity to conduct my master's thesis with them. In particular to my thesis supervisors Aikaterini Tziotziou and Ali Akyildiz, for your unwavering support, guidance and expertise throughout the project; your mentorship has been of great help and I am truly grateful for it. I would also like to express my gratitude to the committee members, Jolanda Wentzel and Mohammad Mirzaali; I appreciate the time and effort you dedicated to this master's thesis.

Finally but not least, I am thankful to all the friends I have made along my stay in Delft. My Jumbo people, thanks for all the amazing time we have spent together. I feel like the luckiest person to have met all of you, you make my life more joyful and enriching. I know this is only the beginning of an amazing friendship and I cannot wait to see where it takes us next. What Jumbo has united, let it never be separated. And how to forget my Aan't Verlaat people, the first people I met and that became friends instantly. The year living with all of you could not have been better and I am so fortunate to have you in my life. If we have survived Aan't Verlaat, we can survive anything.

Thank you again to everyone, this is for you!

Amalia

Table of Contents

List of Figures

List of Tables

List of Acronyms

Acronym	Definition
AD	Advanced-diseased
CFD	Computational Fluid Dynamics
CVD	Cardiovascular disease
ECG	Electrocardiogram
EEL	External elastic lamina
HR	Heart rate
IEL	Internal elastic lamina
IMT	Intima media thickness
IVUS	Intravascular ultrasound
LAD	Left anterior descending
LCx	Left circumflex
LP	Lipid-pool
MD	Mildly-diseased
OCT	Optical coherence tomography
PB	Plaque burden
RCA	Right coronary artery
rLPT	Relative lipid-pool thickness
SMC	Smooth muscle cell
T1	Time point 1
T2	Time point 2
T3	Time point 3
TAWSS	Time average wall shear stress
VSMC	Vascular smooth muscle cell
WMS	Wall mechanical stress
WSS	Wall shear stress

1 Introduction

1.1 Atherosclerosis disease

Atherosclerosis is a chronic, inflammatory arterial disease where arteries become narrow and hardened due to accumulation mainly of lipid tissue, forming what is known as atherosclerotic plaque [1,2]. It is considered as a main cause of cardiovascular diseases (CVD), including ischemic heart disease and ischemic stroke as its primary clinical symptoms [3]; and, as stated by The European Society of Cardiology Atlas, CVDs are the most common cause of death in Europe. Every year more than 11 million new cases of CVD are registered, which represents a cost of €210 billion a year [4].

Different factors contribute to the initiation and progression of the disease, being major risk factors dyslipidemia, hypertension, smoking, diabetes mellitus, history of CVD, sedentary life style, older age and male sex [5,6]. These risk factors lead to impairment of the endothelial cells of the arterial wall, followed by an inflammatory reaction and accumulation of lipid, calcium and fibrous tissue within the intima layer (inner layer of the arterial wall) leading to plaque formation. The plaque continues growing until it occludes the artery (critical stenosis) or the fibrous cap (fibrous tissue separating the plaque from the lumen) breaks creating a thrombus (see Figure 1), leading to any adverse event [7–9].

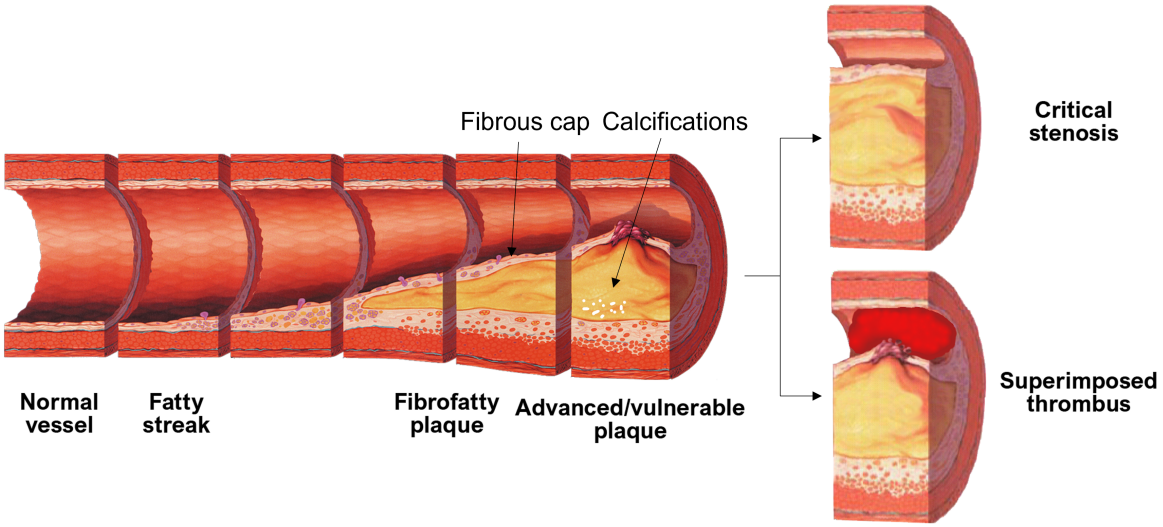

Figure 1: Progression of atherosclerosis [10].

Atherosclerosis is not a linear disease, its progression is not consistent, predictable, or occurring in a straightforward, uniform manner; some plaques may stay stable in time while others may develop into advanced lesions with large lipid-pools (LPs) and thin fibrous caps [11]. Early lesions begin with the accumulation of smooth muscle cells (SMCs) in the intima, later progressing to areas with extracellular lipid accumulation and the development of a fibrous cap. Advanced lesions feature nodular calcifications, fibrocalcific plaque, and non-occlusive thrombus, which may contain necrotic core [12]. In advanced atherosclerosis, the buildup of lipids, cells, and matrix components leads to structural disorganization, intima thickening, and arterial wall deformation [13]. Despite the fact that the lumen may not be narrowed, the advanced lesion could rupture and cause sudden adverse events.

1.2 Wall shear and wall mechanical stress

Moreover, local mechanical factors are regarded as significant in the development of the disease. Coronary arteries experience two main biomechanical forces: wall shear stress (WSS) and wall mechanical stress (WMS) (see Figure 2). The former is the frictional force exerted by the dynamic blood flow parallel to the the inner arterial wall [11]. It is influenced by the geometry of the vessel and the blood flow velocity; regions with tortuous shapes and oscillatory blood flow velocity experience low WSS whereas regions with uniform shapes and constant blood flow velocity experience high WSS [11]. Wall mechanical stress, also known as structural stress, is defined as the stress inside of an artery due to vessel expansion and stretch induced by arterial pressure, acting in circumferential, radial and axial directions [14]. Different factors influence WMS, including plaque dimensions, composition and the geometry of the lumen. WMS seems to increase in regions with large LPs [15,16] and high WMS is linked to the occurrence of plaque rupture, rupture location that could be predicted by the region with higher WMS [15].

Under physiological conditions, endothelial cells within the endothelium are subject to both WSS and WMS simultaneously, while all other cells, including vascular smooth muscle cells (VSMCs), within the wall structure, are mainly subject to WMS only [17]. In regard to WSS, it has been reported that high WSS acts on the phenotype of the endothelial cells making them atheroprotective while under low WSS the phenotype of these cells is switched to atherogenic [11, 18]. In contrast, additional studies have shown an association between high WSS and the development of vulnerable plaques in atherosclerosis progression [19, 20]. Regarding WMS, VSMCs are capable of sensing this stress through multiple mechanisms and transducing it into intracellular signals that might contribute to the initialization and development of atherosclerosis [21]. Both WSS and WMS represent a possible resource to employ for evaluating plaque development and identifying vulnerable plaques. These stresses can enhance clinical decision-making in medical treatment [22] and they can be calculated through computational fluid dynamics (CFD) and finite element analysis (FEA), respectively [23, 24].

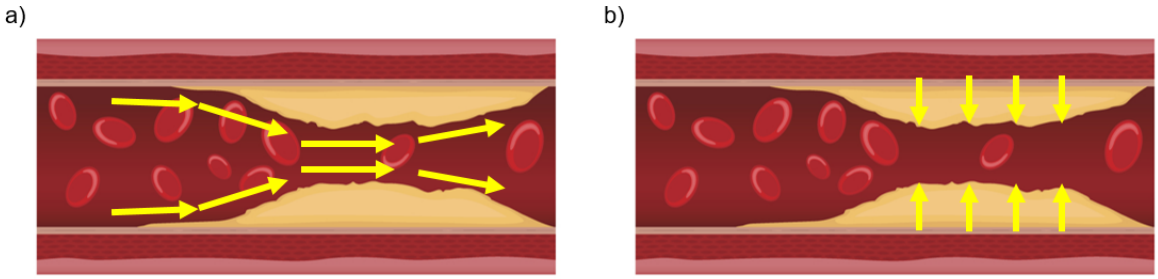

Figure 2: **a)** Wall shear stress. **b)** Wall mechanical stress [25].

1.3 Aim

The aim of the project is to analyse biomechanical arterial wall factors in atherosclerotic coronary arteries, by the use of IVUS and OCT modalities, focusing on the geometry and the lipid component of coronary arteries.

2 Methodology

In this section, the methodology employed to achieve the study aim is presented. The methods presented herein are structured to provide a comprehensive understanding of the data acquisition and its subsequent processing. The flow-chart of the followed methodology can be seen in Figure 3.

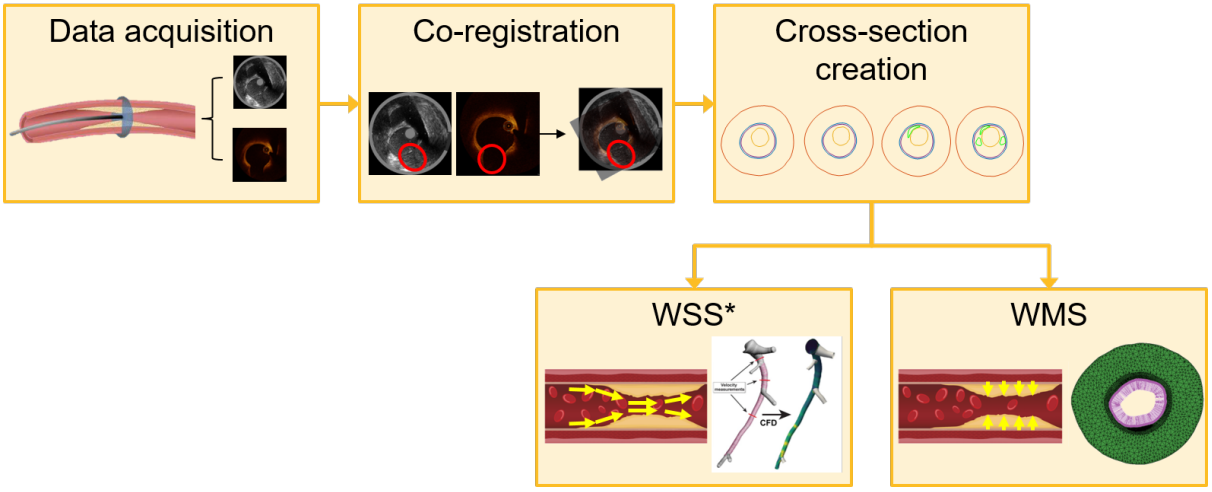

Figure 3: Flow-chart of the project. *Calculated by Hoogendoorn et al. [26].

2.1 Pig model and data acquisition

For the project, data from the study carried out by Hoogendoorn et al. [26] were used, involving 10 FH Bretonchelles Meishan castrated male minipigs homozygous for the *LDLR* R84C mutation. Only castrated males were selected for the study as females from the breed have significantly lower coronary atherosclerosis development [26]. At approximately 34±3 months of age, the pigs were put on a high-fat atherogenic diet, consisting of 10% lard and 0.75% cholesterol. The development of plaque in the coronary arteries was monitored by performing invasive imaging of the left anterior descending (LAD), the left circumflex (LCx), and the right coronary artery (RCA) using both IVUS and OCT imaging modalities. This imaging protocol was conducted at three different time points: 3 months (T1), 9 months (T2), and 12 months (T3) after starting the atherogenic diet, allowing for the assessment of changes in plaque size and composition [26].

The imaging procedure involved advancing an OCT catheter as distally as possible into the artery, up to a maximum depth of 75 mm, followed by a pullback at a rate of 36 mm/s. Subsequently, an IVUS catheter was positioned at the same anatomic location as the OCT catheter, and a pullback at a rate of 0.5 mm/s was performed. Throughout the IVUS pullback, the heart rate was monitored and recorded for future use in IVUS triggering. Two pigs were early euthanized (shortly after T2), due to cardiovascular complications. However, the data of T1 and T2 of these pigs were used for analysis. All pigs were euthanized after T3 [26].

2.2 Co-registration and creation of cross-sections

The structures of the lumen, intima-media layer, and LPs were reconstructed to create an accurate representation of the arteries. In order to do so, the lumen-intima, the external elastic lamina (EEL) and the LPs contours were obtained (see Figure 4a). All other present components,

such as calcifications, were excluded from the study. The lumen-intima and EEL contours[1] were extracted out of the IVUS images while the cap (front of LP) contours were obtained out of the OCT images (Figure 4b and c). For the project, the intima and media layers are analysed as one, referred from now on as intima, due to IVUS inability to identify the internal elastic lamina (IEL) and, therefore, the intima-media border (see Table 1) [27].

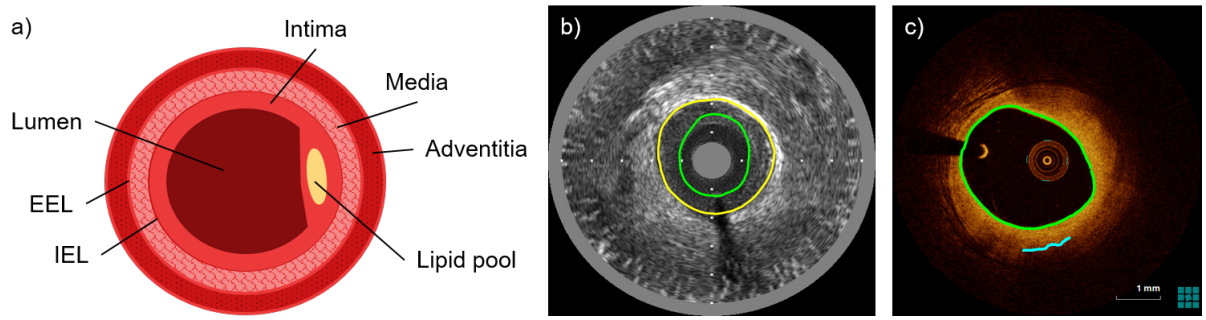

Figure 4: **a)** Cross-section of a coronary artery with a LP. **b)** IVUS image of the cross-section of a coronary artery with the lumen and the EEL delineated in green and yellow respectively. **c)** OCT image of the cross-section of the same coronary artery as in b) with the lumen and the cap contours delineated in green and blue respectively.

	Lumen	**IEL**	**EEL**	**Lipid-pool**	**Adventitia**
IVUS	✓	×	✓	×	×
OCT	✓	×	×	✓*	×

* only front part (cap)

Table 1: IVUS and OCT imaging modalities and the information that can be retrieved from them. The tick symbol (✓) means that those contours can be obtained from the specific imaging modality. The cross (×) depicts that the specific imaging modality cannot retrieve the contours of those components. Even though OCT can retrieve the lumen contours, for this project only lumen contours from IVUS were used.

The images of both techniques needed to be co-registered based on anatomical landmarks in order to obtain correct cross-sections with LP, in case they were present. The co-registration consisted on 3 steps, which were carried out by a scientist from the department: firstly, a longitudinal co-registration was done by detecting the position of the side-branches of each artery (reference frames) in both IVUS and OCT images; secondly, a circumferential co-registration was done by rotating the reference OCT frames so that they were aligned to the corresponding reference IVUS frame; thirdly, between the reference frames a linear interpolation of matching and rotations was done so that all OCT frames would match IVUS frames (see Figure 5).

[1] Side-branches were not represented in the contours.

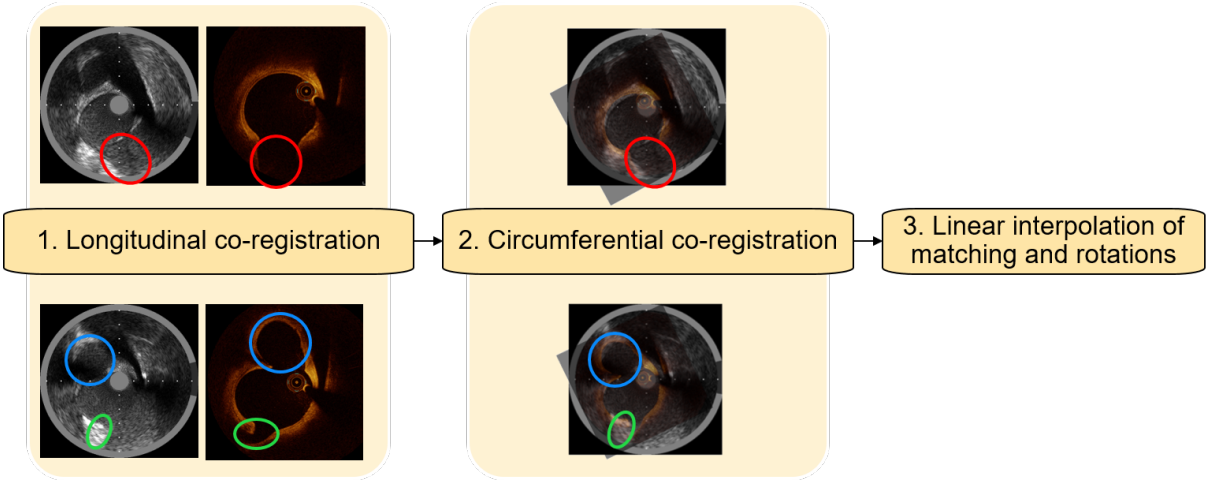

Figure 5: Process for co-registration for IVUS and OCT frames. **1.** Longitudinal co-registration indicating in red, blue and green circles side-branch 1, 2 and 3 respectively (left: IVUS frame, right: OCT frame). **2.** Circumferential co-registration with IVUS and OCT frames overlapping and indicating in red, blue and green circles side-branch 1, 2 and 3 respectively. **3.** Linear interpolation of frame matching and rotations between the reference frames.

For T1, OCT images were directly co-registered with IVUS images. However, for T2 and T3, IVUS images were not directly co-registered with their corresponding OCT images; instead, a sequence of three intermediary steps was employed. Firstly, IVUS images at T_i were co-registered with IVUS images at T1. Secondly, the co-registration of IVUS and OCT images at T1 was carried out and; thirdly, OCT images at T1 were co-registered with OCT images at T_i, with $i = 2, 3$. An example of the co-registration of IVUS and OCT images at T2 can be seen in Figure 6.

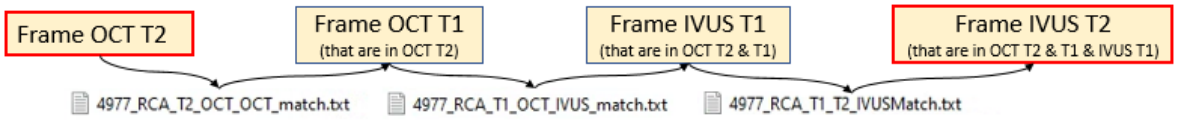

Figure 6: Process for matching the co-registration for IVUS and OCT frames, example from RCA artery of pig 4977 at T2.

Once the co-registration between IVUS and OCT frames was done, the cross-sections of the arteries could be obtained. Nevertheless, there were issues with the co-registration, with certain caps extending beyond the EEL and some contour lines intersecting each other, resulting in an inconsistent geometry. Consequently, a thorough reevaluation of the co-registration process became necessary. Firstly, the contours were checked by fitting them into the raw IVUS and OCT images (see Figure 7a). Secondly, the longitudinal co-registration was revised by matching the raw IVUS and OCT images. Lastly, the circumferential co-registration was checked by rotating OCT images to be aligned with IVUS images. At the end of the reevaluation, it was then seen that the rotations were not correct as the side-branches did not align (see Figure 7b).

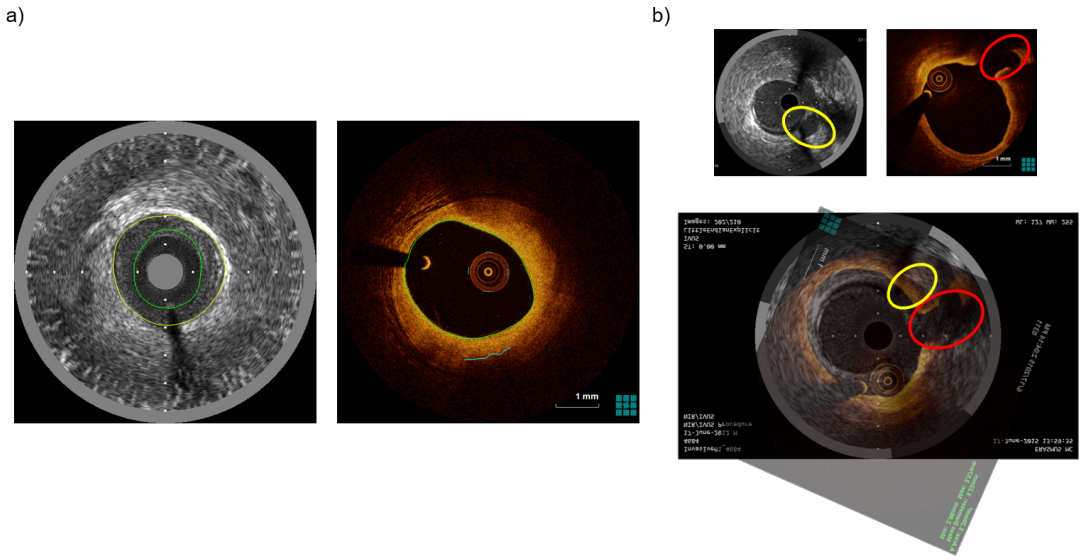

Figure 7: Followed steps to check whether the co-registration was correct. **a)** Contours of EEL and lumen and lumen and front of lipid-pool fitted onto the corresponding raw IVUS and OCT images respectively (yellow: EEL, green: lumen, blue: cap); **b)** OCT image rotated to align with its corresponding IVUS image, in red and yellow the same side-branch is marked and it can be seen how the rotation did not aligned them.

It was assumed that the rotations were inaccurate and, as there was a possibility that the matching was also not correct, a manual co-registration was again performed. The manual co-registration consisted on detecting side-branches in raw IVUS and OCT images and matching them. Afterwards, the matched OCT frames were rotated to fit into the matched IVUS frame. The results, both the frame-matching and the rotations, were compared with the original one. After co-registering 4 arteries, it was observed that the original and new frame-matching co-incided while some of the rotations did not. The generation of cross-sections was more into detailed analysed, in order to understand why some OCT frames had the correct rotation to match IVUS frames and some not. The problem was identified in how the linear interpolation of rotations was done, and it was subsequently fixed. Once the problem was solved, the obtained cross-sections were checked again with the raw IVUS and OCT images to ensure their accuracy. Despite having solved the problem, the existence of some LPs was doubtful, as OCT technique is very sensitive to soft tissue and could detect false positive LPs. After consulting an OCT expert from the department, 2 LPs were removed from their cross-section: one due to its non-existence and one due to uncertainty of its existence. This last LP was removed so that the project was done analysing only LPs with 100% certainty of existence.

As stated previously, OCT modality is able to detect the lumen and the front side of the LP but not its backside (Table 1). This cap was mapped to the corresponding IVUS image in such a way that the cap thickness remained consistent (Figure 8), meaning that the shortest distance between the cap and the lumen coincided both in OCT and IVUS.

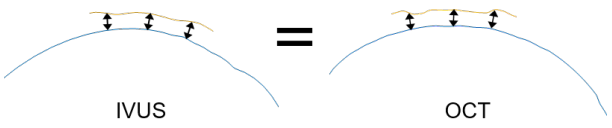

Figure 8: Cap and part of lumen contours in IVUS and OCT matched-images showing same cap thickness.

An in-house developed algorithm was used for the reconstruction of LPs' backside. The reconstruction was based on estimating the relative LP thickness (rLPT) at 3 different locations along each LP; for which plaque specific parameters were used. The boundaries of the LPs were defined and connected with the previous 3 points by a polynomial function, thereby generating

the complete geometry of the LP. In Figure 9, the reconstruction process is depicted and more information about it can be found in the paper by Kok et al. [28].

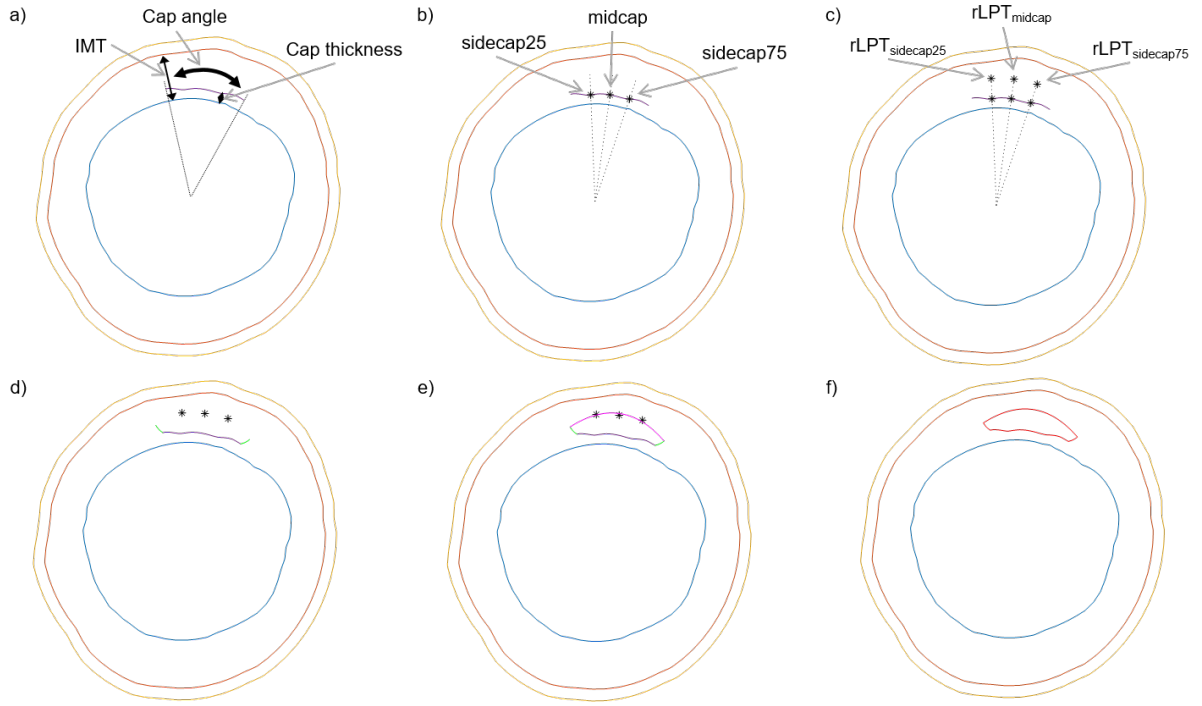

Figure 9: Lipid-pool reconstruction process (blue: lumen; orange: EEL; yellow: adventitia; purple: cap; red: complete lipid-pool). **a)** Schematic overview of the coronary plaque specific properties; **b)** location of mid and sidecap points; **c)** calculation of the relative lipid-pool thicknesses (rLPT) for the mid and sidecaps; **d)** generation of the lipid-pool edges (green); **e)** reconstruction of the backside of the lipid-pool (pink); **f)** complete geometry of the lipid-pool.

In contrast to the intima layer contours, the adventitia layer contour could not be provided by any of the imaging modalities (see Table 1), thus there was the need to reconstruct it. The outer contour of the adventitia was assumed to be the same as the EEL contour but with a greater diameter, based on the ratio of adventitia and media thickness [29]. The main role of adventitia within the arterial wall is to protect it from overstretch and rupture when exposed to pressure, reaching its collagen fibers to their straightened length [30, 31]. Herein lay the importance of including it.

2.3 Wall shear stress

WSS was computed at T1 and T2 by Hoogendoorn et al. and the study can be found at [23]. Nevertheless, the fundamental information about how the computation of WSS was carried out is provided in this section.

At T1 and T2, a 3D model of each coronary artery was generated by combining the lumen and EEL lamina contours with a 3D centerline derived from computed tomography angiography. This process yielded a luminal surface containing data on local wall thickness distribution. WSS was computed at T1 and T2 using unsteady CFD simulations performed in Fluent (v.17.1, ANSYS Inc.). For it, the luminal 3D geometry was meshed with tetrahedral elements in ICEM CFD (v.17.1, ANSYS Inc., Canonsburg, PA, USA) and intravascular Doppler-derived velocity measurements were used to determine flow distribution in segments between side branches. As inlet condition, a time-dependent velocity waveform was applied, based on the most proximal reliable flow measurement. In addition, the lumen was treated as rigid with a no-slip boundary condition, while the blood was modelled as a shear-thinning fluid using the Carreau model.

2.4 Wall mechanical stress calculation

Stress calculations were conducted using finite element analysis. To execute this analysis, the 2D plaque geometries were converted into ABAQUS (version 6.13, Dassault Systemes Simulia Corp., Providence, RI, USA). They were brought into ABAQUS using a Python script (developed in the Biomechanics lab, Biomedical Engineering, Cardiology, Erasmus Medical Center, Rotterdam); and within the ABAQUS environment, the geometry was prepared for stress calculations.

Every cross-section geometry comprised three parts, or four in the presence of a LP: the intima, adventitia, and buffer; and, if applicable, the LP (see Figure 10). The buffer component is in reality not part of the arterial wall; however, it was created to limit the rigid body motion during the finite element analysis.

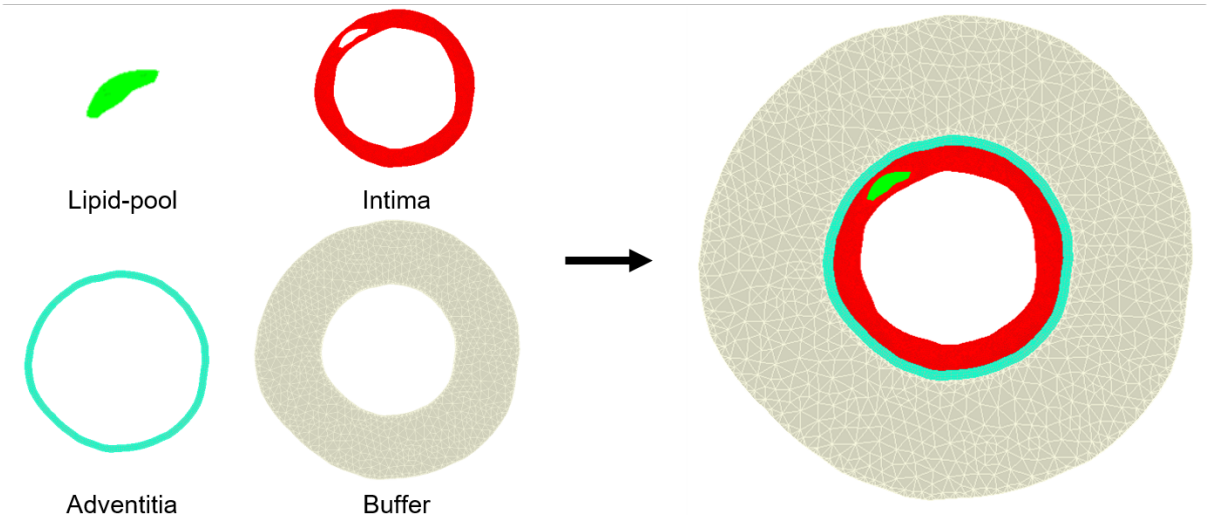

Figure 10: Parts of a cross-section with presence of lipid-pool.

2.4.1 Material properties

Each component of the cross-sections was modeled as incompressible, homogeneous, hyperelastic and nonlinear isotropic [29,32], except the buffer component which was modeled as compressible. The intima was described by the modified Mooney-Rivlin strain energy density function [32]

$$W_{MMR} = C_1(I_1 - 3) + D_1[exp(D_2(I_1 - 3)) - 1] + k(J - 1) \tag{1}$$

where C_1, D_1 and D_2 are material constants; I_1 is the first invariant of the modified right Cauchy-Green tensor; J is the Jacobian of the deformation gradient tensor; and k is the Lagrange multiplier.

The nonlinear mechanical behavior of the adventitia was modeled as incompressible and hyperelastic Yeoh model. The Yeoh model is characterised by the strain energy density function

$$W_Y = \sum_{i=1}^{3} C_i(I_1 - 3)^i + \frac{1}{D_i}(J - 1)^{2i} \tag{2}$$

where C_i and D_i are material constants; I_i is the first deviatoric strain invariant; and J the Jacobian of the deformation gradient tensor. Due to the incompressible behaviour of the material, D_i was set to 10^{-5} kPa^{-1}.

The chosen material properties for the buffer were optimized to ensure that it absorbed less than 1% of the energy dissipated in the simulation, minimizing its impact on the other components as much as possible. The optimal model was a hyperelastic, compressible Neo-Hookean model, characterised by the strain energy density function

$$W_{NH} = C_1(I_1 - 2 - 2lnJ) + D_1(J-1)^2 \tag{3}$$

where C_1 and D_1 are material constants; I_1 is the first invariant; and J the Jacobian of the deformation gradient tensor. Same strain energy density function was used for the LP, setting D_1 to 10^{-5} kPa^{-1} for its incompressibility.

The material constants for each tissue are displayed in Table 2.

Tissue	**Material constants**
Intima [32]	$C_{10} = 0.138$ kPa, $D_1 = 3.833$ kPa^{-1}, $D_2 = 18.803$ kPa^{-1}
Adventitia [29]	$C_{10} = 2.4$ kPa, $C_{20} = 80$ kPa, $C_{30} = 345$ kPa, $D_1 = D_2 = D_3 = 10^{-5}$ kPa^{-1}
Lipid-pool [29]	$C_{10} = 0.1667$ kPa, $D_1 = 10^{-5}$ kPa^{-1}
Buffer	$C_{10} = 1$ kPa, $D_1 = 0.1$ kPa^{-1}

Table 2: Material constants of the components.

To check that the selected materials were indeed hyperelastic, a uniaxial test was performed in 2D rectangular shell for the 4 materials (Figure 11).

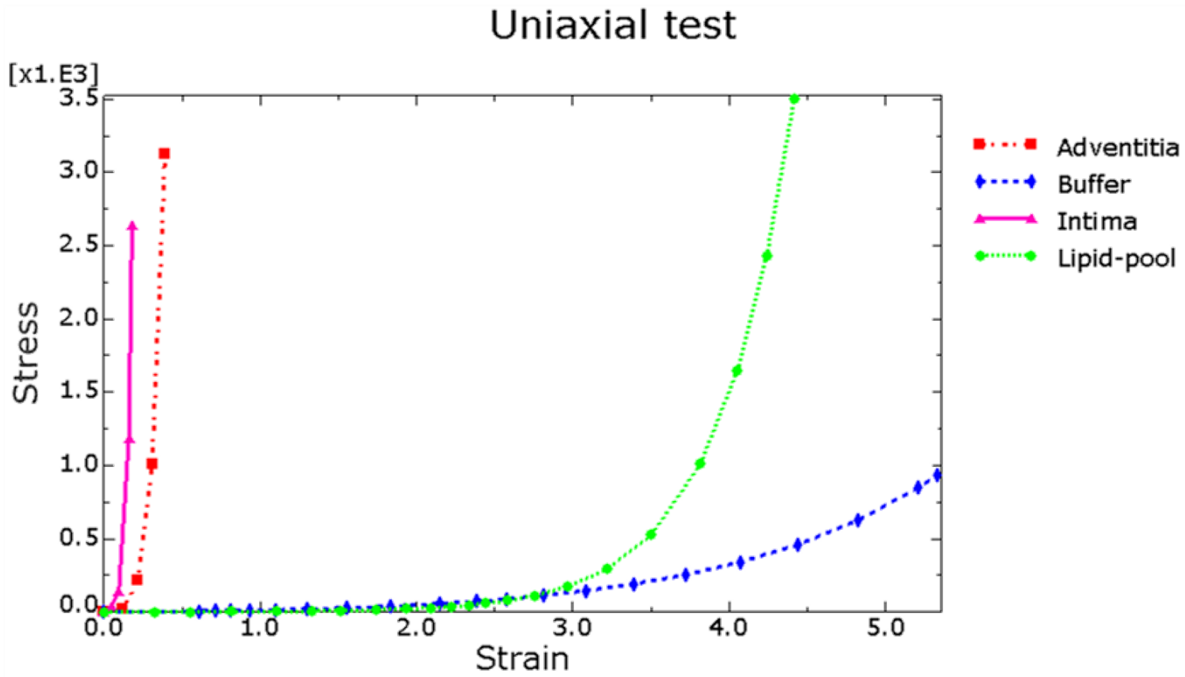

Figure 11: Stress and strain function of the uniaxial test performed for the 4 different materials. In pink with △ and solid line: intima; in blue with ♢ and dashed line: buffer; in red with □ and dash-dotted line: adventitia; and in green with ∘ and dotted line: lipid-pool.

2.4.2 Load (pressure) and boundary conditions

For the wall mechanical stress calculation, pressure needed to be applied to the internal wall of the artery. As the blood pressure varies within the cardiac cycle (see Figure 12), ECG-gated IVUS images were recorded 6 frames before the R-peak, therefore removing differences

in lumen size induced by movement of the catheter or by cardiac contraction [26][Supplemental material]. For the finite element analysis, two different pressures needed to be obtained: the systolic pressure and the pressure 6 frames prior to the R-peak. These pressures were determined for each of the arteries, and the same was assumed along their entire length.

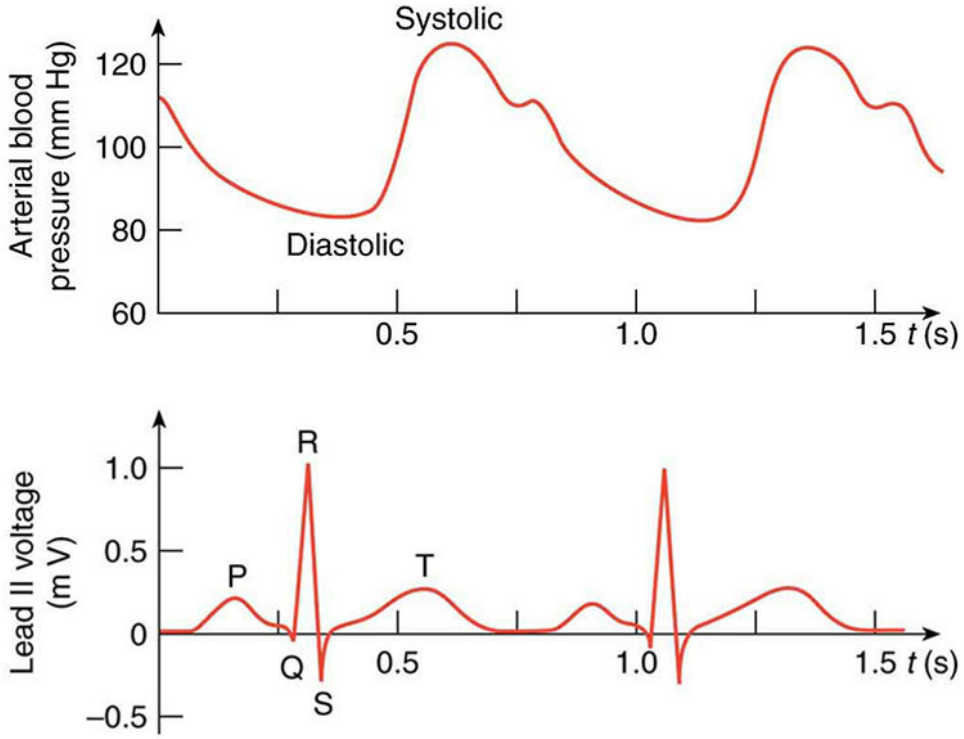

Figure 12: A lead II ECG with corresponding arterial blood pressure [33].

For T1, each pressure was obtained out of a document generated during the IVUS pullback containing the recorded time, pressure and electrocardiogram (ECG) for every 5 ms, specifying the moment where the R-peak was detected. Knowing the exact time of the R-peak and the frame rate, both the systolic pressure and the one experienced by each artery 6 frames before the R-peak were obtained. However, for T2, it was not specified where the R-peak was in the ECG, being not possible to obtain the pressures in the same way as in T1. An algorithm developed by D. Sadhukan and M. Mitra [34] was implemented in order to detect the R-peaks from the ECG and, consequently, obtain the systolic pressure and that one of 6 frames before the R-peak (see Appendix A).

The algorithm was tested and validated with different pigs' ECG at T1, where it could be checked that the R-peaks detected by the algorithm coincided with the R-peaks detected during the IVUS pullback, as it can be seen in Figure 13. Once the adequacy of the algorithm was confirmed, the next step involved obtaining the systolic pressure as well as the pressure 6 frames before the R-peak for all pigs at T2, the same way it was done at T1.

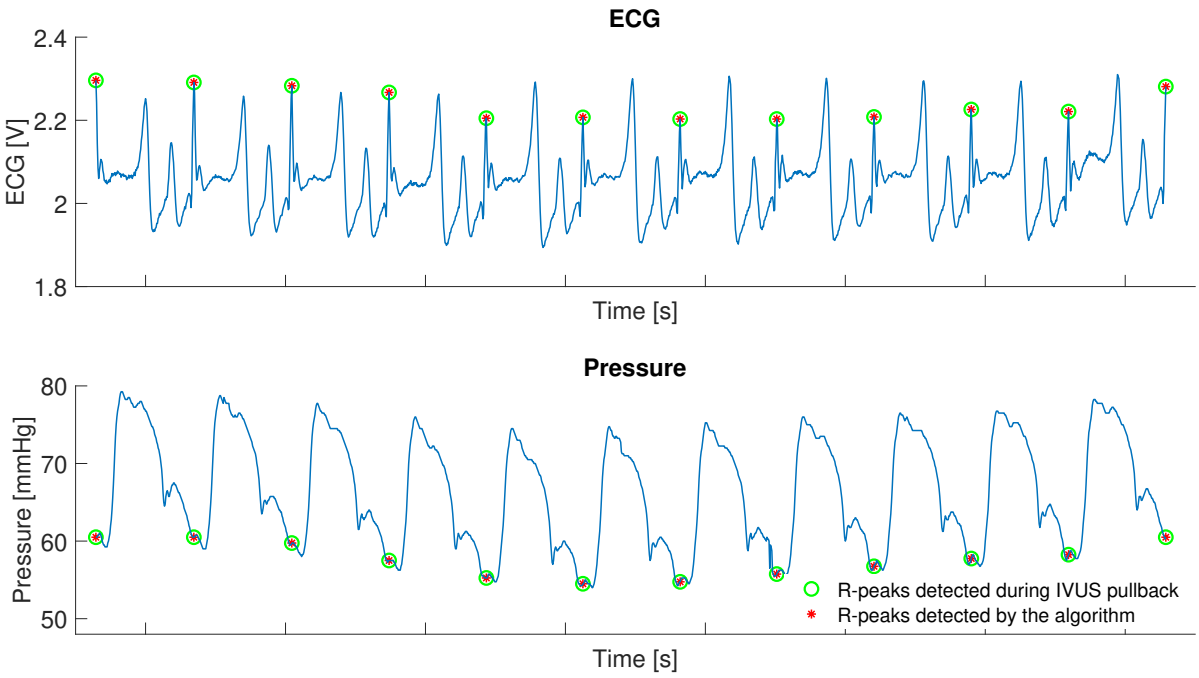

Figure 13: R-peaks detected by the algorithm and during the IVUS pullback in the ECG and pressure graphs.

A boundary condition was established at the outer edge of the buffer to restrict both its displacement and rotation in any direction.

2.4.3 Mesh and element type

A mesh convergence analysis was carried out for 3 different types of geometries: plaque-free cross-section, cross-section with plaque but no LP and cross-section with LP. In all the cases, the intima, adventitia, buffer and LP (in the last case) components were analysed, performing 10 different stress calculations in 4 cross-sections per type of geometry. Each time, the seed size was decreased. Convergence was obtained at seed sizes of 0.4 for intima and LP, and 1.4 for adventitia and buffer (see Figure 14). Both the intima edge and the LP edge had a smaller seed size so that the stresses in the thinner parts or where the LP and the intima interacted could be better simulated. On average, cross-sections without LP were composed of 11261 elements, whereas cross-sections with LP contained 10385. The intima component had 942 elements, adventitia had 1305, buffer contained 8138, and LP consisted of 876 elements. Even though the same mesh was set for all the cross-sections of the arteries, errors due to deformations too large as compared with the model were solved by manually increasing the seed size of intima and LP.

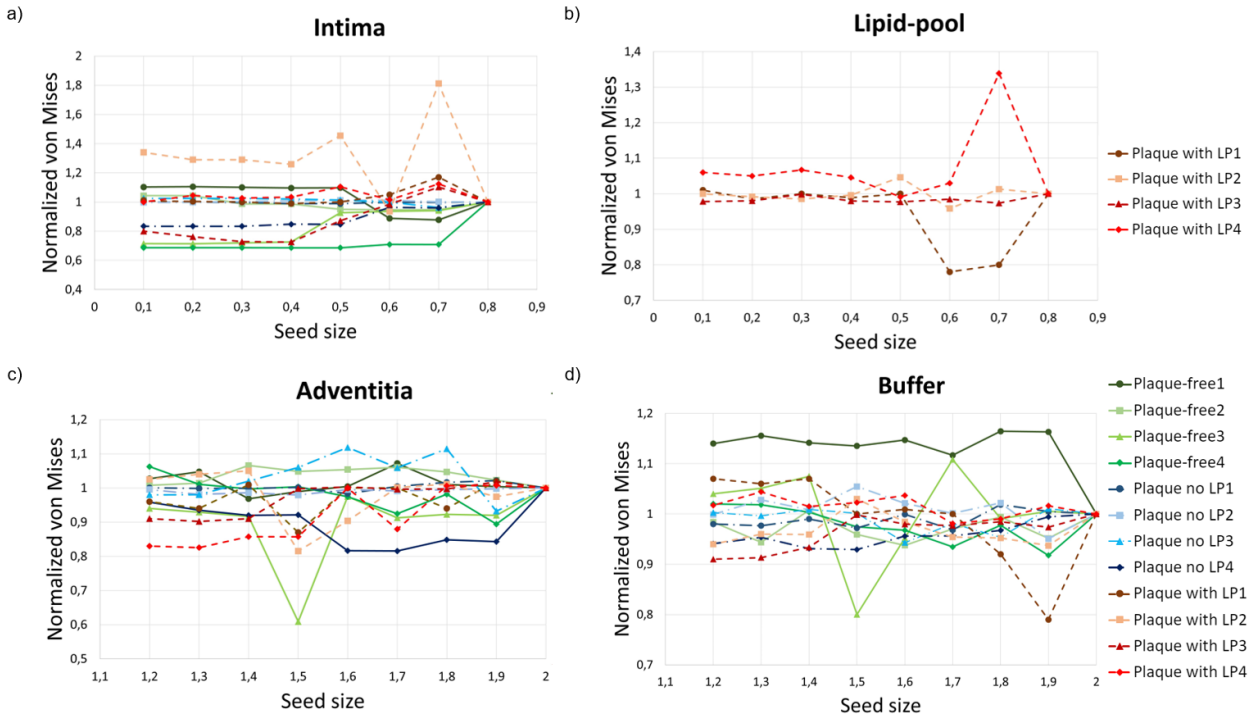

Figure 14: Mesh convergence analysis for: **a)** intima; **b)** lipid-pool; **c)** adventitia; and **d)** buffer.

The shape of the intima, adventitia and lipid-pool components was quadrilateral, and plane strain element CPE4H (4-node bilinear, hybrid with constant pressure) was utilized. The expression "4-node bilinear" signifies that each element is composed of four nodes and exhibits linear deformation behaviour. The term "hybrid" indicates that the element's volume remains constant under applied pressure. Hybrid elements include an additional degree of freedom that determines the pressure stress in the element directly. The words "constant pressure" denotes that the pressure is uniformly distributed across the entire element. A triangular element shape was used for the buffer, as well as a CPE3H (3-node linear, hybrid with constant pressure) element type.

2.4.4 Backward Incremental Method

When imaging the arteries, the acquired geometries intrinsically exist under the influence of blood pressure and, thus, under stress. This initial stress cannot be ignored, as it would result in an underestimation of wall stresses [35]. In order to compute the initial stress, an in-house developed algorithm based on the backward incremental method was used [35–37]. The method aimed to incorporate the initial stress into the model's geometry, ensuring that when the peak systolic pressure was applied, the geometry already accounted for the initial stress [35, 37]. The backward incremental method consisted of 16 steps or iterations. In each step, intraluminal pressure was applied causing deformation in the geometry of the model, and calculating stresses. In the immediate subsequent step, the geometry of the model was reset and the previously obtained stresses were incorporated as initial conditions. Throughout each step, the applied pressure was gradually increased until, in the final step, it reached the pressure 6 frames before the R peak, i.e. the pressure at imaging time. Once the original geometry integrated the initial stress, the peak systolic pressure was applied in 2 steps, enabling the computation of stresses and model's deformation.

2.5 Arterial division and tertile analysis

For analysis, every artery was divided in 3 mm long and 45° sectors. This division has been applied in previous studies of coronary atherosclerosis [38–42], achieving the highest possible alignment between T1 and T2 data while also effectively addressing spatial variations, reflecting accurately local plaque characteristics and being appropriate for serial comparisons [42]. In addition, the wall mechanical and wall shear stress metrics at both time points were divided into low, mid and high tertiles. This division within the coronary system enhances the comprehension of the pathophysiology associated with plaque progression and plaque rupture [43]. Three different types of tertile division were considered: artery-specific, pig-specific and absolute. The first was chosen because it provided the most effective data distribution, while ensuring that all pigs had data in every tertile. In appendix B, the data distribution for the 3 types of tertile division as well as the defined thresholds for the tertiles are displayed. Plaque burden (PB) and wall thickness, as well as its change over the follow-up period, were used as indicator for atherosclerosis progression.

Additionally, sectors were classified as plaque-free, plaque without LP or plaque with LP. Plaque-free sectors were considered sectors with PB$<$40% [44], plaque sectors without LP were sectors with PB$\geq$40% and did not contain LPs, and plaque sectors with LP were those sectors with PB$\geq$40% and with presence of LP.

3 Results

After 9 months of follow-up, 2 of the 10 pigs died, one due to a presumed myocardial infarction and one due to an acute thrombotic occlusion of a femoral artery. Nevertheless, data of these 2 pigs were included in the analysis for T1 and T2, and their last time point was T2. For the rest of the cohort, T3 was considered as last time point.

3.1 Morphometrical measurements

Even though all pigs were fed the same high-fat diet and had the same baseline conditions (non-diabetic, no difference in weight, cholesterol and arterial tension) (see appendix C), 5 of them developed limited atherosclerosis while the other 5 developed large lumen-intruding plaques. The cohort was then divided into 2 groups: mildly-diseased (MD) pigs with average PB<40% at last time point and advanced-diseased (AD) pigs with average PB≥40% at last time point; the results and posterior analysis will be presented per group.

Mildly-diseased pigs

In the MD group, 15 arteries were analysed with a total of 3172 3mm/45° sectors at each time point. At T1, all sectors were plaque-free with the exception of 2 sectors that had plaque but no LP; no sectors with LP were present. At T2, there were exclusively plaque-free sectors; and at T3, 3161 sectors were plaque-free, 10 had plaque with no LP and 1 had plaque with LP (Table 3 and Figure 15).

	T1	T2	T3
Plaque-free (%)	3170 (99.94)	3172 (100)	1361 (99.65)
Plaque no LP (%)	2 (0.06)	0 (0)	10 (0.32)
Plaque with LP (%)	0 (0)	0 (0)	1 (0.03)

Table 3: Number and percentage of plaque-free, plaque without lipid-pool and plaque with lipid-pool of MD sectors for T1 to T3.

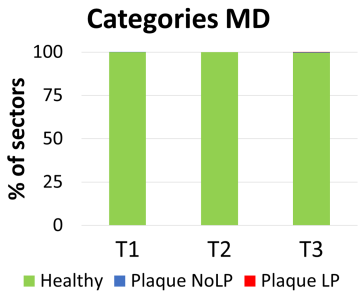

Figure 15: Average percentage of plaque-free, plaque without LP and plaque with LP of MD sectors for T1 to T3.

The majority of the sectors were plaque-free at baseline and during follow-up. Moreover, at T2 all sectors that had plaque but no LP became plaque-free and no sector developed LP (Table 4a). At last time point, 0.31% of sector which were plaque-free at T2 developed plaque without LP and only 0.03% developed plaque with LP (Table 4b). In Figure 16, the number of sectors per category at each time point and how they changed is visualized. In addition, sector categories and their change during follow-up per pig can be found in appendix D.1.

		T2		
		Plaque-free	Plaque no LP	Plaque with LP
T1	Plaque-free	100%	0%	0%
	Plaque no LP	100%	0%	0%
	Plaque with LP	0%	0%	0%

(a) Percentage of MD sectors that changed categories between T1 and T2.

		T3		
		Plaque-free	Plaque no LP	Plaque with LP
T2	Plaque-free	99.65%	0.32%	0.03%
	Plaque no LP	0%	0%	0%
	Plaque with LP	0%	0%	0%

(b) Percentage of MD sectors that changed categories between T2 and T3.

Table 4: Percentage of MD sectors in each category from one time point to its following.

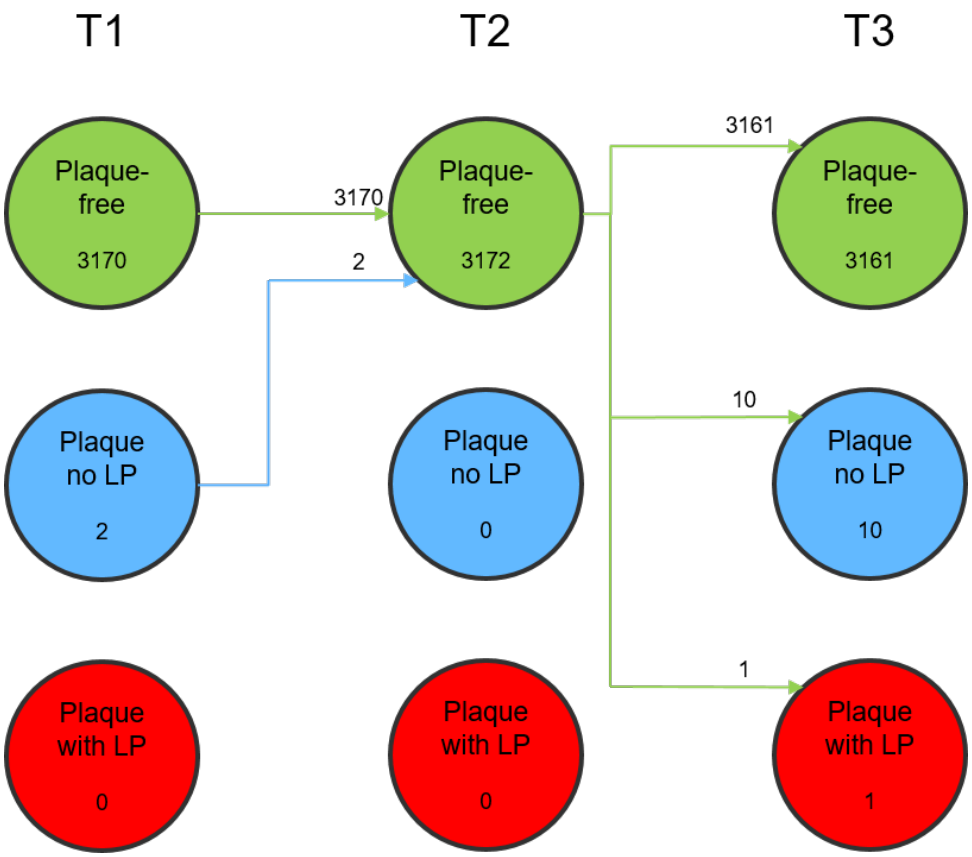

Figure 16: Infographic of the number of MD sectors in each category from T1 to T3, and how they changed over time.

Advanced-diseased pigs

In the AD, 15 arteries were analysed with a total of 3035 3mm/45° sectors at T1 and T2. Due to death of 2 pigs after T2, 9 arteries with a total of 1989 3mm/45° sectors were remaining for T3 analysis. At all time points, more than 65% of the sectors were plaque-free: 2990 (98.52%) sectors at T1, 2367 (77.99%) at T2 and 1323 (66.52%) at T3. 43 sectors with plaque but no LP were present at T1, 635 at T2 and 655 at T3; while 2, 33 and 11 sectors had plaque with LP at T1, T2 and T3 respectively (Table 5 and Figure 17).

	T1	**T2**	**T3**
Plaque-free (%)	2990 (98.52)	2367 (77.99)	1323 (66.52)
Plaque no LP (%)	43 (1.42)	635 (20.92)	655 (32.93)
Plaque with LP (%)	2 (0.06)	33 (1.09)	11 (0.55)

Table 5: Number and percentage of plaque-free, plaque without lipid-pool and plaque with lipid-pool of AD sectors for T1 to T3.

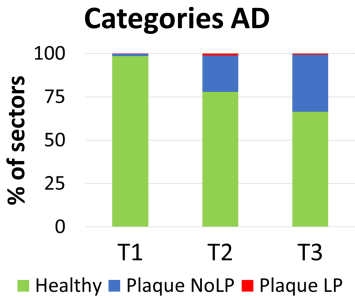

Figure 17: Average percentage of plaque-free, plaque without LP and plaque with LP of AD sectors for T1 to T3.

9 months after starting the high-fat diet (T2), around 21% of sectors that were plaque-free at baseline developed atherosclerosis, of which 1% had LP. 7% of sectors with plaque without LP at baseline became plaque-free while around 4% developed LPs. Out of the two sectors with plaque containing a LP at T1, one of them resolved or disappeared (Table 6a). At T3, more than 20% of sectors which were plaque-free at T2 developed plaque, forming LPs in 0.3% of them. In contrast, around 20% of sectors with plaque, with or without LP, shifted to plaque-free sectors.

Merely 1.5% of sectors without LP at T2 had it at the last time point (Table 6b). For the results of T3, data from pigs that did not survive beyond T2 were omitted. In other words, T2 data from these pigs was not considered when calculating the percentage of AD sectors that changed categories between T2 and T3. In Figure 18, the number of sectors per category at each time point and how they changed is visualized. In addition, sector categories and their change during follow-up per pig can be found in appendix D.2.

		T2		
		Plaque-free	Plaque no LP	Plaque with LP
T1	Plaque-free	79.06%	19.93%	1%
	Plaque no LP	6.98%	88.37%	4.65%
	Plaque with LP	0	0.5	0.5

(a) Percentage of AD sectors that changed categories between T1 and T2.

		T3		
		Plaque-free	Plaque no LP	Plaque with LP
T2	Plaque-free	78.06%	21.62%	0.32%
	Plaque no LP	21.61%	77.13%	1.26%
	Plaque with LP	22.22%	66.67%	11.11%

(b) Percentage of AD sectors that changed categories between T2 and T3.

Table 6: Percentage of AD sectors in each category from one time point to its following.

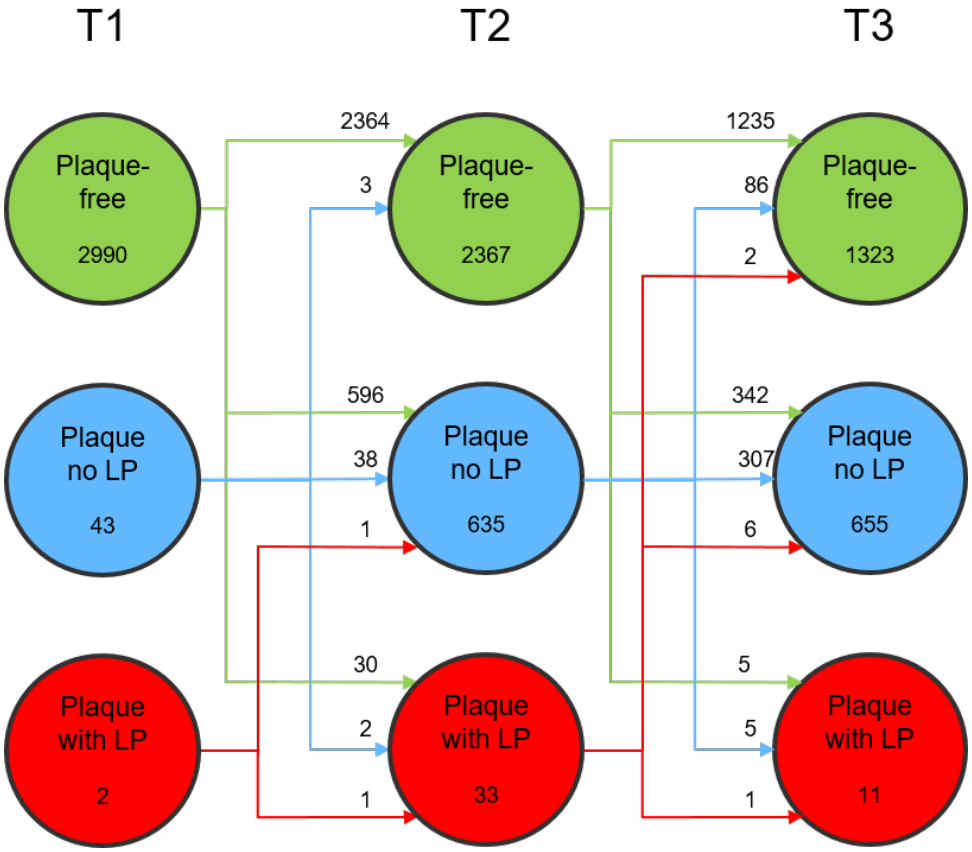

Figure 18: Infographic of the number of AD sectors in each category from T1 to T3, and how they changed over time.

Overall, wall thickness was higher in sectors with plaque than in plaque-free sectors for both groups at all time points. In none of the groups were plaque-free sectors with wall thickness greater than 0.25 mm while sectors with plaque never had wall thickness lower than 0.3 mm. A slight increase of wall thickness of around 0.01 mm was observed throughout time in plaque-free sectors whereas sectors that had plaque experienced a reduction in wall thickness of 0.057 mm between T1 and T2 followed by a significant growth between T2 and T3 of 0.19 mm and 0.29 mm (plaque with and without LP respectively), having thicker walls at T3 than at baseline. The wall of sectors with LP was thinner than the wall of sectors with plaque without LP at all time points for AD group, having at T3 an average wall thickness of 0.6 mm and 0.82 mm

respectively. Due to little atherosclerosis development on MD group, sectors with plaque with or without LP cannot be analysed. Nevertheless, AD group had thicker walls at all categories and time points than MD group (Figure 19).

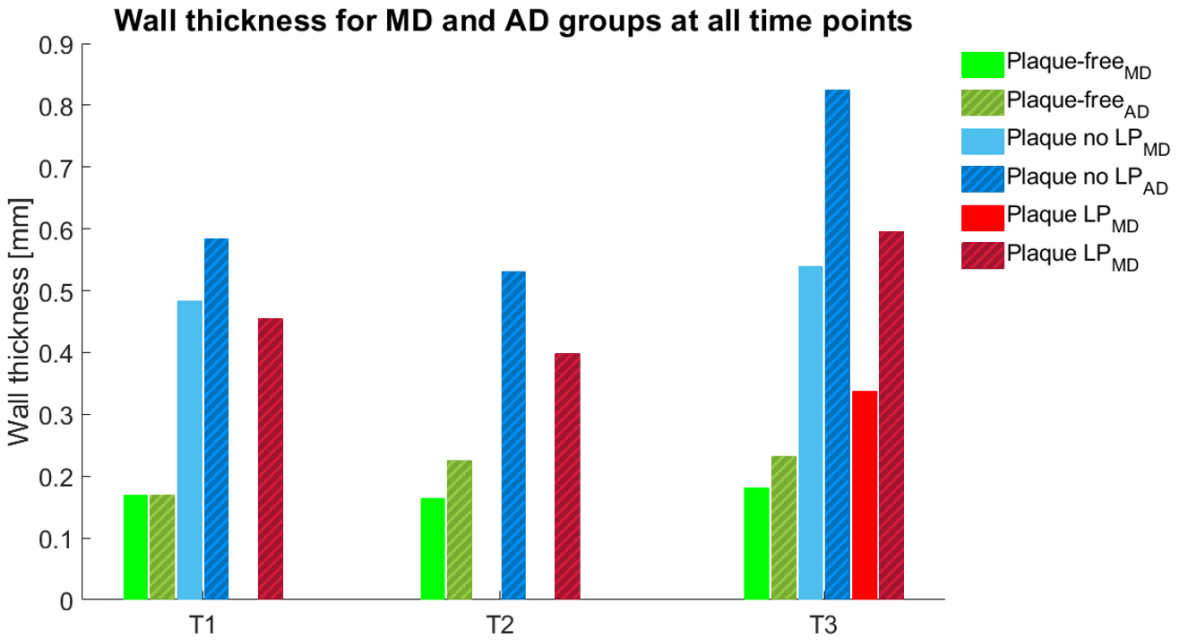

Figure 19: Wall thickness per group per time point. Blank spaces are due to none existence of that category at that time point, i.e, no plaques with lipid-pool at T1 and no plaques with or without lipid-pool at T2.

3.2 Wall stresses and morphometrical measurements

In this section, the results of wall stresses and wall thickness are displayed. For PB results, see Appendix E.

3.2.1 Wall Shear Stress

Mildly-diseased pigs

In Figure 20 the relationship between wall thickness with WSS for MD pigs is depicted. Wall thickness decreased as WSS increased, that is, in regions with low WSS the arterial wall was thicker whereas regions with high WSS had thinner arterial walls. The same behaviour was observed at the three time points, in all cases having at T3 greatest wall thickness, and at T2 lowest. On average, the wall thickness experienced a greater reduce from low to medium WSS than the one experienced from medium to high WSS (0.03 mm vs. 0.015 mm).

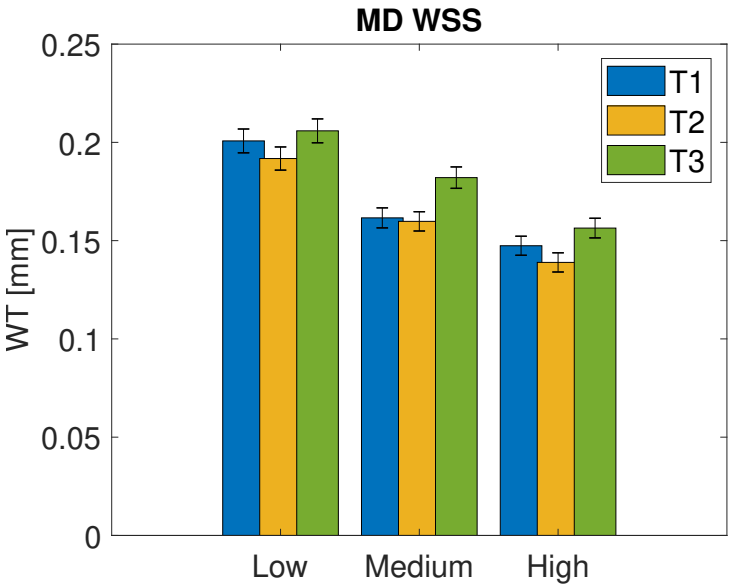

Figure 20: Wall thickness of MD pigs and low, medium and high WSS at each time point. The 95% confidence interval is represented by vertical lines.

Advanced-diseased pigs

The interaction of wall thickness with WSS for AD pigs can be observed in Figure 21. At every time point, a reduction of wall thickness was observed as WSS increased for all cases. A significant difference of wall thickness was noted between T1 and T2 or T3, being walls thicker at T2 or T3 when comparing with T1, and being higher at T3 when comparing T2 and T3. The reduction rate for wall thickness between tertiles was greatest for T3 and lowest for T2 (average of 0.06 mm vs. 0.0014 mm respectively).

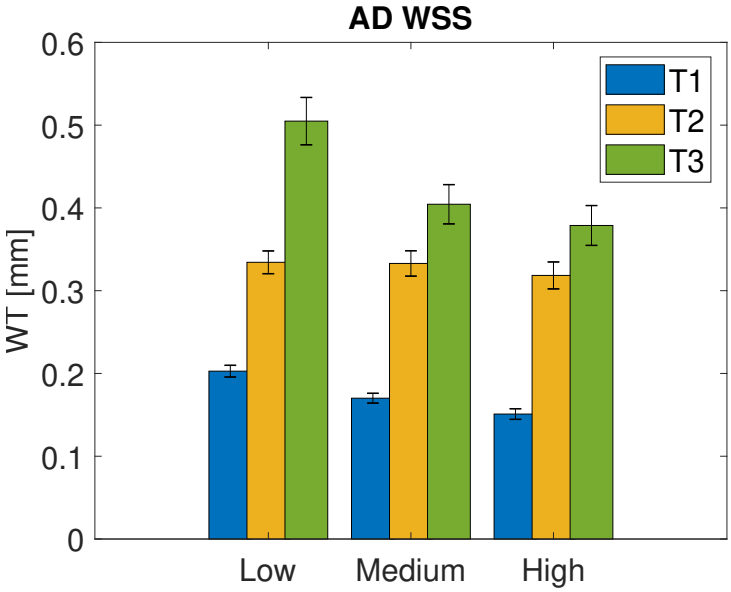

Figure 21: Wall thickness of AD pigs and low, medium and high WSS at each time point. The 95% confidence interval is represented by vertical lines.

Sectors belonging to AD pigs were classified as plaque-free, diseased without LP and diseased with LP. In the following paragraphs, the results of each category are presented independently.

Regarding plaque-free sectors belonging to AD pigs, a progressive decrease in wall thickness was observed as WSS increased (see Figure 22). Wall thickness was lowest at T1 and highest at T3. The reduction rate was consistent between WSS tertiles, observing a reduction of 0.03 mm and 0.04 mm between low and medium WSS and medium and high WSS respectively.

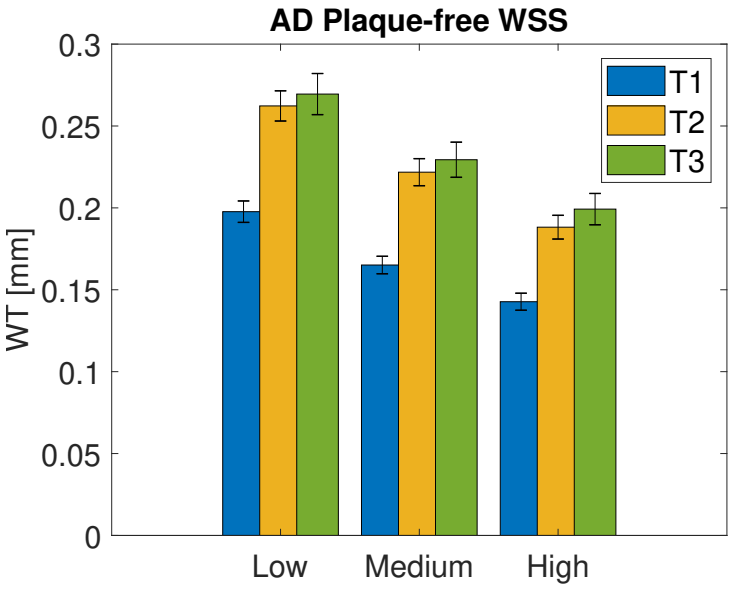

Figure 22: Wall thickness of plaque-free sectors belonging to AD pigs and low, medium and high WSS at each time point. The 95% confidence interval is represented by vertical lines.

Figure 23 shows the relation of sectors with plaque but no lipid-pool between wall thickness and WSS. On average, wall thickness remained constant as WSS increased at T1 and T2 (wall thickness of 0.57 mm and 0.7 mm respectively) whereas at T3 a decrease of wall thickness with WSS increase was observed (0.12 mm between low and mid WSS and 0.04 mm between mid and high WSS). It was also noted that wall thickness increased with time in all WSS levels, witnessing the highest wall thickness increase in sectors undergoing low WSS (0.22 mm increase).

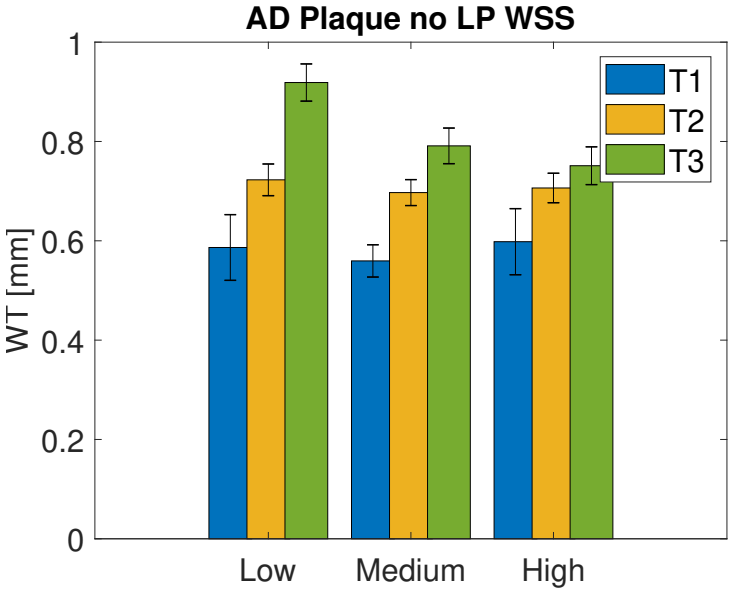

Figure 23: Wall thickness of sectors with plaque but no lipid-pool belonging to AD pigs and low, medium and high WSS at each time point. The 95% confidence interval is represented by vertical lines.

In Figure 24, the interaction of WSS on wall thickness for diseased sectors with LP is visualized. Wall thickness experienced a greater increase in sectors exposed to medium WSS than sectors exposed to low WSS (increase of 0.24 mm). This increase was subsequently reduced by 0.2 mm in sectors with high WSS. Wall thickness values at T3 were higher than at T2, maintaining the difference in the three WSS levels (0.08 mm difference). Data from T1 was ignored due to few or none presence of sectors that had plaque with LP.

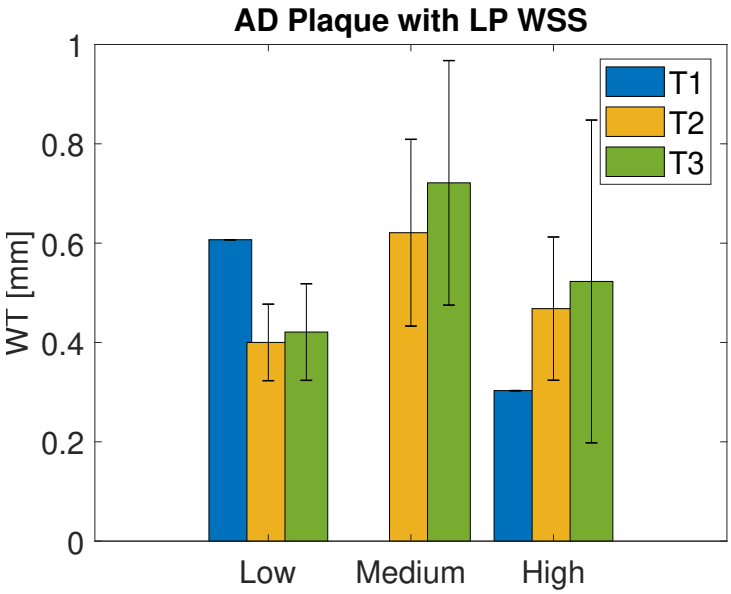

Figure 24: Wall thickness of sectors with plaque with lipid-pool belonging to AD pigs and low, medium and high WSS at each time point. The 95% confidence interval is represented by vertical lines.

3.2.2 Wall Mechanical Stress

Mildly-diseased pigs

Wall thickness experienced a reduction of 0.05 mm as WMS increased from low to medium, that is, sectors exposed to low WMS had higher wall thickness than sectors with medium WMS (see Figure 25). On the contrary, a modest increased of wall thickness was observed when WMS increased from medium to high (0.01 mm increase). With the exception of sectors with high WMS, wall thickness had the highest values at T3 while the lowest values were observed at T2.

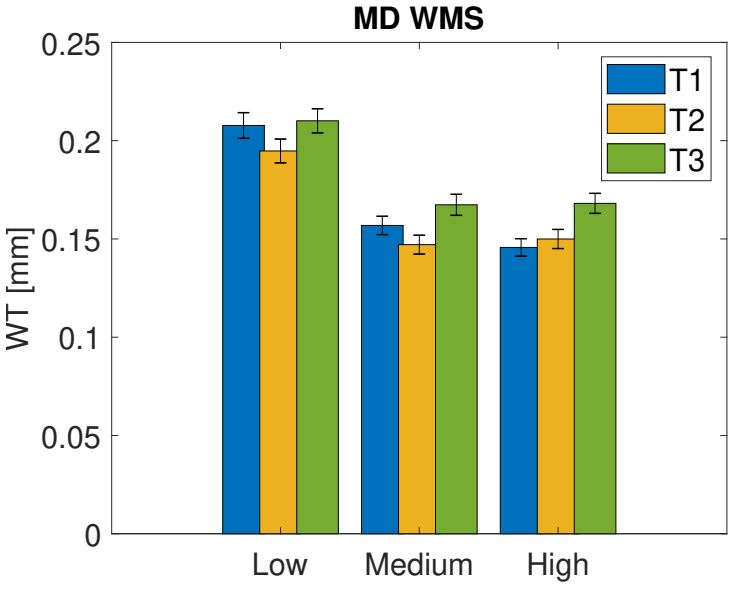

Figure 25: Wall thickness of MD pigs and low, medium and high WMS at each time point. The 95% confidence interval is represented by vertical lines.

Advanced-diseased pigs

The interaction of WMS on wall thickness for AD is displayed in Figure 26. A significant increase in wall thickness was observed at T2 and T3 in comparison with T1. Moreover, at T3 the metric had greater values than at T2. A reduction of wall thickness was observed at all time

points, being the reduction higher at T2 and T3 than at T1 (reduction of 0.1 mm at T2 and T3 vs. reduction of 0.04 mm at T1).

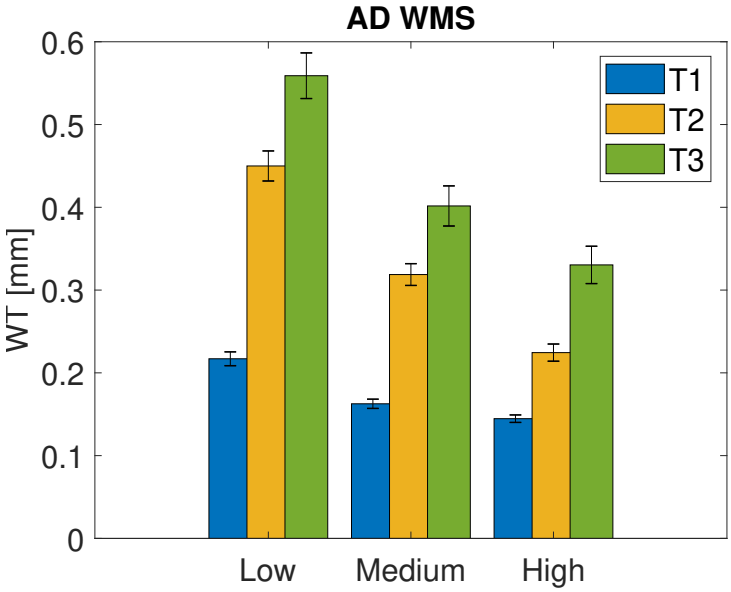

Figure 26: Wall thickness of AD pigs and low, medium and high WMS at each time point. The 95% confidence interval is represented by vertical lines.

Same as before, sectors belonging to AD pigs were classified as plaque-free, diseased without LP and diseased with LP; and the results of each category were independently analysed.

In Figure 27, the interaction of WMS on wall thickness for plaque-free sectors belonging to AD pigs is visualized. The metric had the lowest values at T1 and highest at T3 and the reduction rate was consistent between WMS tertiles. A reduction of 0.04 mm and 0.03 mm between low and medium WMS and medium and high WMS was experienced, respectively.

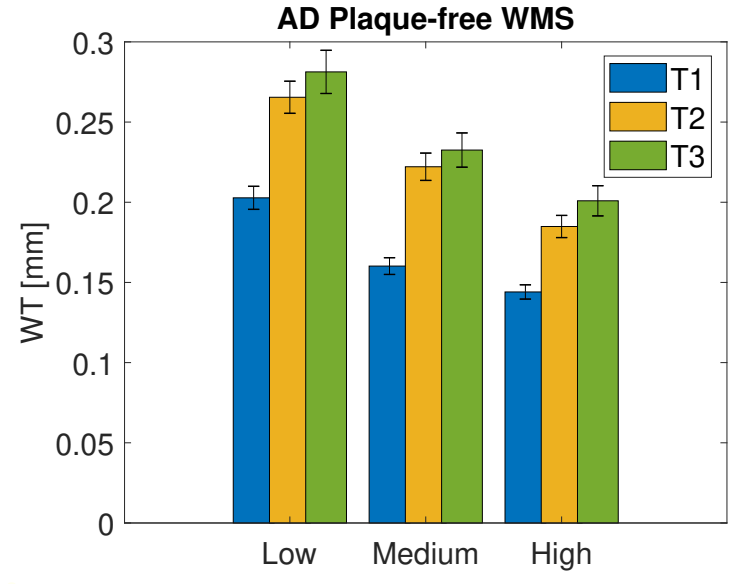

Figure 27: Wall thickness of plaque-free sectors belonging to AD pigs and low, medium and high WMS at each time point. The 95% confidence interval is represented by vertical lines.

The relationship of wall thickness of diseased sectors without lipid-pool can be seen in Figure 28. At T1, the lowest wall thickness was observed no matter the WMS level. Moreover, wall thickness experienced a slight increase of 0.1 mm when WMS level increased from low to medium at T1 to decrease 0.19 mm when high WMS level was reached. On the contrary, wall thickness experienced a decrease of 0.9 mm when WMS level increased from low to medium at T2. In the

remaining cases, the metric stayed stable independently of WMS level.

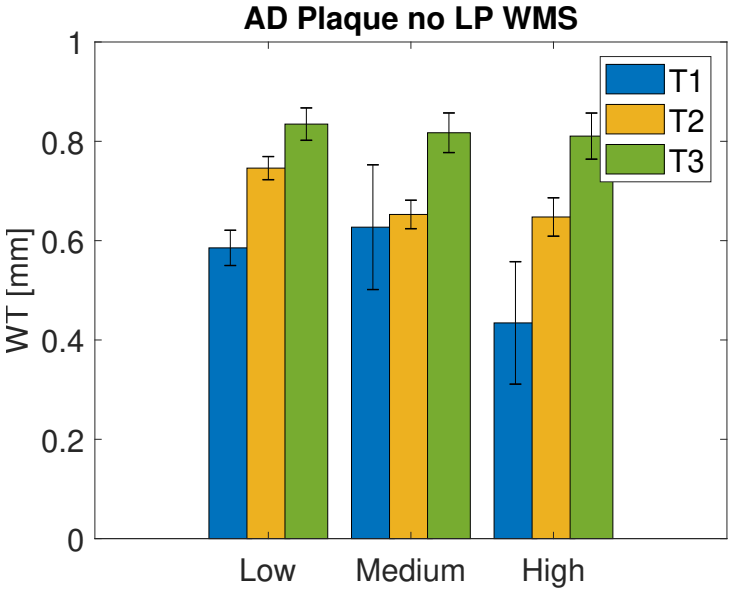

Figure 28: Wall thickness of sectors with plaque but no lipid-pool belonging to AD pigs and low, medium and high WMS at each time point. The 95% confidence interval is represented by vertical lines.

In Figure 29 the interaction between wall thickness with WMS for diseased sectors with LP belonging to AD pigs is depicted. A decrease of wall thickness was observed at every time point as WMS increased. At T3, sectors had thicker walls than at T2 when exposed to low or medium WMS, while wall thickness decreased in time when exposed to high WMS (thickness of 0.38 mm at T2 vs. 0.34 mm at T3). Data from T1 was ignored due to the fact that there were very few or none sectors with LP at T1.

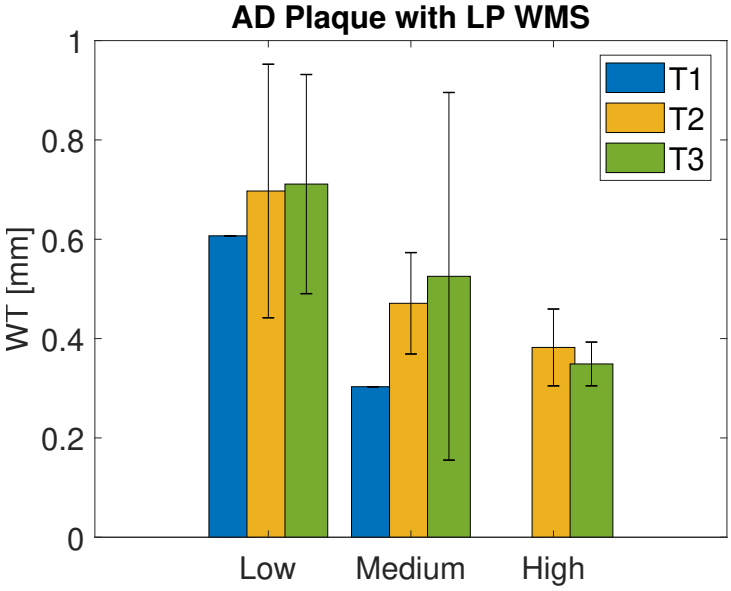

Figure 29: Wall thickness of sectors with plaque with lipid-pool belonging to AD pigs and low, medium and high WMS at each time point. The 95% confidence interval is represented by vertical lines.

3.2.3 Combination of WSS and WMS

The relationship between wall thickness and WSS and WMS at each time point can be found in Figure 30, Figure 31 and Figure 32.

Mildly-diseased pigs

In all time points, the thickest walls of MD group were observed in sectors with low WSS and low WMS while the thinner walls were observed in sectors exposed to high WSS and high WMS. However, at T2 and T3 slightly thinner walls were noticed in sectors with medium WMS and high WSS than in sectors with high WSS and WMS.

Advanced-diseased pigs

At T1 and T3, same behaviour as for MD pigs was observed in AD pigs, highest wall thickness was found in sectors exposed to low WSS and low WMS while smallest wall thickness was observed in sectors exposed to high WSS and high WMS. However, even though wall thickness reduced as WMS increased, at T2 wall thickness did not necessarily decrease as WSS increased. Wall thickness remained consistent at any level of WSS as long as WMS was low; when increasing WMS to medium or high, at low WSS, wall thickness was higher but no difference was observed between medium and high WSS.

Analogously as for WSS and WMS, sectors belonging to AD pigs were classified as plaque-free, diseased without LP and diseased with LP; and the connection of both stresses with wall thickness was analysed independently. At all time points, AD plaque-free sectors with lowest WSS and WMS presented with highest wall thickness whereas sectors exposed to high WSS and WMS exhibited the lowest wall thickness. In all cases, as WSS increased, wall thickness decreased irrespective of WMS level. Regarding sectors with plaque but no LP, no sectors with high WMS and low or medium WSS were present at T1. Nonetheless, it was observed that sectors experiencing high WMS and high WSS had thinner arterial walls. Sectors exposed to low or medium WMS, despite the WSS level, had similar wall thickness. At T2, higher wall thickness was reported in sectors exposed to low WMS independently of their level of WSS, observing the same pattern in sectors with medium and high WMS, where the wall thickness slowly decreased independently of the WSS levels. On the contrary, at T3 an average reduction of wall thickness was observed as WSS increased no matter WMS level, with the exception of high WSS and WMS, where the wall thickness increased 0.06 mm compared to medium WSS and high WMS. Sectors with LP at T1 were ignored due to very few or none present sectors. At both T2 and T3, it was observed that the highest the WMS was, the thinner the wall was independently of WSS level. However, it was also noticeable that sectors experiencing medium WSS combined with low or medium WMS had the thickest arterial walls, followed by sectors exposed to low WMS and high WSS.

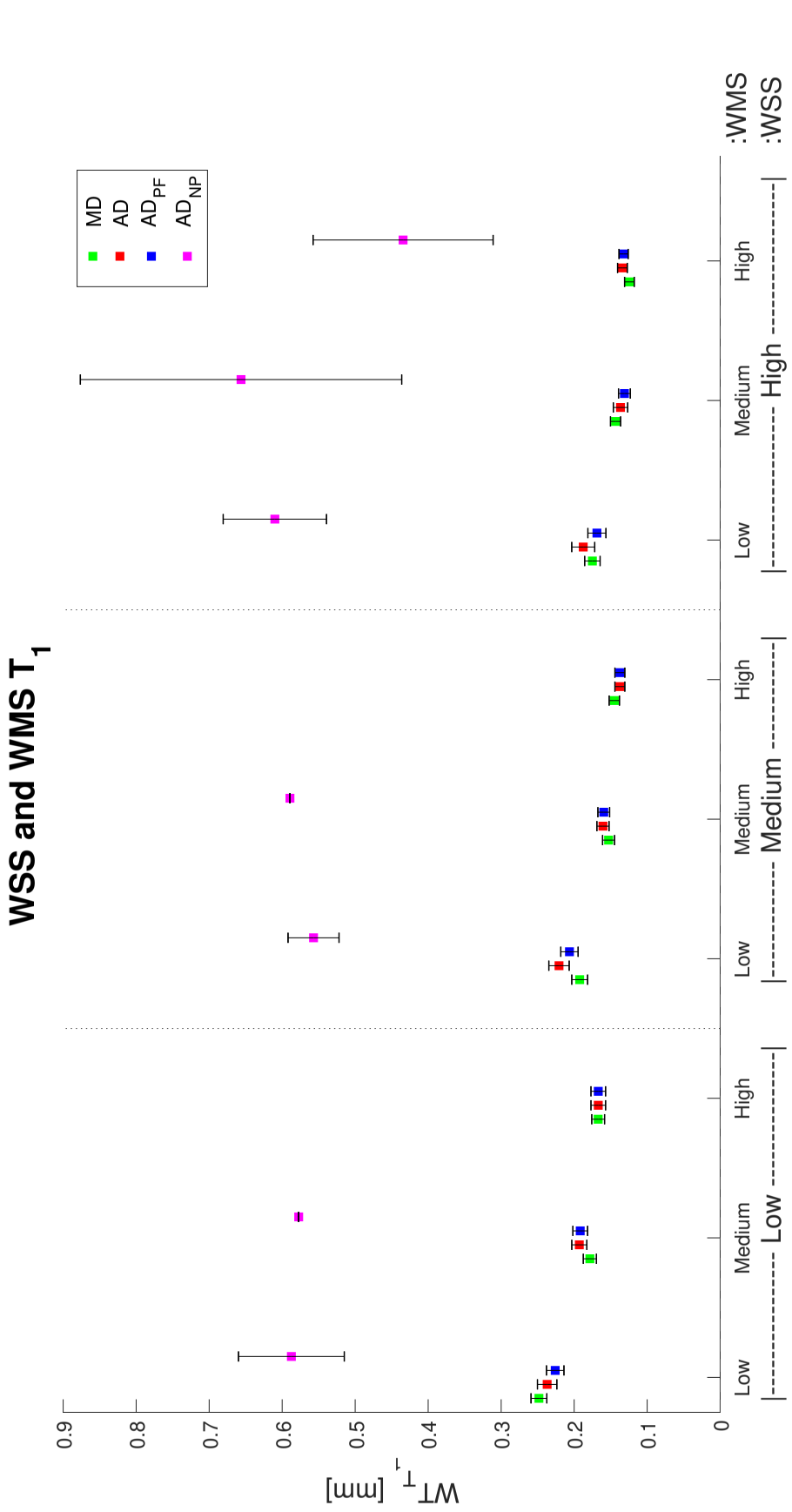

Figure 30: Wall thickness at T1 of all categorised sectors according to low, medium and high WSS and WMS. The 95% confidence interval is represented by vertical lines. MD: mildly-diseased; AD: advanced-diseased; PF: plaque-free; NP: plaque without lipid-pool.

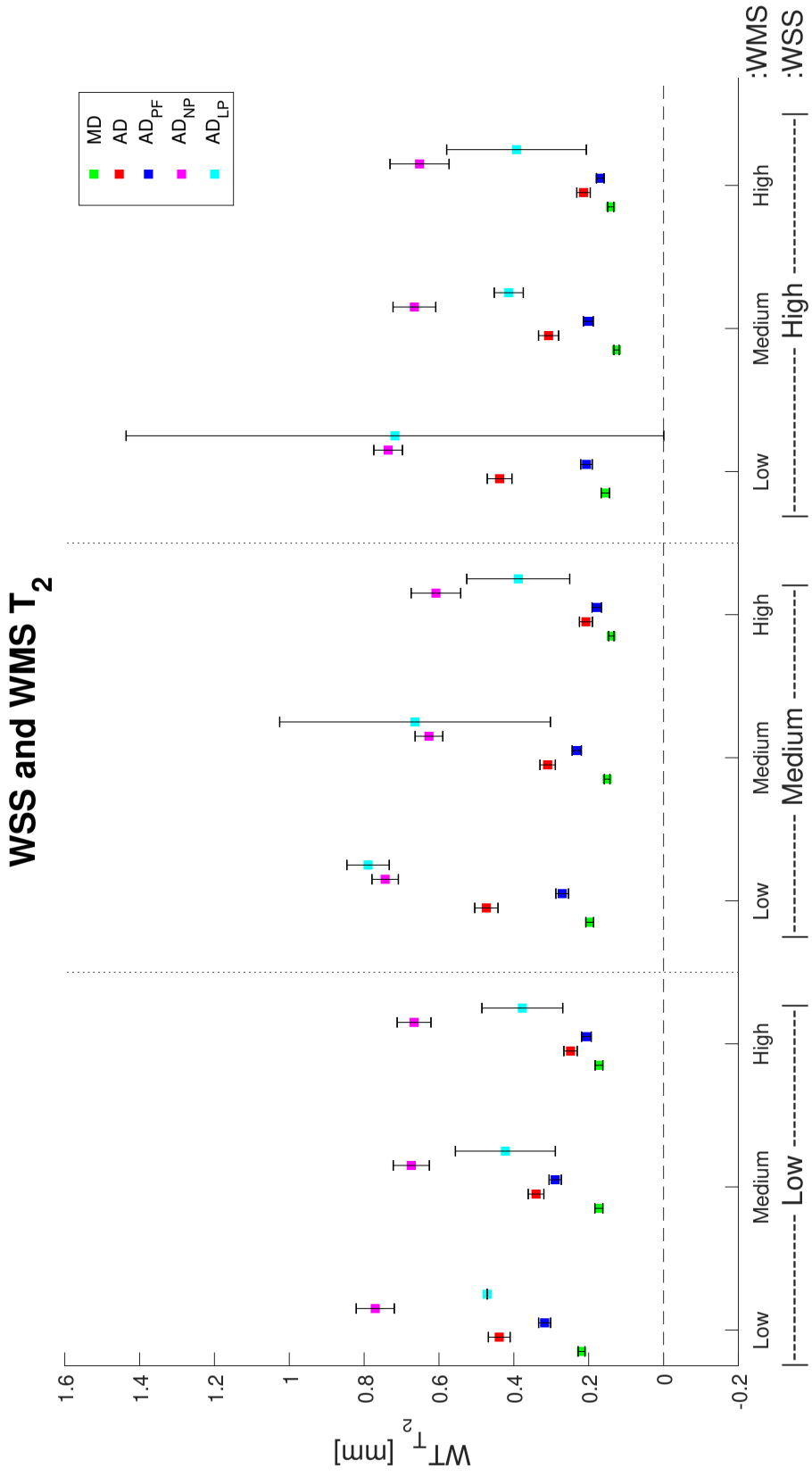

Figure 31: Wall thickness at T2 of all categorised sectors according to low, medium and high WSS and WMS. The 95% confidence interval is represented by vertical lines. MD: mildly-diseased; AD: advanced-diseased; PF: plaque-free; NP: plaque without lipid-pool; LP: plaque with lipid-pool.

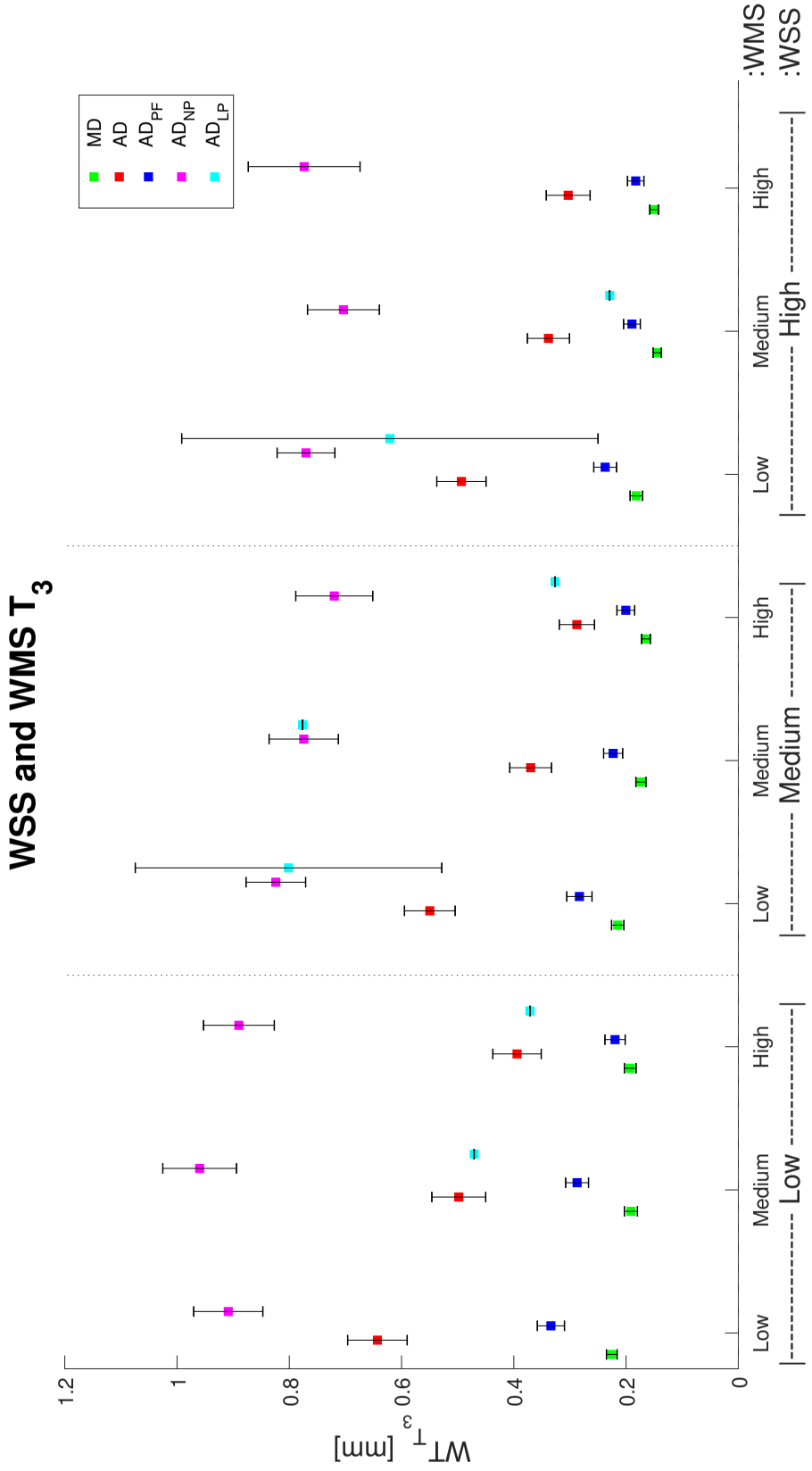

Figure 32: Wall thickness at T3 of all categorised sectors according to low, medium and high WSS and WMS. The 95% confidence interval is represented by vertical lines. MD: mildly-diseased; AD: advanced-diseased; PF: plaque-free; NP: plaque without lipid-pool; LP: plaque with lipid-pool.

3.3 Wall stresses and morphometrical change over time

3.3.1 Wall Shear Stress

Mildly-diseased pigs

Wall thickness change between baseline and T2 in MD pigs was greater in sectors exposed to low or medium WSS at T1 compared to sectors exposed to high WSS (change of 0.01 mm under low and medium WSS vs. 0.004 mm of change under high WSS) (Figure 33). On the contrary, sectors undergoing medium or high WSS at T2 experienced a bigger increase in wall thickness at T3 (change of 0.014 mm, 0.023 and 0.018 mm at low, medium and high WMS respectively) (Figure 34). In any circumstance, the wall thickness variation for MD pigs, both at initiation (T1-T2) and progression (T2-T3), was almost none.

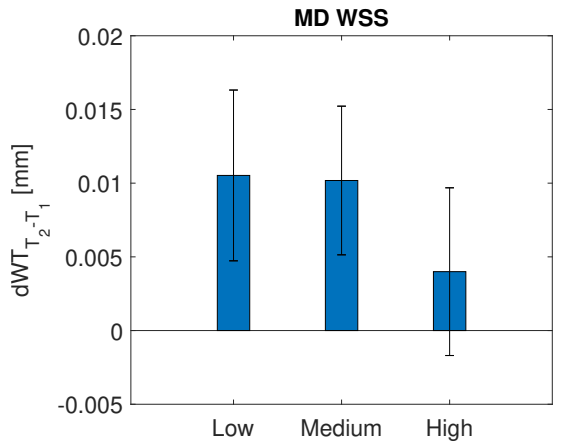

Figure 33: Wall thickness change between T1 to T2 of MD pigs according to low, medium and high WSS at T1. The 95% confidence interval is represented by vertical lines.

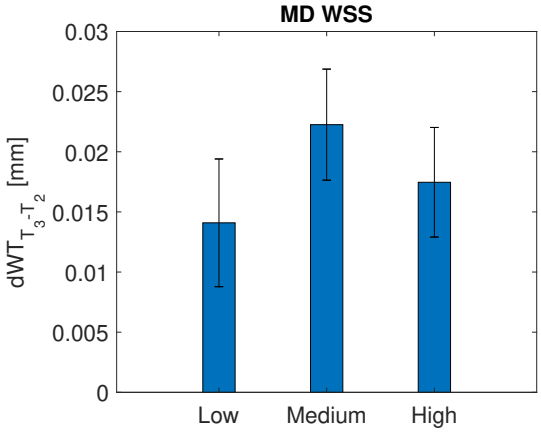

Figure 34: Wall thickness change between T2 to T3 of MD pigs according to low, medium and high WSS at T2. The 95% confidence interval is represented by vertical lines.

Advanced-diseased pigs

The interaction between WSS and wall thickness change at plaque initiation and plaque progression for AD pigs are observed in Figure 35 and Figure 36 respectively. Both at plaque initiation and progression, as WSS increased sectors experienced a progressive decrease of wall thickness growth, being the reduction more remarkable from T2 to T3 (reduction of 0.04 mm per tertile from T1 to T2 vs. an average of 0.49 mm per tertile from T2 to T3).

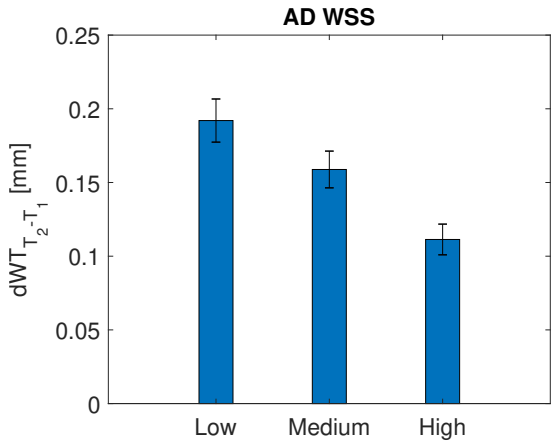

Figure 35: Wall thickness change between T1 to T2 of AD pigs according to low, medium and high WSS at T1. The 95% confidence interval is represented by vertical lines.

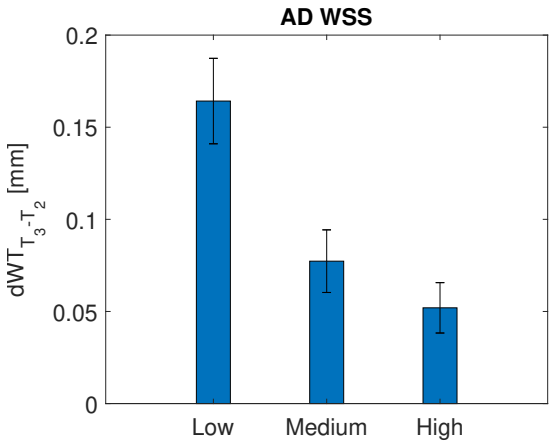

Figure 36: Wall thickness change between T2 to T3 of AD pigs according to low, medium and high WSS at T2. The 95% confidence interval is represented by vertical lines.

In regards to plaque-free sectors from AD pigs, very similar results as the ones for the whole AD group were found (see Figure 37 and Figure 38). At both plaque initiation and progression, an increase in WSS was observed with a gradual reduction in wall thickness growth, with the most significant decrease occurring between T2 and T3 (a decrease of 0.04 mm per tertile between T1 and T2 compared to an average decrease of 0.49 mm per tertile from T2 to T3).

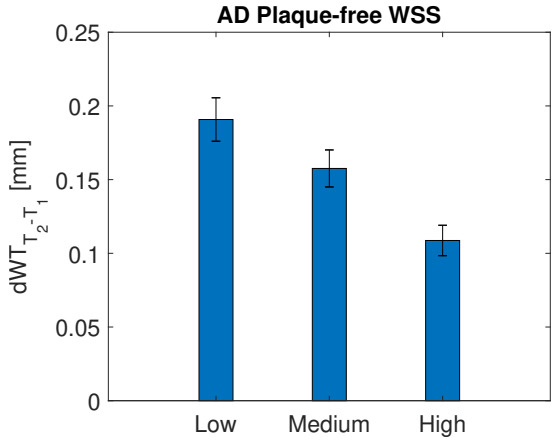

Figure 37: Wall thickness change between T1 to T2 of plaque-free sectors from AD pigs according to low, medium and high WSS at T1. The 95% confidence interval is represented by vertical lines.

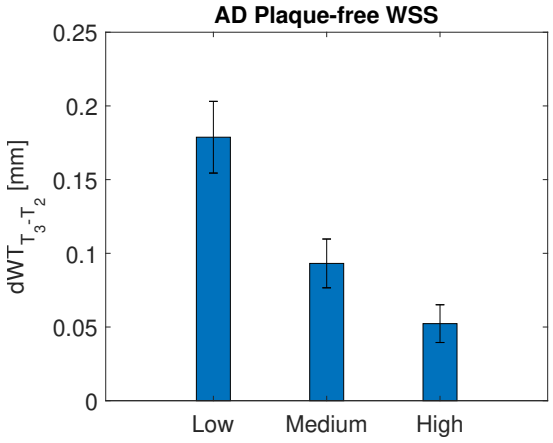

Figure 38: Wall thickness change between T2 to T3 of plaque-free sectors from AD pigs according to low, medium and high WSS at T2. The 95% confidence interval is represented by vertical lines.

When observing sectors with plaque but no LP from AD pigs, it was observed that sectors undergoing low WSS at T1 experienced a greater wall thickness increase at T2 than sectors with higher WSS level (0.29 mm vs 0.23 mm increase respectively) (Figure 39). The difference on wall thickness between T2 and T3 was smaller (average of 0.043 mm) than the one at plaque initiation (0.25 mm), and sectors exposed to low and high WSS had a similar increase while sectors exposed to medium WSS experienced a lower wall thickness growth (0.05 mm vs 0.017 mm) (Figure 40).

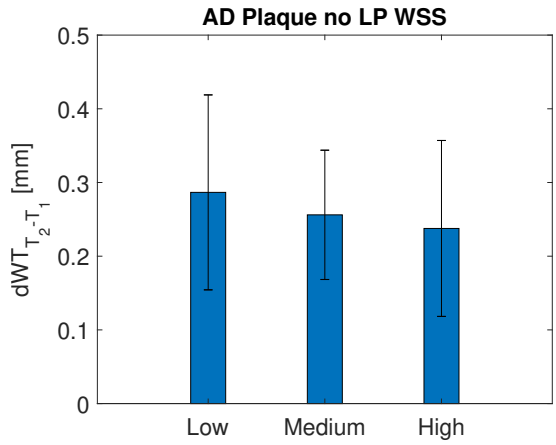

Figure 39: Wall thickness change between T1 to T2 of sectors with plaque but no lipid-pool from AD pigs according to low, medium and high WSS at T1. The 95% confidence interval is represented by vertical lines.

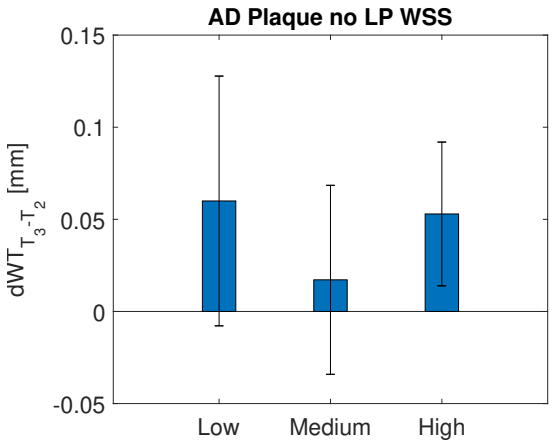

Figure 40: Wall thickness change between T2 to T3 of sectors with plaque but no lipid-pool from AD pigs according to low, medium and high WSS at T2. The 95% confidence interval is represented by vertical lines.

At T1, insufficient sectors with LP were present and the majority of sectors that developed LP belonged to AD pigs that died after T2 so little information could be obtained on the wall thickness change over time for this group. However, in Figure 41 a reduction on wall thickness growth at plaque progression could be observed as WSS level increased.

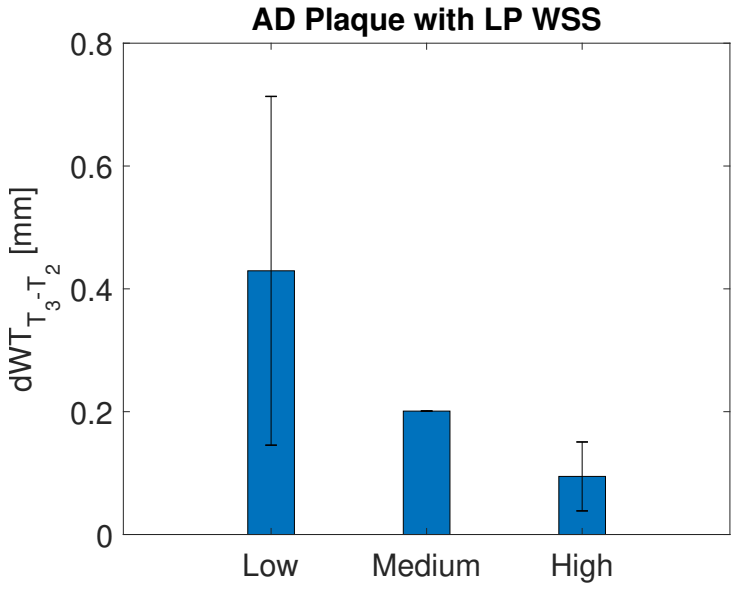

Figure 41: Wall thickness change between T2 to T3 of sectors with lipid-pool from AD pigs according to low, medium and high WSS at T2. The 95% confidence interval is represented by vertical lines.

3.3.2 Wall Mechanical Stress

Mildly-diseased pigs

In Figure 42 and Figure 43, the relationship of WMS and the change in wall thickness over time is visualized. At baseline as well as T2, sectors undergoing low WMS experienced lowest wall thickness growth, while sectors experiencing the highest wall thickness growth were those under high WMS at T1 (0.007 mm, 0.01 mm and 0.017 mm of increase under low, mid and high WMS respectively) and those under medium WMS at T2 (0.015 mm, 0.02 and 0.018 mm of increase under low, mid and high WMS respectively). Nevertheless, the wall thickness change was negligible in both cases.

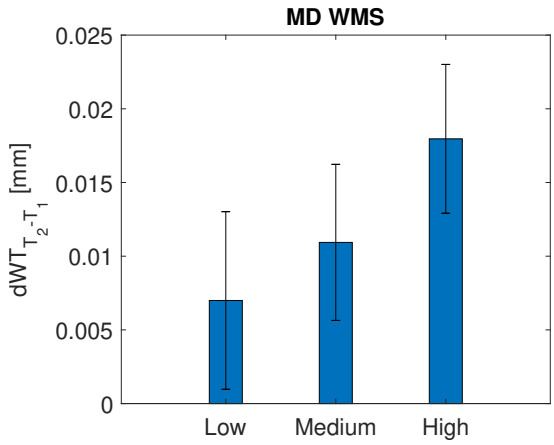

Figure 42: Wall thickness change between T1 to T2 of MD pigs according to low, medium and high WMS at T1. The 95% confidence interval is represented by vertical lines.

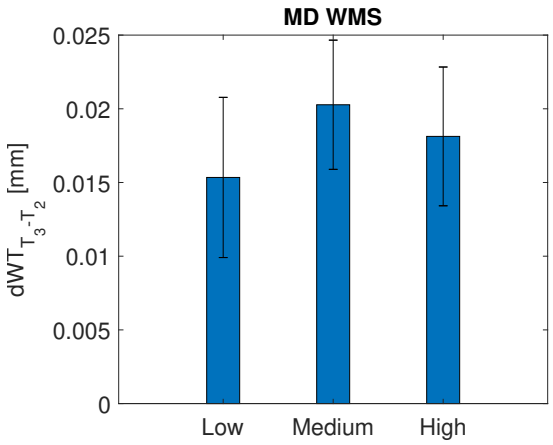

Figure 43: Wall thickness change between T2 to T3 of MD pigs according to low, medium and high WMS at T2. The 95% confidence interval is represented by vertical lines.

Advanced-diseased pigs

An increase on wall thickness of around 0.15 mm was observed from baseline to T2 without effect of WMS levels (see Figure 44). Smaller wall thickness growth (average of 0.095 mm) was seen between T2 and T3, having again no remarkable difference between WMS levels (see Figure 45).

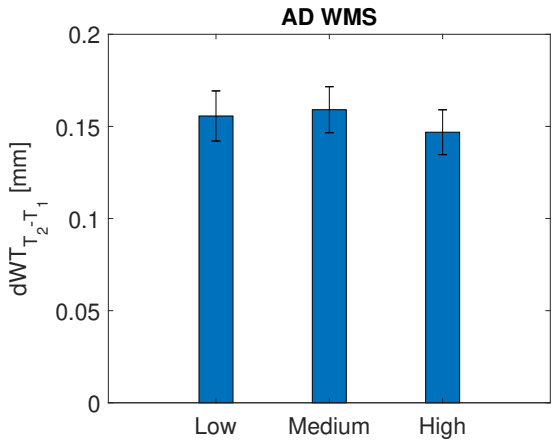

Figure 44: Wall thickness change between T1 to T2 of AD pigs according to low, medium and high WMS at T1. The 95% confidence interval is represented by vertical lines.

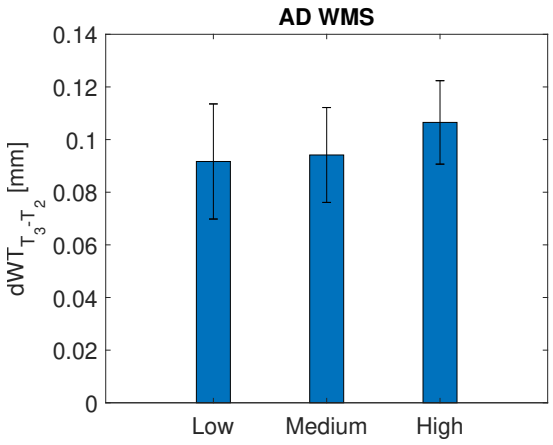

Figure 45: Wall thickness change between T2 to T3 of AD pigs according to low, medium and high WMS at T2. The 95% confidence interval is represented by vertical lines.

Regarding plaque-free sectors from AD pigs, at plaque initiation a wall thickness increase of around 0.15 mm was observed, regardless of WMS level (Figure 46). However, at plaque progression, sectors exposed to low WMS experienced an increase of 0.14 mm while sectors exposed to medium or high WMS experienced a wall thickness growth of 0.1 mm (Figure 47).

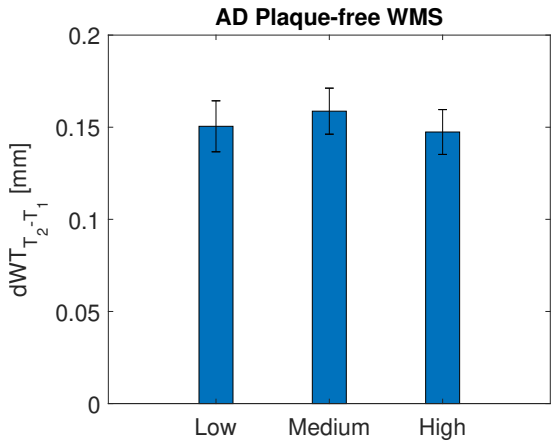

Figure 46: Wall thickness change between T1 to T2 of plaque-free sectors from AD pigs according to low, medium and high WMS at T1. The 95% confidence interval is represented by vertical lines.

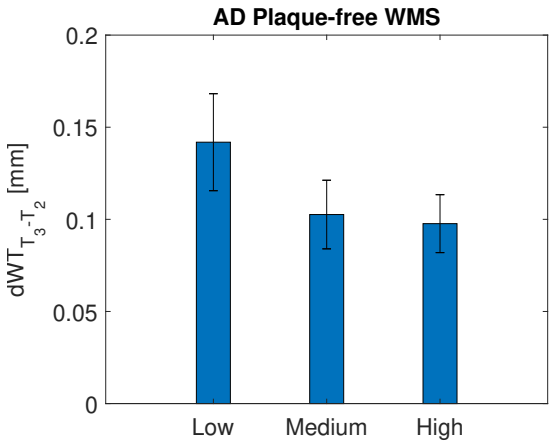

Figure 47: Wall thickness change between T2 to T3 of plaque-free sectors from AD pigs according to low, medium and high WMS at T2. The 95% confidence interval is represented by vertical lines.

On the other hand, when looking only at sectors with plaque but no LP belonging to AD pigs, increase in wall thickness was observed as WMS levels increased (average increase of 0.37 mm and 0.13 mm from T1 to T2 and from T2 to T3 respectively) (Figure 48 and Figure 49). This behaviour was observed at plaque initiation as well as at plaque progression, being the later a more noticeable difference between WMS levels despite of having an overall smaller increase.

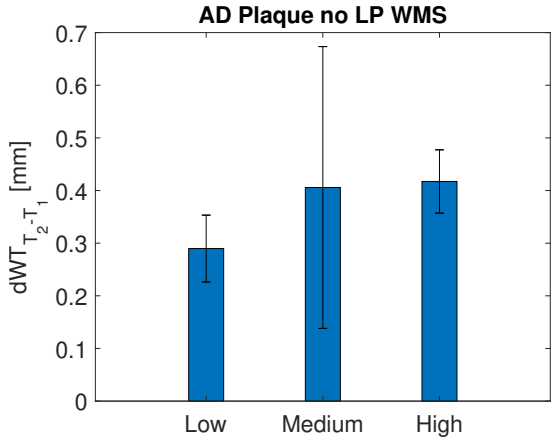

Figure 48: Wall thickness change between T1 to T2 of sectors with plaque but no lipid-pool from AD pigs according to low, medium and high WMS at T1. The 95% confidence interval is represented by vertical lines.

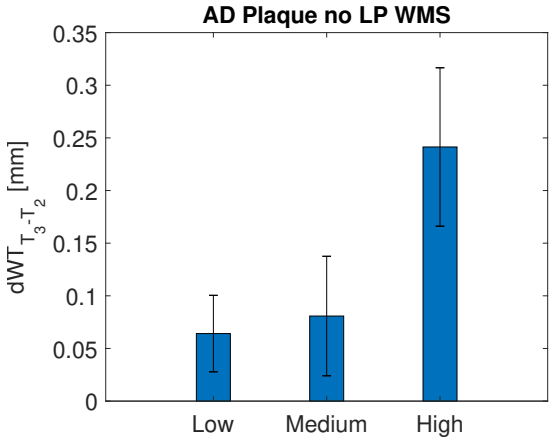

Figure 49: Wall thickness change between T2 to T3 of sectors with plaque but no lipid-pool from AD pigs according to low, medium and high WMS at T2. The 95% confidence interval is represented by vertical lines.

Due to insufficient amount of sectors with LP present at T1 and the subsequent death of 2 AD pigs containing the majority of sectors with LP, little information could be retrieved on the wall thickness change over time. In spite of it, the relationship between wall thickness difference and WMS levels between T2 and T3 is visualised in Figure 50. Following the same pattern previously described, sectors exposed to higher WMS at T2 experienced a higher increase in wall thickness than sectors exposed to low WMS (0.54 mm vs. 0.07 mm).

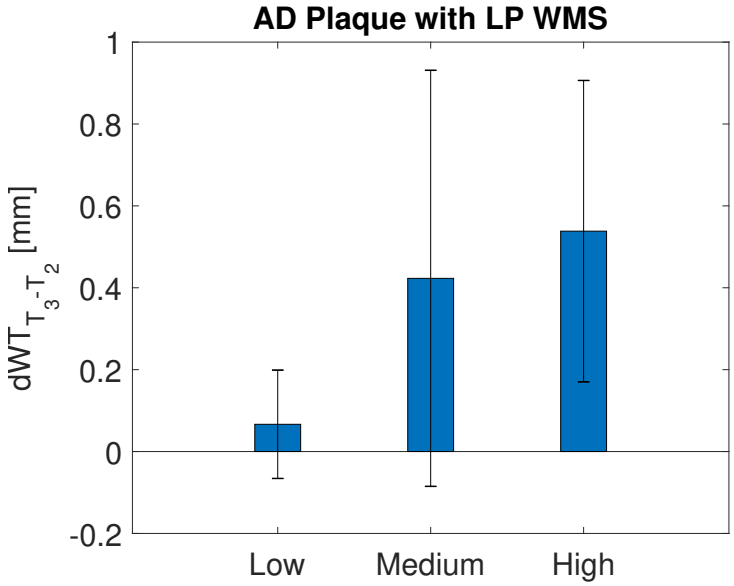

Figure 50: Wall thickness change between T2 to T3 of sectors with lipid-pool from AD pigs according to low, medium and high WMS at T2. The 95% confidence interval is represented by vertical lines.

3.3.3 Combination of WSS and WMS

The effect of WSS and WMS on wall thickness change over time can be seen in Figure 51 and Figure 52.

Mildly-diseased pigs

At plaque initiation, sectors from MD pigs which were under high WSS and high WMS experienced higher increase in wall thickness, whereas the combination of low or medium WMS with high WSS produced wall thickness increase reduction (0.05 mm vs. 0.01 mm). Sectors exposed to medium WMS and low WSS also exhibited greater increase of 0.029 mm in wall thickness. When analysing plaque progression, that is, change in wall thickness between T2 and T3, it was observed that the combinations of low WSS with low WMS and high WSS with high WMS provided the less increase in wall thickness, being it of 0.007 mm. On the contrary, the highest wall thickness increase of 0.026 mm was noted when WSS level was medium with the exception being when WMS was low, with an increase of 0.017 mm. A greater increase of 0.026 mm in wall thickness was additionally observed in sectors with high WSS and low WMS.

Advanced-diseased pigs

Regarding sectors belonging to AD pigs, both at plaque initiation and plaque progression, the higher WSS was, the smaller the wall thickness increase was. This reduction on wall thickness change was more remarkable between T2 and T3 when WSS level increased from low to medium or high (average increase of 0.02 mm at low, 0.012 mm at medium and 0.007 mm at high WSS). Even though WMS did not substantially vary wall thickness growth, it was observed that sectors with medium WMS experienced slightly bigger increase on wall thickness, except at plaque progression when the combination of low WSS with low WMS produced the higher wall thickness change.

As for plaque-free sectors belonging to AD group, at plaque initiation, a lower increase in wall thickness was observed as WSS increased. The highest wall thickness increase of 0.19 mm was found in sectors exposed to low WSS, whereas sectors with high WSS exhibited the lowest wall thickness increase of 0.1 mm. No difference in wall thickness was observed when WMS increased. At plaque progression, a tendency to decrease in wall thickness change was noticed as WSS increased. In sectors with low or medium WSS, a reduction on wall thickness was witness as WMS increased. Nonetheless, sectors exposed to high WSS experienced an increase in wall thickness as WMS increased.

When looking at sectors with plaque which did not contain LP, an increase on wall thickness was noted at plaque initiation as WMS levels increased, with highest increase of 0.73 mm experienced by sectors under low WSS and medium WMS. On the other hand, at initiation stage, not many sectors had developed plaque and, therefore, there was a lack of information about the combination of low or medium WSS with high WMS. At plaque progression stage, greater wall thickness change was observed in sectors exposed to high WMS, in particular those sectors which also experienced high WSS (0.73 mm, 0.73 mm and 0.86 mm on wall thickness increase of sectors under high WMS and low, mid and high WSS respectively). In contrast, sectors under low WMS experienced a lower wall thickness increase, being medium WSS with low WMS the combination that generated the lowest increase (0.09 mm, 0.03 mm and 0.07 mm on wall thickness increase of sectors under low WMS and low, mid and high WSS respectively).

As previously mentioned, not enough sectors with LP were present at T1 so no information could be retrieved for that time point. Despite the fact that at T2 there was not either a large number of sectors with plaque, it was witnessed that the arterial wall of sectors with higher WMS experienced a greater increase in thickness (0.4 mm vs. 0.6mm at low WSS and mid and high WMS respectively; 0.2mm vs. 0.3 mm at high WSS and low and high WMS respectively) . In contrast, as WSS increased, wall thickness increase got reduced, achieving the lowest increase of 0.2 mm when WSS was high and WMS low.

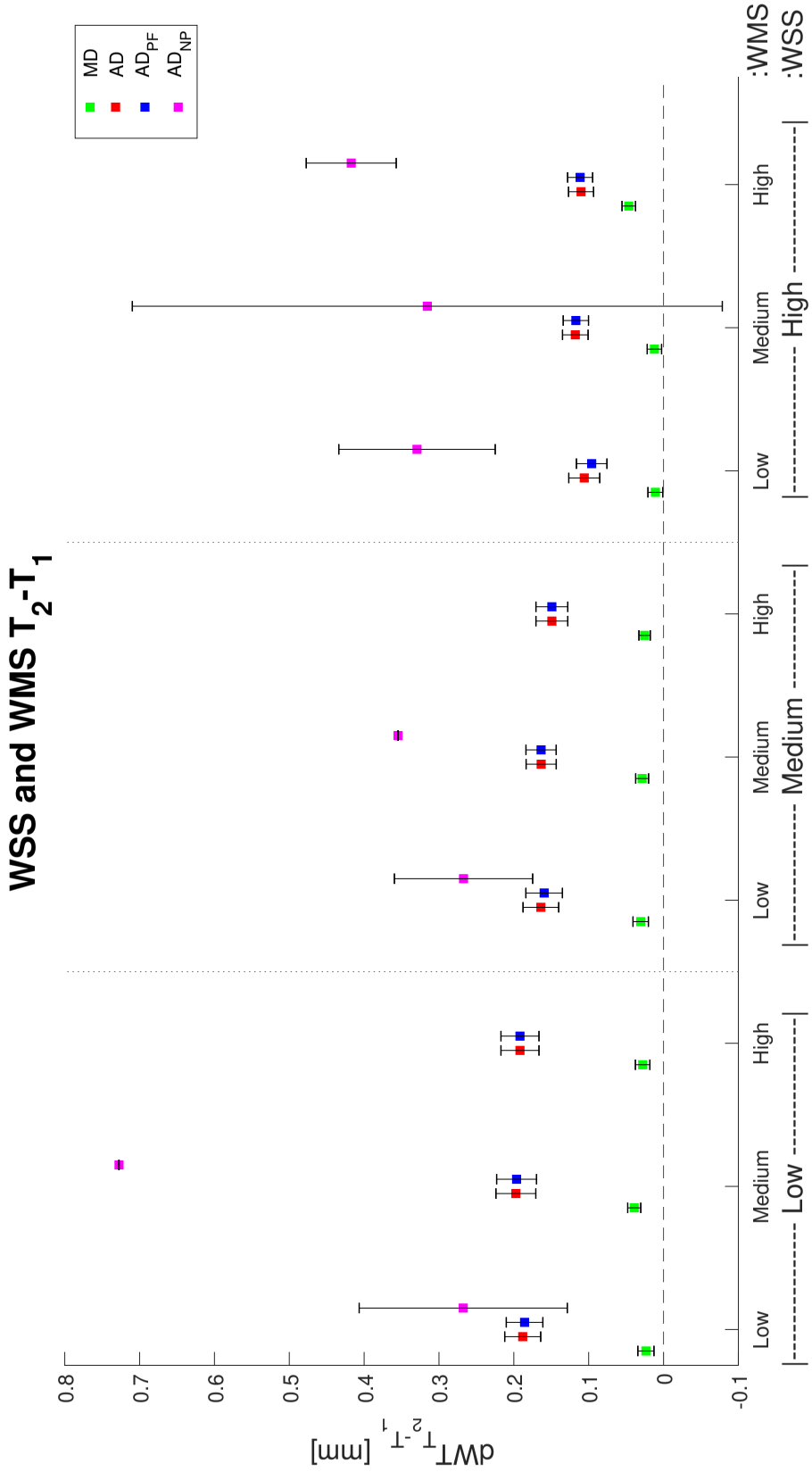

Figure 51: Wall thickness change between T1 to T2 of all categorised sectors according to low, medium and high WSS and WMS at T1. The 95% confidence interval is represented by vertical lines. MD: mildly-diseased; AD: advanced-diseased; PF: plaque-free; NP: plaque without lipid-pool.

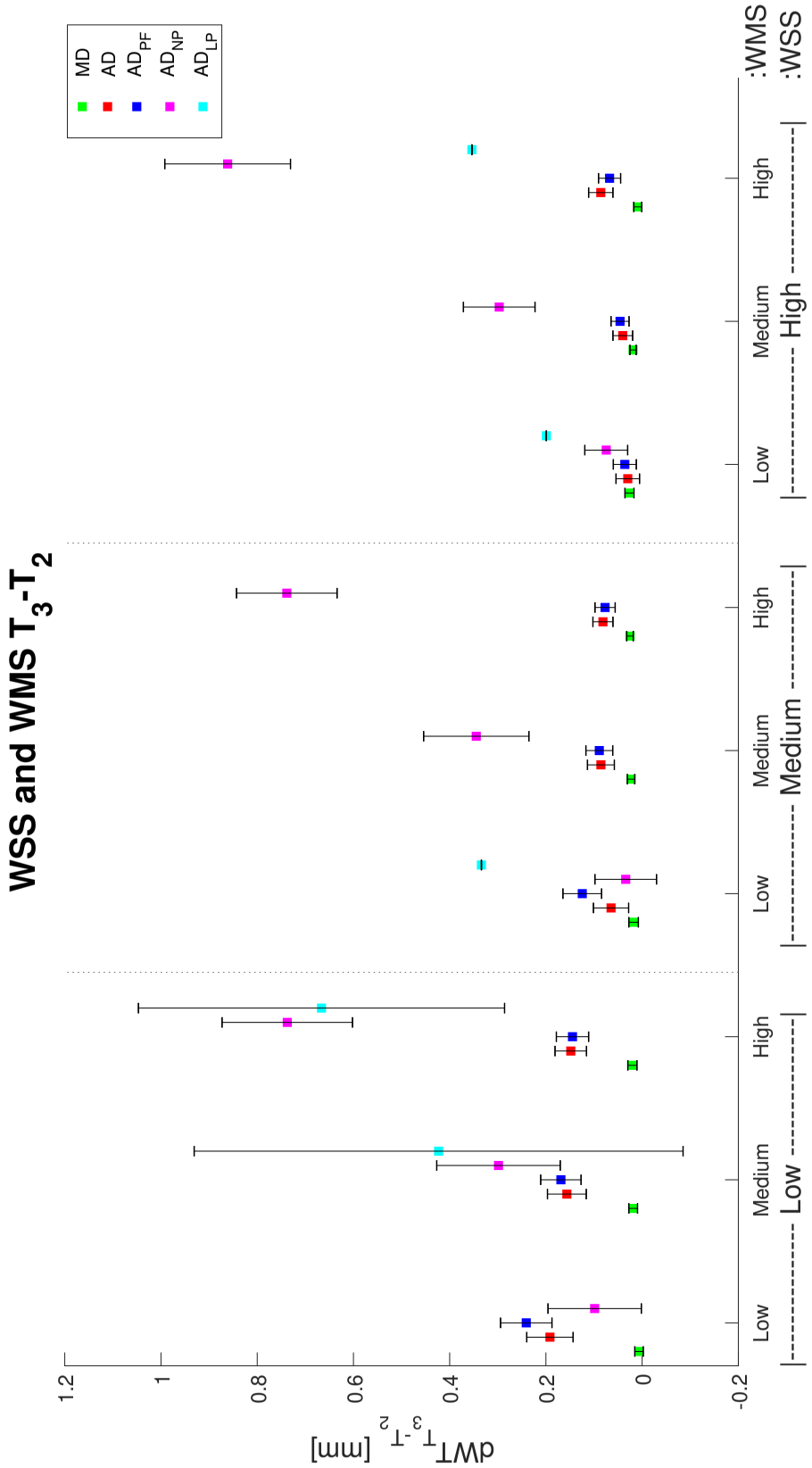

Figure 52: Wall thickness change between T2 to T3 of all categorised sectors according to low, medium and high WSS and WMS at T2. The 95% confidence interval is represented by vertical lines. MD: mildly-diseased; AD: advanced-diseased; PF: plaque-free; NP: plaque without lipid-pool; LP: plaque with lipid-pool.

4 Discussion

In this project, biomechanical arterial wall factors in atherosclerotic coronary arteries were examined by employing IVUS and OCT imaging techniques, with wall thickness as the metric for tracking atherosclerosis progression. Although a small difference in the initiation and progression of atherosclerosis was observed in the MD group, it is ignored for the discussion due to its minimal impact.

4.1 Disease initiation and progression based on morphometrical measurements

After being on a high-fat diet for 9 or 12 months, atherosclerosis development was observed. This observation was also noted in other studies leading to the affirmation that high-fat diet promotes the initiation and progression of the disease [45–47]. Even though the progression in MD pigs was minimal, the growth rate was comparable to that of humans with acute coronary syndrome (median PB increase of 0.93%/year versus 0.34%/year respectively [48]). In the AD group, even though sectors with plaque increased over time, the number of sectors with LP decreased. This observation could be explained by the premature loss of 2 AD pigs which exhibited the majority of LP sectors at T2. Furthermore, the principal limitation of OCT is the incapacity to visualize beyond lipid-rich tissue [49], limitation that could explain the scarcity of sectors with LP presence observed in the entire cohort. This is primarily due to the fact that most LPs had thick caps, with lipid-rich tissue potentially located between these caps and the lumen, shielding their detection by OCT [26, 49]. This progression of atherosclerosis was also evident when examining the wall thickness over the follow-up period, where an increase was observed in both groups. Nevertheless, it may come as a surprise that the average wall thickness seemed to decrease from T1 to T2 in sectors with plaque, whether they had LPs or not, only to experience a substantial increase from T2 to T3. However, it is important to note that at T1, very few sectors had plaque compared to the subsequent time points, making the average wall thickness for sectors with plaque at T1 none reliable for analysis.

Although most sectors either remained in the same condition (healthy or diseased) or progressed on atherosclerosis over time, some sectors experienced regression. Two possible reasons could explain this behaviour: false positive regression induced by errors in the manual co-registration between IVUS and OCT images or real regression in atherosclerosis. For the former reason, manual co-registration could lead to misalignment of sectors between time points, that is, a sector at T1 could not have been precisely aligned with its corresponding sector at T2, for example. So, even if plaque was present in that sector at T1 and at T2, due to the misalignment of sectors, the plaque was reported as not present at T2. For the latter reason, it has been reported that, although it is not the most common occurrence, spontaneous regression can occur in atherosclerosis [50], particularly if the plaque type is intimal xanthoma [51] (the most common type of plaque in this study [26]). In a total of 4.6% of sectors was regression observed, percentage comparable to the one reported in the Bruneck Study, in which 5.2% of lesions regressed [50]. Furthermore, while studying the diameter change of atherosclerotic coronary arteries, Stone et al. [52] reported that after a period of over 2 years 10% of patients experienced spontaneous regression.

It could be seen as contradictory that sectors with plaque but no LP had thicker walls than sectors with LP. Nevertheless, sectors without LP could contain fibrous tissue, calcifications, lipid-rich tissue, cell accumulation [53] or even LPs that were not detected by OCT and, therefore, have thicker walls [54]. Stary et al. [55] reported a rise in the aforementioned components in

severe plaque types. In our study, sectors with plaque lacking LP could pottentially be classified as severe plaques types, as some include these components [26], thus leading to thicker arterial walls.

4.2 Relation of wall stresses with morphometrical measurements

Overall, higher atherosclerosis initiation and progression was observed in sectors exposed to low WSS. This same result was obtained in previous studies; Dhawan et al. [56] observed an inverse correlation between wall thickness and WSS as well as a correlation between low WSS and atherosclerosis progression, and Cibis et al. [57] reported a significant inverse relation between WSS and wall thickness. Analogical to WSS, low WMS could be related to atherosclerosis progression as, on average, wall thickness and PB were highest in sectors exposed to low WMS, while sectors exposed to high WMS had thinner walls and lower PB; same findings as those reported by Costopoulus et al. when analysing the PROSPECT study [58]. Laplace's law states that WMS increases with decreasing wall thickness and increasing luminal radius when arterial pressure remains constant [16]. The wall thickness/luminal radius ratio was obtained per sector to successfully confirm that the obtained results followed this law. When combining WSS and WMS, Costopoulos et al. [14] reported that low WSS with low WMS was the combination generating thicker arterial walls. This statement is in accordance with the results obtained in this study, in which low levels of both stresses seemed to promote atherosclerosis, as thicker walls were observed in areas exposed to those stress levels. In addition, when looking at advanced-diseased pigs, it could be determined that WSS had a greater effect on atherosclerosis initiation and progression than WMS, as when WSS increased the wall thickness decreased independently of WMS levels.

4.3 Relation of wall stresses with morphometrical changes over time

The finding that WSS had an inverse relationship to wall thickness and PB change is consistent with previous studies by Ku et al. [59] and Stone et al. [60], studies which analysed the influence of WSS on carotid and coronary arteries respectively, reporting as results that regions with low WSS exhibited a more pronounced increase in wall thickness over time. As a result, an inverse correlation between WSS magnitude and the development of atherosclerosis was found. Regarding WMS, in this study a positive interaction between WMS and wall thickness and PB change was found, observing a higher increase of wall thickness and PB in regions with higher WMS. In accordance with it, Liu et al. [61], demonstrated that high WMS was associated with increase in plaque volume in coronary arteries and that WMS could predict coronary plaque progression. In addition, Costopoulos et al. [14] studied the influence of biomechanical factors on plaque development, reporting association of high WMS with increase in necrotic core and, therefore, increase in wall thickness. Regarding the combination of WSS and WMS with wall thickness change over time, Costopoulus et al. [14] documented that low WSS was associated with larger increase in PB while high WMS was still associated with larger wall thickness increase. Furthermore, low WSS produced greater increase in PB when combined with low WMS while the smallest increase was observed in regions with high WSS and high WMS. This trend of increased wall thickness in lower WSS levels was also observed in this project; however, the smallest increase was not observed when both stress levels were high but when WSS was high and WMS was low or medium. Costopoulus et al. [14] also reported that WSS had an impact on areas with progression as well as regression, while WMS exclusively affected regions with progression. These findings supported the observation of a higher increase in wall thickness and PB in sectors with plaques as WMS increased, while sectors free of plaques appeared to be less influenced by WMS increase. Moreover, a slightly bigger impact of WMS was perceived on wall

thickness in atherosclerosis progression than in initiation, which aligns with what is reported by Brown et al. [11].

4.4 Limitations and future improvements

When examining the findings, it is important to consider some limitations present in the project. Fist of all, the sample size was limited, which became even smaller when considering only the pigs with advanced atherosclerosis progression. Additional studies with larger sample size are needed to draw more widely applicable conclusions. Secondly, OCT cannot differ LPs from necrotic cores [49], so the advanced stage of the plaque cannot be fully known. Thirdly, in this project only LP component was taken into consideration, excluding sectors with calcifications. Calcium has stiffer material properties that affect the stress calculations and, its addition, could lead to a better understanding of the relation between wall stress and atherosclerosis progression [62]. Moreover, LPs were assumed to be homogeneous with same material properties. However, in reality, LPs consist of a mixture of water, cholesterol monohydrate, cholesterol esters, phospholipids, SMCs and elastic and collagen fibers [63, 64]; composition that could change over time and cause different effects in the biomechanical behaviour of LPs. These changes may result in stiffer or more flexible LPs, altering wall stresses [63]. Fourthly, the study did not include a control group, which would have been of help to confidently determine the relation between atherosclerosis progression and a high-fat diet and wall stresses, as well as to get better understanding of why half of the pigs developed limited atherosclerosis. Lastly, performing statistical analysis would be of interest in order to obtain the association of wall stresses with the analysed morphometrical measurements.

5 Conclusion

The aim of this project is to analyse the biomechanical arterial wall factors in atherosclerotic coronary arteries. It was concluded that (i) atherosclerosis progresses when feeding a high-fat diet and this progression is observed in the increase of arterial wall thickness; (ii) regions with low WSS and low WMS have thicker arterial walls; (iii) regions with low WSS are thought to promote atherosclerosis initiation and progression while regions with high WMS are thought to promote atherosclerosis progression; and (iv) WSS is suggested to have greater impact on atherosclerosis development than WMS.

Appendices

A R-peak detection algorithm

The algorithm to detect the R-peaks in an ECG consisted of 3 stages:

1. Detection of QRS region
    a) The squared double differences were computed across all points from the ECG data array *e(n)*, resulting in the creation of the difference array *d(j)*.

$$d1(j) = e(i+1) - e(i), \quad i = 1, 2, ..., n-1 \tag{4}$$

$$d2(j) = d1(j+1) - d1(j), \quad j = 1, 2, ..., n-2 \tag{5}$$

$$d(j) = [d2(j)]^2 \tag{6}$$

    b) The array of differences *d(j)* was arranged in a descending order based on their magnitudes, and the difference-peaks that exceed a fixed threshold value of 3% of the maximum were selected.
    c) Given that the maximum duration of QRS regions for pigs is 70 ms [65], in order to prevent the potential identification of multiple peaks within the same QRS region, all difference-peaks falling within a range of ±35 ms around each selected difference-peak were removed.
    d) The QRS regions were identified within a time window of ±35 ms around each of the selected peaks in the ECG data array.
2. Detection of R peaks
    a) Within each identified QRS window, the ECG data array's maximum and minimum amplitude values were computed.
    b) The average of these maximum and minimum values was deducted from every data point within that window, obtaining the relative magnitudes.
    c) The maximum position of the relative magnitudes shows the R-peak location for the corresponding QRS window. The absolute highest value within the QRS window was not chosen as the R-peak location to avoid potential S-peak detection.
3. Processing of RR intervals
    a) It is assumed that the minimum time between two consecutive R peaks for pigs is 570 ms. Any peaks detected within a difference less than 570 ms were considered false peaks and were removed. This way, only true positive R-peaks were detected, even if some false negative R-peaks were discarded.
    b) The mean RR interval was established using five consecutive R-peaks, with two on each side of the R-peak associated with the highest difference peak. This average RR interval was taken as the benchmark for RR interval processing.
    c) All succeeding RR intervals underwent processing by comparison with the computed average RR interval.
        i. If the RR interval between any two identified peaks was less than 70% of the average RR interval, the second peak was excluded.

ii. If the RR interval between any two identified peaks exceeded 180% of the average interval, a search for an additional R peak within that interval was initiated, utilizing a lowered threshold for the difference signal.

For the algorithm detecting R-peak from the ECG, the selected QRS and minimum RR interval time were selected from the article by U Paslawska et al. [65].The pigs participating in the study had a mean body weight of 86 kg (58-106 kg) so 70 ms was chosen as QRS interval time, as it can be seen in Table 7.

Body weight (kg)	**Duration of QRS interval (seconds)**
20-29	0.07 ± 0.01
30-39	0.07 ± 0.01
40-49	0.07 ± 0.01
50-59	0.07 ± 0.01
60-69	0.07 ± 0.01
70-79	0.07 ± 0.01
80-89	0.07 ± 0.01
90-99	0.07 ± 0.01
100-109	0.07 ± 0.01
110-119	0.08 ± 0.01
120-129	0.08 ± 0.01
130-139	0.08 ± 0.01
140-149	0.08 ± 0.01
150-159	0.09 ± 0.01

Table 7: Duration of QRS interval of lead II electrocardiograms in healthy domestic swine according to their body weight in 10 kg increments [65]

The minimum RR interval time was selected from the graph shown in Figure 53; the heart rate (HR) was obtained and conversed to RR duration (converse from beats per minute to seconds per beat). It was observed that as the body weight decreased, the HR increased, thus reducing the duration of the RR interval. As for the algorithm only the minimum RR interval time was needed, the HR for the lowest body weight was chosen; corresponding to 105 HR for 58 kg, what resulted in 570 ms of duration.

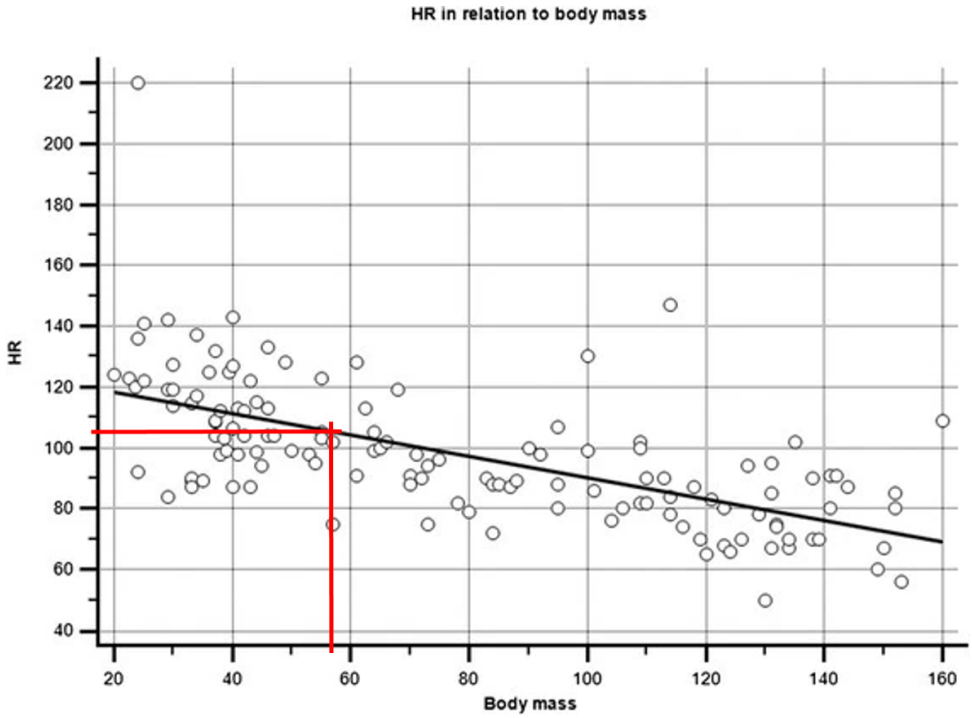

Figure 53: The correlation between heart rate (beats per minute) and body weight (kg) in healthy domestic swine [65]. In red, the lowest body weight and the corresponding HR are shown.

B Stress tertiles

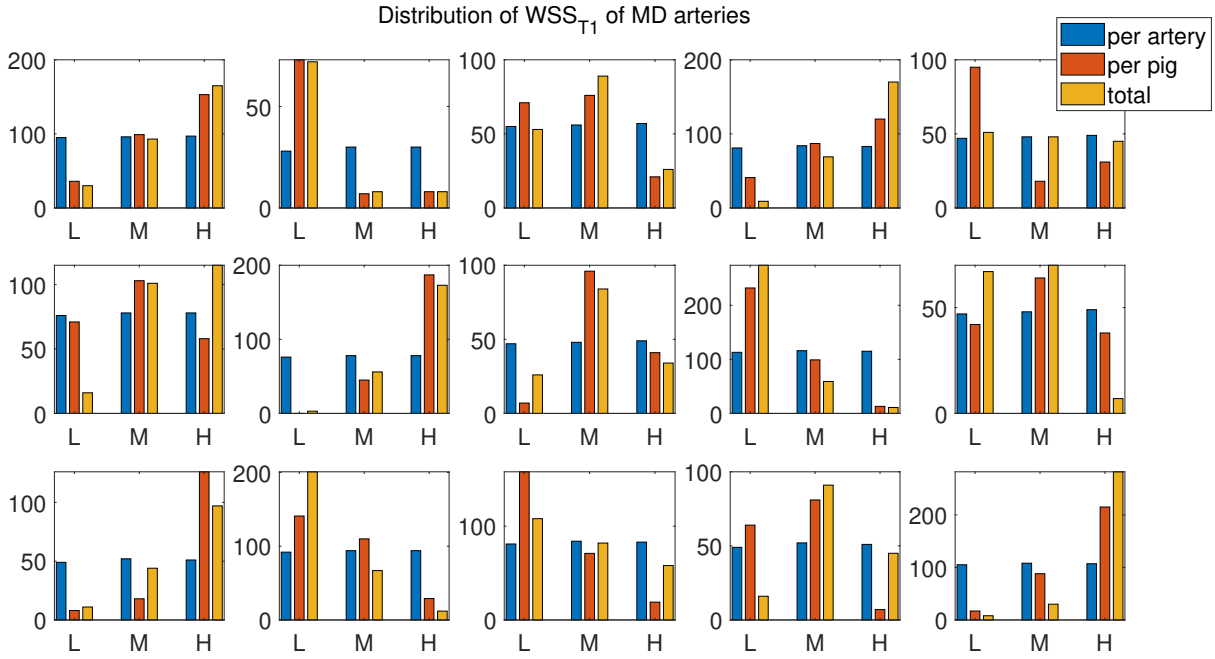

Figure 54: Distribution of baseline wall shear stress in low (L), medium (M) and high (H) tertiles for MD arteries in 3 different types of divisions: per artery, per pig and total. Each graph represents one artery.

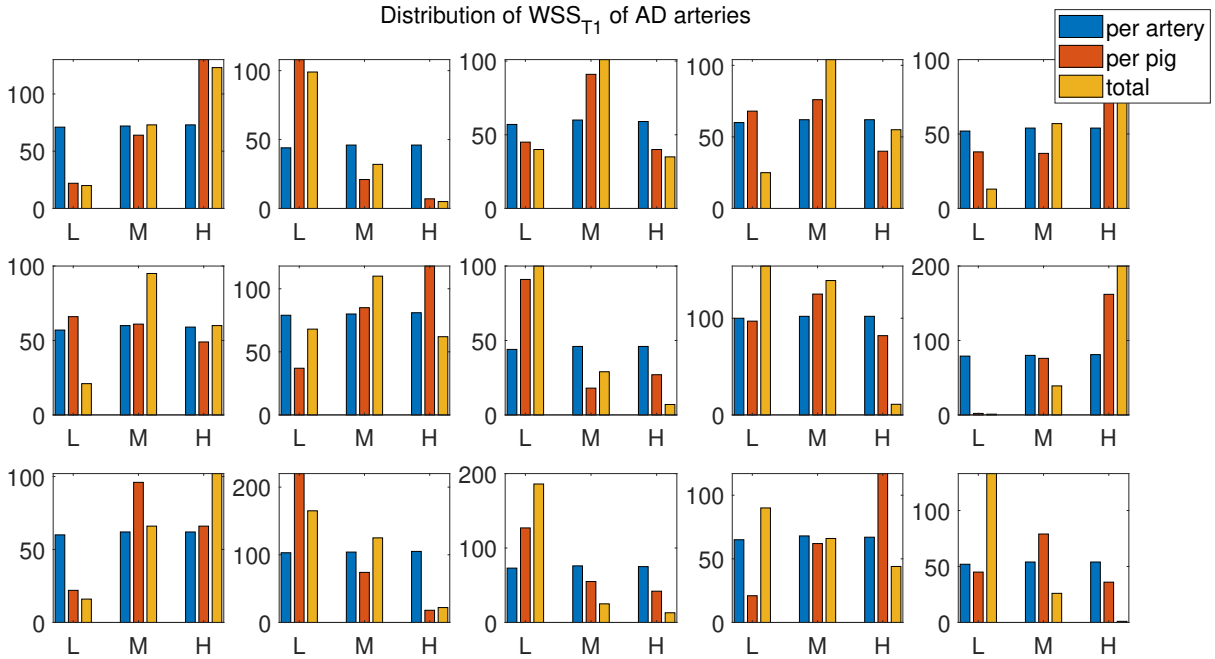

Figure 55: Distribution of baseline wall shear stress in low (L), medium (M) and high (H) tertiles for AD arteries in 3 different types of divisions: per artery, per pig and total. Each graph represents one artery.

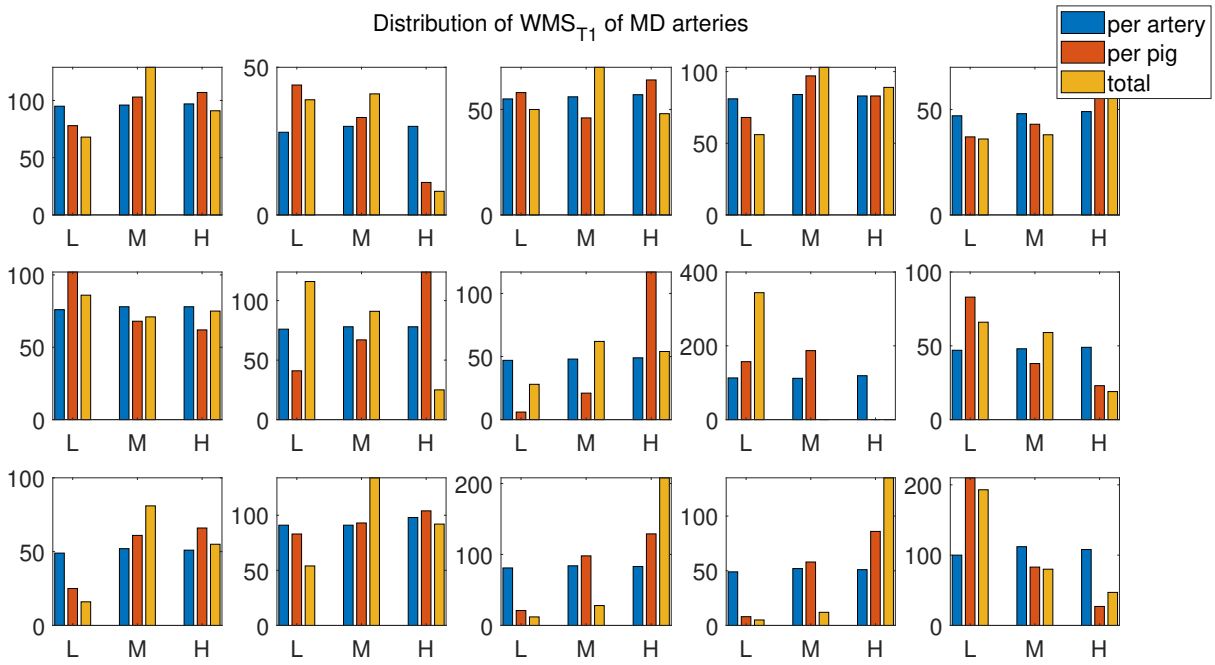

Figure 56: Distribution of baseline wall mechanical stress in low (L), medium (M) and high (H) tertiles for MD arteries in 3 different types of divisions: per artery, per pig and total. Each graph represents one artery.

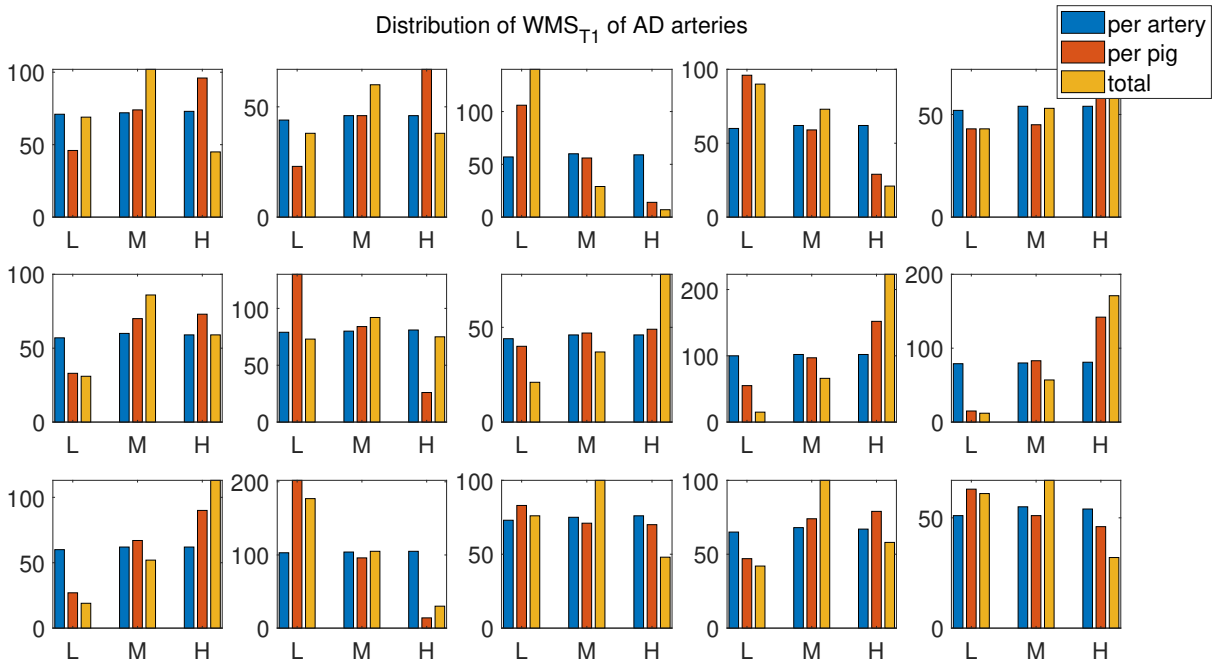

Figure 57: Distribution of baseline wall shear stress in low (L), medium (M) and high (H) tertiles for AD arteries in 3 different types of divisions: per artery, per pig and total. Each graph represents one artery.

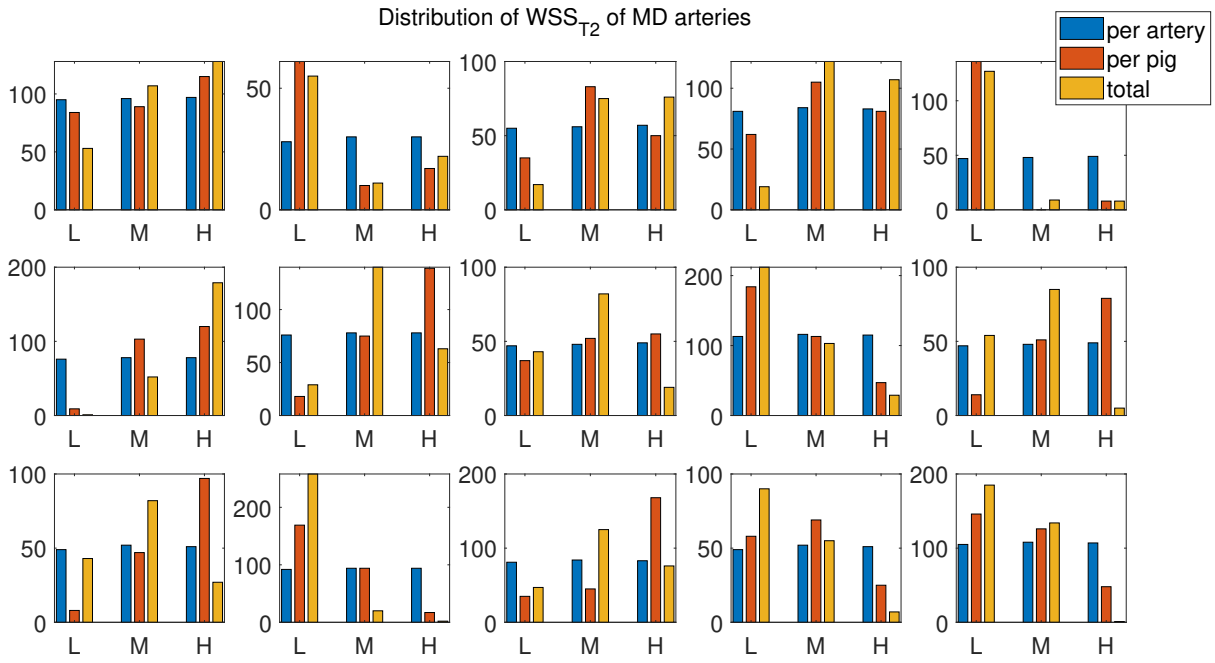

Figure 58: Distribution of T2 wall shear stress in low (L), medium (M) and high (H) tertiles for MD arteries in 3 different types of divisions: per artery, per pig and total. Each graph represents one artery.

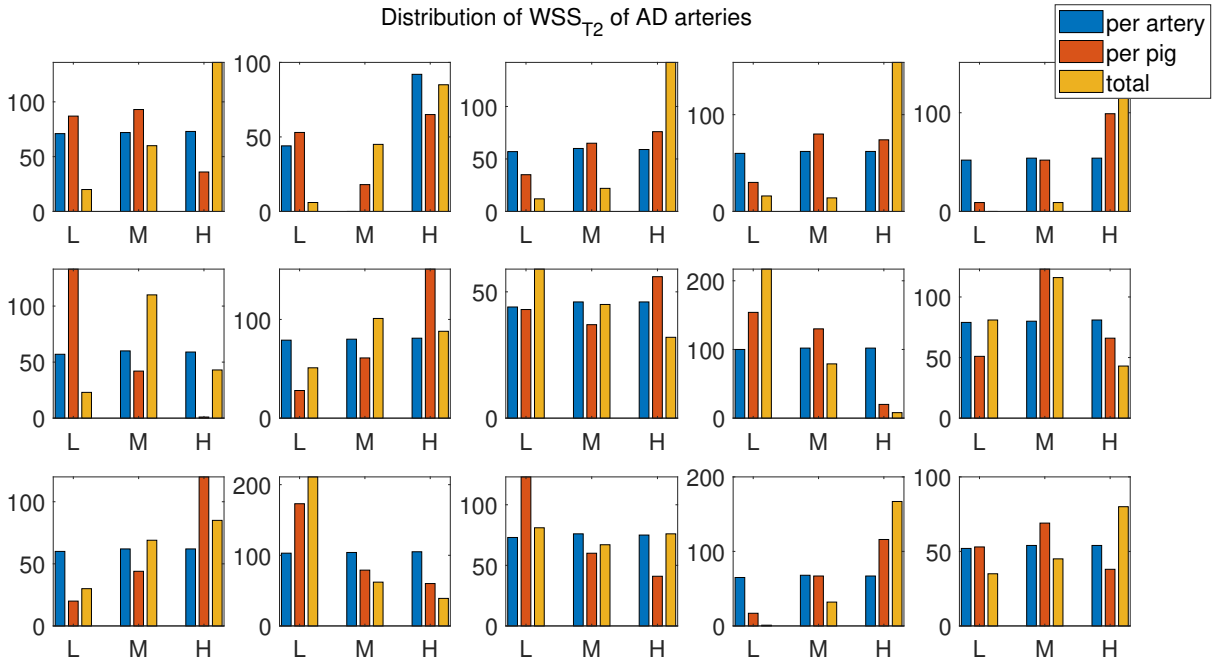

Figure 59: Distribution of T2 wall shear stress in low (L), medium (M) and high (H) tertiles for AD arteries in 3 different types of divisions: per artery, per pig and total. Each graph represents one artery.

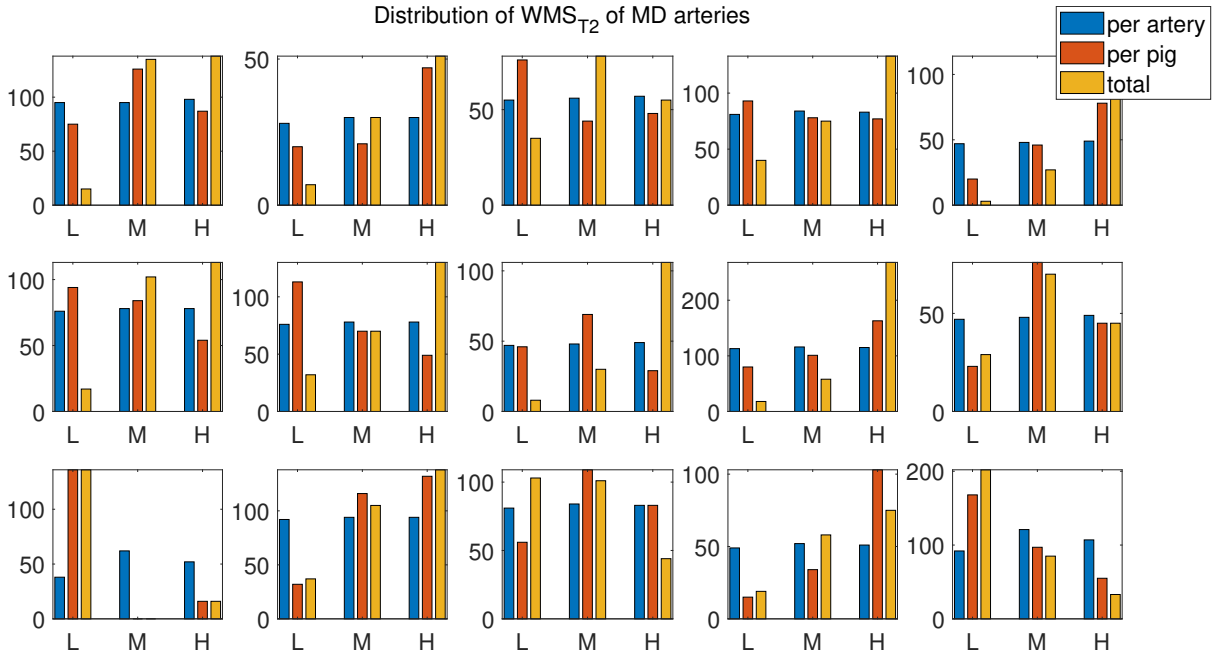

Figure 60: Distribution of T2 wall mechanical stress in low (L), medium (M) and high (H) tertiles for MD arteries in 3 different types of divisions: per artery, per pig and total. Each graph represents one artery.

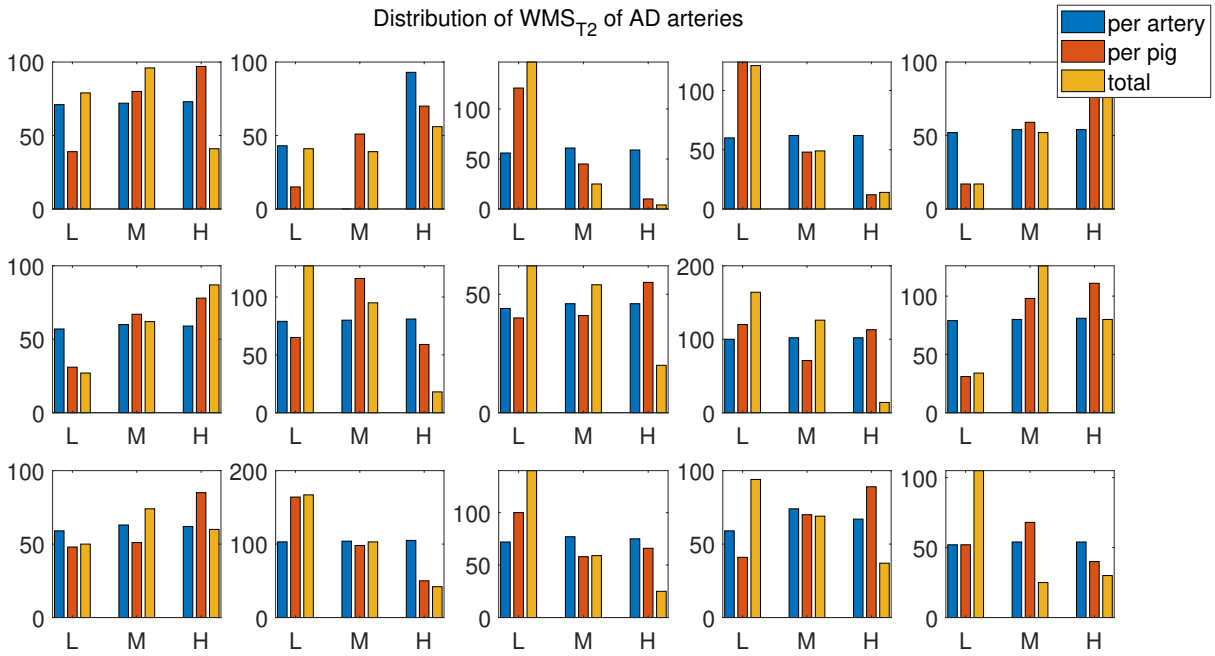

Figure 61: Distribution of T2 wall shear stress in low (L), medium (M) and high (H) tertiles for AD arteries in 3 different types of divisions: per artery, per pig and total. Each graph represents one artery.

	Pig	Artery	T1				T2			
			WSS [Pa]		WMS [kPa]		WSS [Pa]		WMS [kPa]	
			L-M	M-H	L-M	M-H	L-M	M-H	L-M	M-H
MD	4602	LAD	0.9468	1.4192	290.0390	446.6559	0.6039	1.2811	308.5081	408.3902
		LCX	0.3202	0.4849	236.1942	3325.1242	0.4316	0.5486	327.4810	540.6176
		RCA	0.6568	0.8814	264.3204	446.0795	0.6811	0.9507	190.5680	372.0800
	4656	LAD	1.0840	1.5328	304.7704	473.7966	0.6930	0.9873	302.0785	481.6216
		LCX	0.6455	0.8960	353.0715	548.2130	0.2273	0.2985	437.0210	577.0617
		RCA	0.9187	1.2126	245.3746	442.5242	0.9015	1.1780	295.9529	435.5527
	4700	LAD	1.1420	1.4883	197.9056	357.8420	0.5839	0.7924	292.5712	479.5842
		LCX	0.7358	0.9336	335.2826	493.0025	0.5249	0.6297	403.5664	528.4030
		RCA	0.4551	0.5385	137.0700	173.8740	0.4520	0.5211	447.1330	829.1950
	4716	LAD	0.5887	0.7307	231.8849	326.4809	0.4975	0.6025	204.8160	347.9390
		LCX	1.0333	1.6960	347.6526	480.6280	0.5310	0.6444	75.9787	83.7420
		RCA	0.5384	0.6370	312.9964	459.3330	0.3397	0.4044	277.1706	444.1200
	4953	LAD	0.6032	0.8849	693.9759	1022.1057	0.6071	0.8140	145.4500	279.2525
		LCX	0.8456	0.9736	695.4310	1012.8900	0.4617	0.5338	281.1300	437.4387
		RCA	1.5094	2.1831	240.7140	329.3360	0.4434	0.5419	89.1007	169.1264
AD	4609	LAD	0.9615	1.3600	269.8660	403.4830	0.7974	1.1797	145.2558	304.7138
		LCX	0.5526	0.6315	292.3178	442.7617	0.7694	0.9757	139.7378	239.3150
		RCA	0.7318	0.9305	142.3491	227.9010	1.0976	1.8864	60.7829	108.0320
	4684	LAD	0.8217	1.0359	177.8881	329.4350	1.1001	1.6495	96.4093	172.0872
		LCX	0.9292	1.4138	284.2258	535.9541	1.3987	2.0872	283.7060	509.7043
		RCA	0.8256	1.0655	305.4521	461.9612	0.6172	0.7901	281.8680	484.6600
	4945	LAD	0.6878	0.9672	267.3380	442.9600	0.6130	0.8821	128.9637	195.5160
		LCX	0.4317	0.5355	378.5800	667.8920	0.4284	0.6907	116.0779	244.5831
		RCA	0.5525	0.7330	492.5040	769.5195	0.3457	0.4871	95.2621	239.2380
	4961	LAD	1.2653	1.8254	481.2905	775.0980	0.5108	0.6683	229.8710	366.0460
		LCX	0.9643	1.3129	419.4009	685.7040	0.6913	1.0034	177.2605	361.3531
		RCA	0.5358	0.7160	191.4777	288.1110	0.4008	0.5044	136.5400	212.3020
	4977	LAD	0.3991	0.5343	254.8590	403.0790	0.4858	0.8378	58.9070	185.9593
		LCX	0.5927	0.8680	302.8573	437.6743	1.0059	1.3069	117.3180	263.8190
		RCA	0.5014	0.5650	255.7550	390.2049	0.6647	0.9596	86.4201	181.8749

Table 8: Overview of stress threshold levels for each tertile per artery and time point. L-M: low-medium; M-H: medium-high.

C Pig characteristics

	MD pigs			AD pigs		
	T1	**T2**	**T3**	**T1**	**T2**	**T3**
Age [months]	37 (36-42)	43 (42-48)	47 (46-52)	36 (35-54)	42 (41-60)	46 (45-64)
Weight [kg]	86 (69-90)	87 (79-99)	93 (78-106)	77 (58-105)	92 (68-106)	93 (68-106)
Cholesterol [mmol/L]	12.8 (9.6-17.1)	10.7 (9.2-12.4)	8.8 (7.8-10.9)	11 (8.6-13)	11 (10-23.5)	9.1 (8.5-21)
LDL-C [mmol/L]	10.7 (7.6-14.3)	8.4 (6.7-10.7)	6.5 (5.8-9.3)	9.1 (7.1-28.6)	8.9 (8.1-20.5)	7.6 (6.7-20.7)
HDL-C [mmol/L]	2.7 (2.5-4.6)	2.5 (2.4-5)	2.6 (2.2-5.1)	2.6 (1.9-4.35)	3.3 (2.3-4.5)	3 (2.9-3.2)

Table 9: General pig characteristics with values expressed as median, being the range between brackets. Data obtained from [26][Supplemental material].

D Category of sectors per pig at each time point and their category change

D.1 Mildly-diseased pigs

Pig 4602

	T1	T2	T3
Healthy (%)	536 (100)	536 (100)	533 (99.44)
Plaque no LP (%)	0 (0)	0 (0)	2 (0.37)
Plaque with LP (%)	0 (0)	0 (0)	1 (0.19)

Table 10: Number and percentage of sectors of pig 4602 at the 3 time points that were healthy, had plaque without lipid-pool and had plaque with lipid-pool.

		T2		
		Healthy	**Plaque no LP**	**Plaque with LP**
T1	**Healthy**	536	0	0
	Plaque no LP	0	0	0
	Plaque with LP	0	0	0

(a) Number of sectors of pig 4602 that changed categories between T1 and T2.

		T3		
		Healthy	**Plaque no LP**	**Plaque with LP**
T2	**Healthy**	533	2	1
	Plaque no LP	0	0	0
	Plaque with LP	0	0	0

(b) Number of sectors of pig 4602 that changed categories between T2 and T3.

Table 11: Sectors of pig 4602 in each category from one time point to its following.

Pig 4656

	T1	T2	T3
Healthy (%)	619 (99.84)	620 (100)	618 (99.68)
Plaque no LP (%)	1 (0.16)	0 (0)	2 (0.32)
Plaque with LP (%)	0 (0)	0 (0)	0 (0)

Table 12: Number and percentage of sectors of pig 4656 at the 3 time points that were healthy, had plaque without lipid-pool and had plaque with lipid-pool.

		T2		
		Healthy	Plaque no LP	Plaque with LP
T1	Healthy	619	0	0
	Plaque no LP	1	0	0
	Plaque with LP	0	0	0

(a) Number of sectors of pig 4656 that changed categories between T1 and T2.

		T3		
		Healthy	Plaque no LP	Plaque with LP
T2	Healthy	618	2	0
	Plaque no LP	0	0	0
	Plaque with LP	0	0	0

(b) Number of sectors of pig 4656 that changed categories between T2 and T3.

Table 13: Sectors of pig 4656 in each category from one time point to its following.

Pig 4700

	T1	T2	T3
Healthy (%)	720 (100)	720 (100)	719 (99.86)
Plaque no LP (%)	0 (0)	0 (0)	1 (0.14)
Plaque with LP (%)	0 (0)	0 (0)	0 (0)

Table 14: Number and percentage of sectors of pig 4700 at the 3 time points that were healthy, had plaque without lipid-pool and had plaque with lipid-pool.

		T2		
		Healthy	Plaque no LP	Plaque with LP
T1	Healthy	720	0	0
	Plaque no LP	0	0	0
	Plaque with LP	0	0	0

(a) Number of sectors of pig 4700 that changed categories between T1 and T2.

		T3		
		Healthy	Plaque no LP	Plaque with LP
T2	Healthy	719	1	0
	Plaque no LP	0	0	0
	Plaque with LP	0	0	0

(b) Number of sectors of pig 4700 that changed categories between T2 and T3.

Table 15: Sectors of pig 4700 in each category from one time point to its following.

Pig 4716

	T1	T2	T3
Healthy (%)	575 (99.83)	576 (100)	576 (100)
Plaque no LP (%)	1 (0.17)	0 (0)	0 (0)
Plaque with LP (%)	0 (0)	0 (0)	0 (0)

Table 16: Number and percentage of sectors of pig 4716 at the 3 time points that were healthy, had plaque without lipid-pool and had plaque with lipid-pool.

		T2		
		Healthy	Plaque no LP	Plaque with LP
T1	Healthy	575	0	0
	Plaque no LP	1	0	0
	Plaque with LP	0	0	0

(a) Number of sectors of pig 4716 that changed categories between T1 and T2.

		T3		
		Healthy	Plaque no LP	Plaque with LP
T2	Healthy	576	0	0
	Plaque no LP	0	0	0
	Plaque with LP	0	0	0

(b) Number of sectors of pig 4716 that changed categories between T2 and T3.

Table 17: Sectors of pig 4716 in each category from one time point to its following.

Pig 4953

	T1	T2	T3
Healthy (%)	720 (100)	720 (100)	715 (99.3)
Plaque no LP (%)	0 (0)	0 (0)	5 (0.7)
Plaque with LP (%)	0 (0)	0 (0)	0 (0)

Table 18: Number and percentage of sectors of pig 4953 at the 3 time points that were healthy, had plaque without lipid-pool and had plaque with lipid-pool.

		T2		
		Healthy	Plaque no LP	Plaque with LP
T1	Healthy	720	0	0
	Plaque no LP	0	0	0
	Plaque with LP	0	0	0

(a) Number of sectors of pig 4953 that changed categories between T1 and T2.

		T3		
		Healthy	Plaque no LP	Plaque with LP
T2	Healthy	715	5	0
	Plaque no LP	0	0	0
	Plaque with LP	0	0	0

(b) Number of sectors of pig 4953 that changed categories between T2 and T3.

Table 19: Sectors of pig 4953 in each category from one time point to its following.

D.2 Advanced-diseased pigs

Pig 4609

Pig died after T2.

	T1	T2
Healthy (%)	517 (97.92)	396 (75)
Plaque no LP (%)	11 (2.08)	113 (21.4)
Plaque with LP (%)	0 (0)	19 (3.6)

Table 20: Number and percentage of sectors of pig 4609 at the 3 time points that were healthy, had plaque without lipid-pool and had plaque with lipid-pool.

		T2		
		Healthy	**Plaque no LP**	**Plaque with LP**
T1	**Healthy**	396	102	19
	Plaque no LP	0	11	0
	Plaque with LP	0	0	0

Table 21: Number of sectors of pig 4609 that changed categories between T1 and T2.

Pig 4684

Pig died after T2.

	T1	**T2**
Healthy (%)	495 (95.56)	389 (75.1)
Plaque no LP (%)	21 (4.05)	124 (23.94)
Plaque with LP (%)	2 (0.39)	5 (0.96)

Table 22: Number and percentage of sectors of pig 4684 at the 3 time points that were healthy, had plaque without lipid-pool and had plaque with lipid-pool.

		T2		
		Healthy	**Plaque no LP**	**Plaque with LP**
T1	**Healthy**	389	104	2
	Plaque no LP	0	19	2
	Plaque with LP	0	1	1

Table 23: Number of sectors of pig 4684 that changed categories between T1 and T2.

Pig 4945

	T1	T2	T3
Healthy (%)	680 (100)	599 (88.09)	462 (67.94)
Plaque no LP (%)	0 (0)	80 (11.76)	218 (32.06)
Plaque with LP (%)	0 (0)	1 (0.15)	0 (0)

Table 24: Number and percentage of sectors of pig 4945 at the 3 time points that were healthy, had plaque without lipid-pool and had plaque with lipid-pool.

		T2		
		Healthy	**Plaque no LP**	**Plaque with LP**
T1	**Healthy**	599	80	1
	Plaque no LP	0	0	0
	Plaque with LP	0	0	0

(a) Number of sectors of pig 4945 that changed categories between T1 and T2.

		T3		
		Healthy	**Plaque no LP**	**Plaque with LP**
T2	**Healthy**	459	140	0
	Plaque no LP	3	77	0
	Plaque with LP	0	1	0

(b) Number of sectors of pig 4945 that changed categories between T2 and T3.

Table 25: Sectors of pig 4945 in each category from one time point to its following.

Pig 4961

	T1	T2	T3
Healthy (%)	726 (98.64)	577 (78.4)	461 (62.63)
Plaque no LP (%)	10 (1.36)	157 (21.33)	269 (36.55)
Plaque with LP (%)	0 (0)	2 (0.27)	6 (0.82)

Table 26: Number and percentage of sectors of pig 4961 at the 3 time points that were healthy, had plaque without lipid-pool and had plaque with lipid-pool.

		T2		
		Healthy	**Plaque no LP**	**Plaque with LP**
T1	**Healthy**	575	149	2
	Plaque no LP	2	8	0
	Plaque with LP	0	0	0

(a) Number of sectors of pig 4961 that changed categories between T1 and T2.

		T3		
		Healthy	**Plaque no LP**	**Plaque with LP**
T2	**Healthy**	425	149	3
	Plaque no LP	34	120	3
	Plaque with LP	2	0	0

(b) Number of sectors of pig 4961 that changed categories between T2 and T3.

Table 27: Sectors of pig 4961 in each category from one time point to its following.

Pig 4977

	T1	T2	T3
Healthy (%)	572 (99.83)	406 (70.85)	400 (69.8)
Plaque no LP (%)	1 (0.17)	161 (28.1)	168 (29.32)
Plaque with LP (%)	0 (0)	6 (1.05)	5 (0.88)

Table 28: Number and percentage of sectors of pig 4977 at the 3 time points that were healthy, had plaque without lipid-pool and had plaque with lipid-pool.

		T2		
		Healthy	**Plaque no LP**	**Plaque with LP**
T1	**Healthy**	405	161	6
	Plaque no LP	1	0	0
	Plaque with LP	0	0	0

(a) Number of sectors of pig 4977 that changed categories between T1 and T2.

		T3		
		Healthy	**Plaque no LP**	**Plaque with LP**
T2	**Healthy**	351	53	2
	Plaque no LP	49	110	2
	Plaque with LP	0	5	1

(b) Number of sectors of pig 4977 that changed categories between T2 and T3.

Table 29: Sectors of pig 4977 in each category from one time point to its following.

E Plaque burden analysis

E.1 Wall stresses and morphometrical measurements

E.1.1 Wall Shear Stress

Mildly-diseased pigs

In Figure 62 the relationship between PB with WSS for MD pigs is depicted. PB decreased as WSS increased, that is, in regions with low WSS, PB was greater whereas regions with high WSS had lower PB. The same behaviour was observed at the three time points, in all cases having at T3 greatest PB, and at T2 lowest. Nevertheless, for the case of high WSS at T1, PB increased 1% with respect to medium WSS at T1. On average, PB experienced a greater reduce from low to medium WSS than the one experienced from medium to high WSS (1.7% vs. 1.03%).

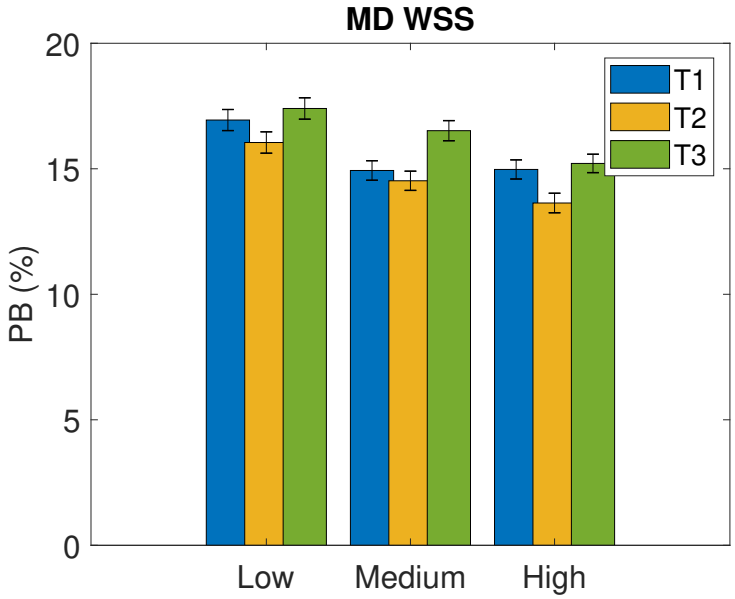

Figure 62: Plaque burden of MD pigs and low, medium and high WSS at each time point. The 95% confidence interval is represented by vertical lines.

Advanced-diseased pigs The interaction of PB with WSS for AD pigs can be observed in Figure 63. At every time point, a reduction of PB was observed as WSS increased for all cases with the exception of PB at T2, where it increased 1.68% as WSS increased. A significant difference of PB was noted between T1 and T2 or T3, being walls with higher PB at T2 or T3 when comparing with T1, and being higher at T3 when comparing T2 and T3. The reduction rate for PB between tertiles was lowest at T1 while, at T2, an increase of similar rate was observed (1% of reduction and increase respectively).

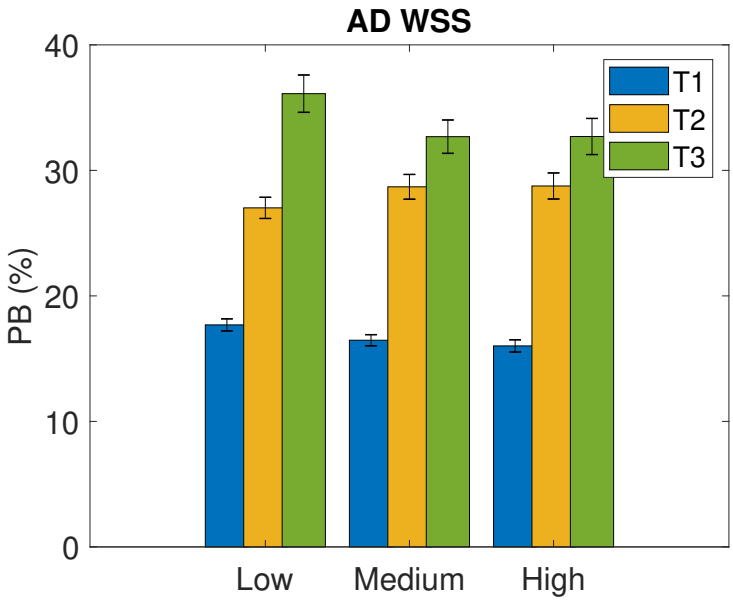

Figure 63: Plaque burden of AD pigs and low, medium and high WSS at each time point. The 95% confidence interval is represented by vertical lines.

Sectors belonging to AD pigs were classified as plaque-free, diseased without LP and diseased with LP. In the following paragraphs, the results of each category are presented independently.

Regarding plaque-free sectors belonging to AD pigs, a progressive decrease in PB was observed as WSS increased (see Figure 64). PB was lowest at T1 and highest at T3. The reduction rate was consistent between WSS tertiles, observing a reduction of 1% between WSS levels.

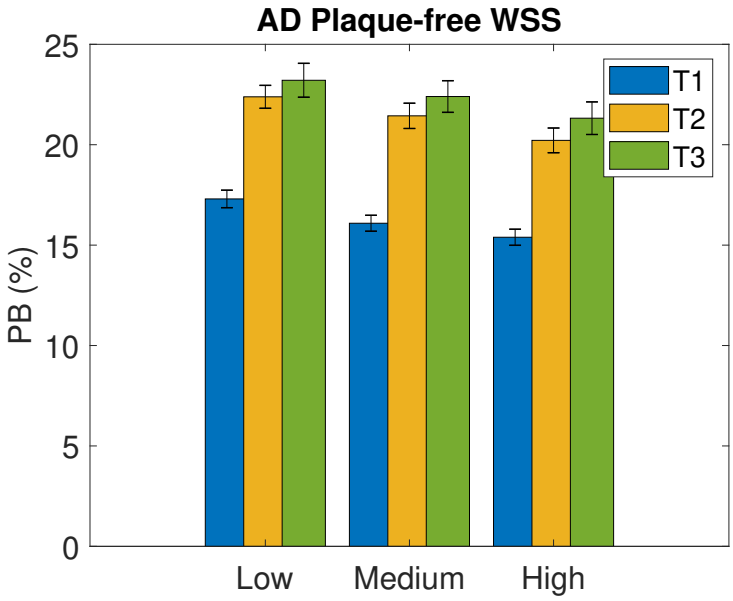

Figure 64: Plaque burden of plaque-free sectors belonging to AD pigs and low, medium and high WSS at each time point. The 95% confidence interval is represented by vertical lines.

Figure 65 shows the relation of sectors with plaque but no lipid-pool between PB and WSS. On average, PB remained constant as WSS increased at T1 and T2 (47% and 52% respectively) whereas it decreased 3% at T3. Over time PB increased in all WSS levels, experiencing the greatest increase in sectors with low WSS (6% increase).

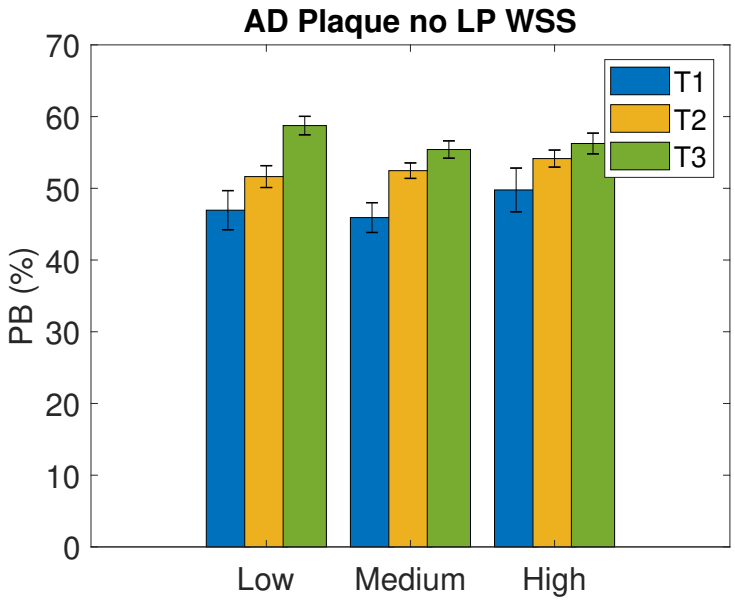

Figure 65: Plaque burden of sectors with plaque but no lipid-pool belonging to AD pigs and low, medium and high WSS at each time point. The 95% confidence interval is represented by vertical lines.

In Figure 66, the interaction of WSS on PB for diseased sectors with LP is visualized. PB experienced a greater increase in sectors exposed to medium WSS than sectors exposed to low WSS (increase of 13%). This increase was subsequently reduced 7% in sectors with high WSS. PB values at T3 were higher than at T2, maintaining the difference in the three WSS levels (4% difference). Data from T1 was ignored due to few or none presence of sectors that had plaque with LP.

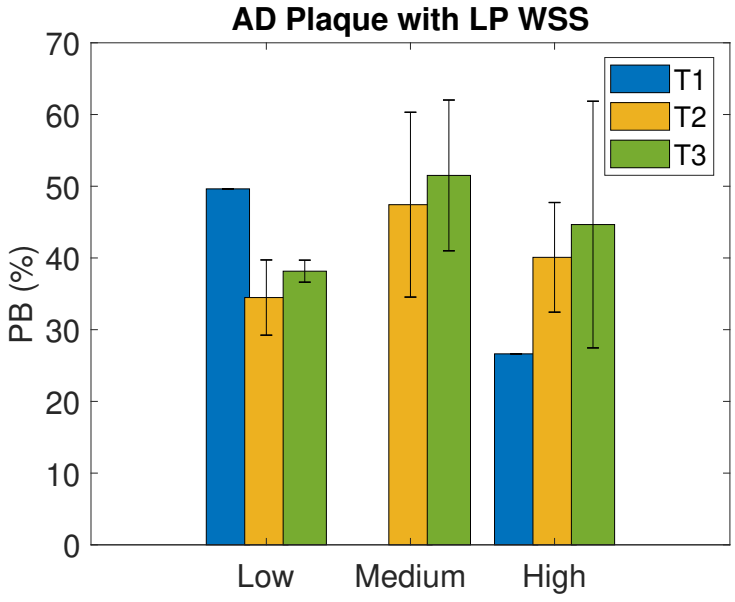

Figure 66: Plaque burden of sectors with plaque with lipid-pool belonging to AD pigs and low, medium and high WSS at each time point. The 95% confidence interval is represented by vertical lines.

E.1.2 Wall Mechanical Stress

Mildly-diseased pigs

PB experienced a reduction of 3% as WMS increased from low to medium, that is, sectors exposed to low WMS had higher PB than sectors with medium WMS (see Figure 67). PB had the highest values at T3 while the lowest values were observed at T2.

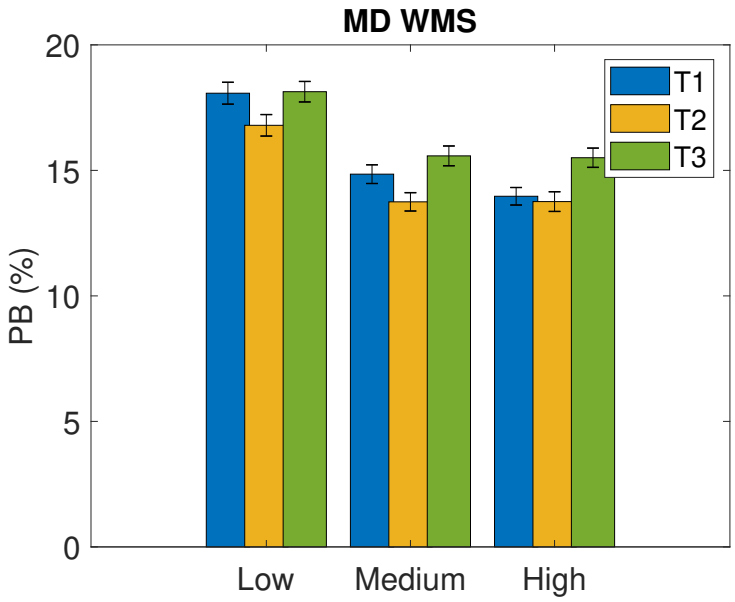

Figure 67: Plaque burden of MD pigs and low, medium and high WMS at each time point. The 95% confidence interval is represented by vertical lines.

Advanced-diseased pigs

The interaction of WMS on PB for AD is displayed in Figure 68. A significant increase in PB was observed at T2 and T3 in comparison with T1. Moreover, at T3 the metric had greater values than at T2. A reduction of PB was observed at all time points, being the reduction higher at T2 and T3 than at T1 (reduction of 8% at T2 and T3 vs. reduction of 3% at T1).

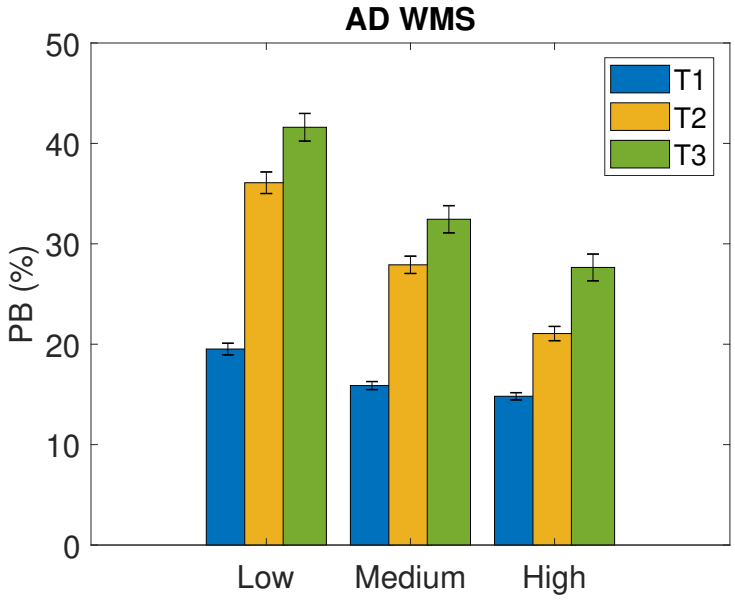

Figure 68: Plaque burden of AD pigs and low, medium and high WMS at each time point. The 95% confidence interval is represented by vertical lines.

Same as before, sectors belonging to AD pigs were classified as plaque-free, diseased without LP and diseased with LP; and the results of each category were independently analysed.

In Figure 69, the interaction of WMS on PB for plaque-free sectors belonging to AD pigs is visualized. The metric had the lowest values at T1 and highest at T3 and the reduction rate was consistent between WMS tertiles. A reduction of 4% was observed between low and mid WMS whereas between mid and high WMS a reduction of 2% was observed.

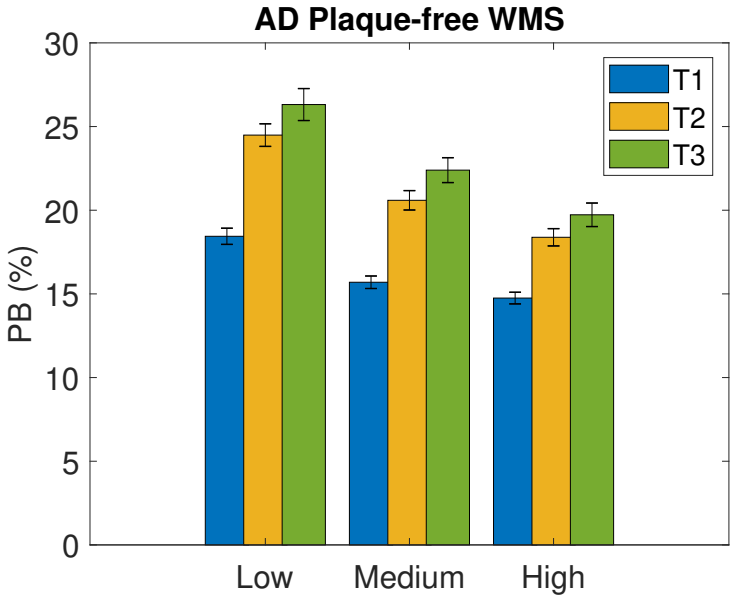

Figure 69: Plaque burden of plaque-free sectors belonging to AD pigs and low, medium and high WMS at each time point. The 95% confidence interval is represented by vertical lines.

The relationship of PB of diseased sectors without lipid-pool can be seen in Figure 70. At T1, the lowest PB was observed no matter the WMS level with the exception of sectors exposed to medium WMS, where PB was 4% higher than at T2. The metric experienced a slight increase of 4% when WMS level increased from low to medium at T1 to decrease 4% when high WMS level was reached. On the contrary, PB experienced a decrease of 4% when WMS level increased from low to medium at T2. In the remaining cases, PB stayed stable independently of WMS level.

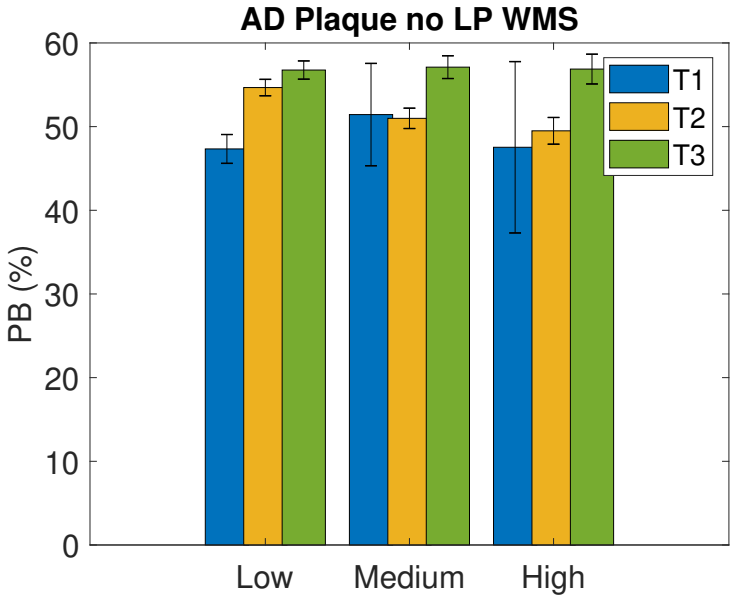

Figure 70: Plaque burden of sectors with plaque but no lipid-pool belonging to AD pigs and low, medium and high WMS at each time point. The 95% confidence interval is represented by vertical lines.

In Figure 71 the interaction between PB with WMS for diseased sectors with LP belonging to AD pigs is depicted. A decrease of PB was observed at every time point as WMS increased. Sectors with medium and high WMS had higher PB at T3 than at T2 whereas sectors with low WMS had higher PB at T2. Data from T1 was ignored due to the fact that there were very few or none sectors with LP at T1.

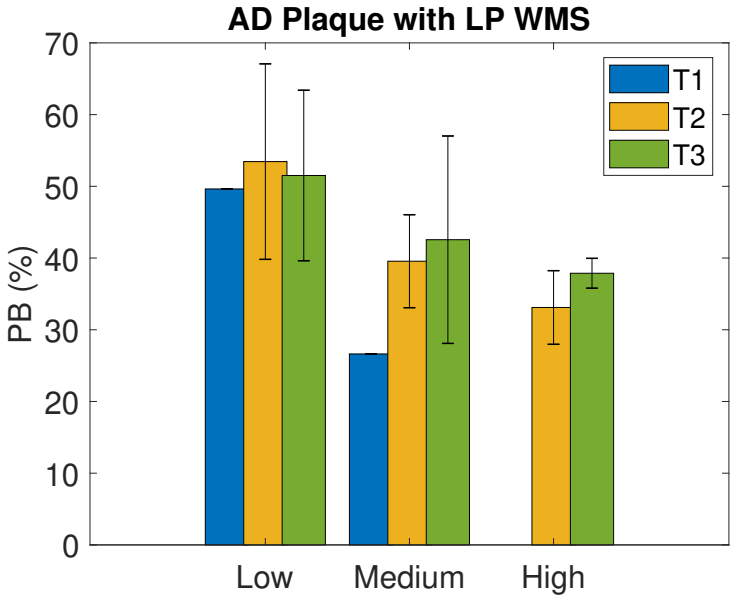

Figure 71: Plaque burden of sectors with plaque with lipid-pool belonging to AD pigs and low, medium and high WMS at each time point. The 95% confidence interval is represented by vertical lines.

E.1.3 Combination of WSS and WMS

The relationship between PB and WSS and WMS at each time point can be found in Figure 72, Figure 73 and Figure 74.

Mildly-diseased pigs

At all time points, PB remained stable independently of WSS level, noticing a 2% higher PB in sectors exposed to low WMS.

Advanced-diseased pigs

A reduction in PB was observed as WMS increased, although no difference was noted with WSS increase. In addition, PB increased over time, having an average PB of 17.1% at T1, 27.8% at T2 and 35.8% at T3. Analogously as for WSS and WMS, sectors belonging to AD pigs were classified as plaque-free, diseased without LP and diseased with LP; and the connection of both stresses with wall thickness was analysed independently. PB decreased as WMS increased independently of WSS. At T1, PB remained at all stress levels under 20% while, at T2, only sectors exposed to high WMS had PB<20% and at T3 no sectors had PB lower than 20%, being the minimum PB 20.6% in sectors under high WSS and high WMS. Regarding sectors with plaque but no LP, no sectors with high WMS and low or medium WSS were present at T1. Nonetheless, PB stayed stable around 53% at the 3 time points regardless of stress levels, even though a tendency to decrease could be observed as WMS increased. Sectors with LP at T1 were ignored due to very few or none present sectors. In contrast to the other categories, PB of sectors with LP increased as WSS increased from low to high, both at T2 and at T3. Sectors exposed to medium WSS exhibited the highest PB, regardless of their WMS level. Nevertheless, the previously observed trend of decreasing PB as WMS increased remained evident.

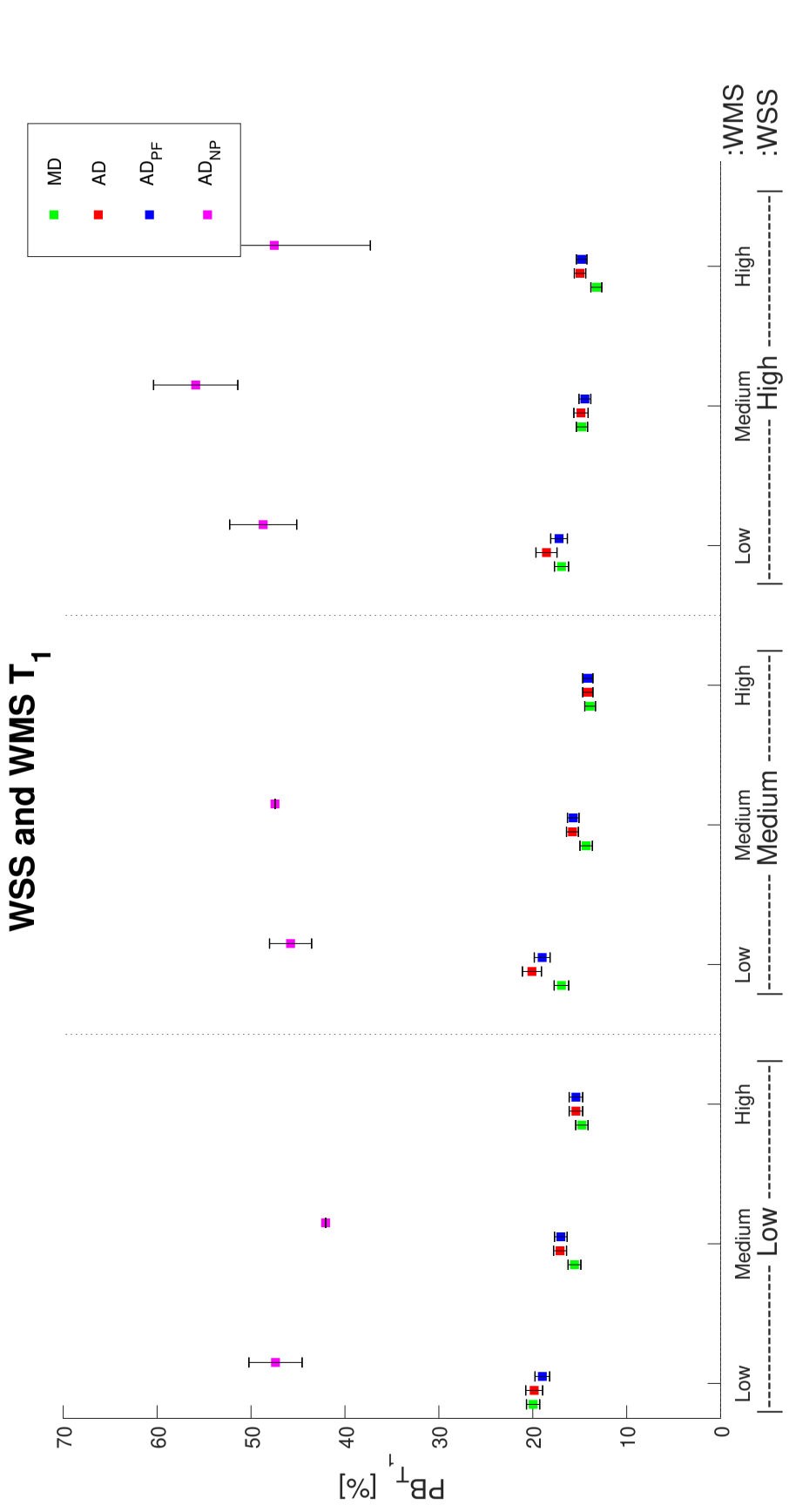

Figure 72: Plaque burden at T1 of all categorised sectors according to low, medium and high WSS and WMS. The 95% confidence interval is represented by vertical lines. MD: mildly-diseased; AD: advanced-diseased; PF: plaque-free; NP: plaque without lipid-pool.

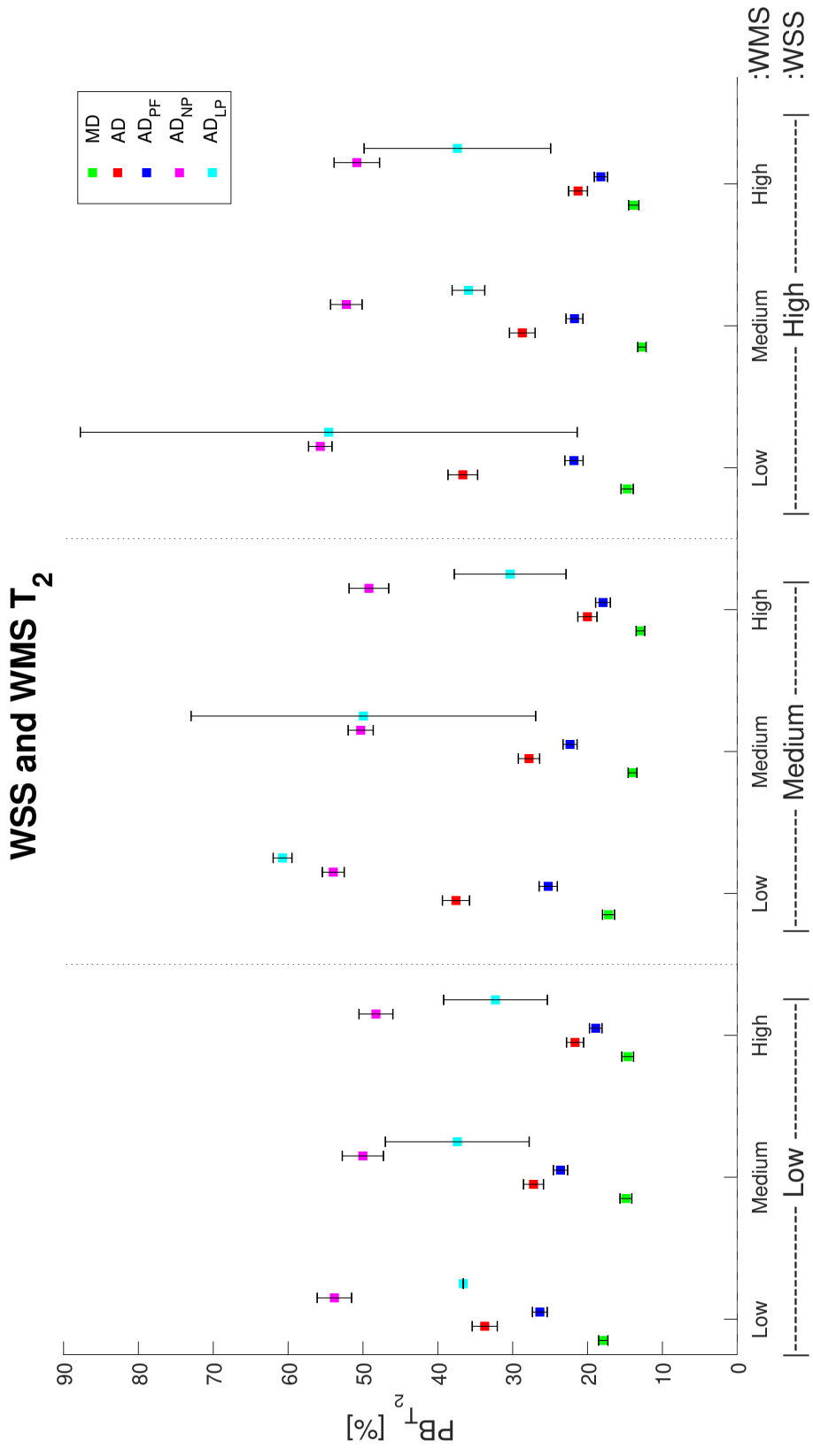

Figure 73: Plaque burden at T2 of all categorised sectors according to low, medium and high WSS and WMS. The 95% confidence interval is represented by vertical lines. MD: mildly-diseased; AD: advanced-diseased; PF: plaque-free; NP: plaque without lipid-pool; LP: plaque with lipid-pool.

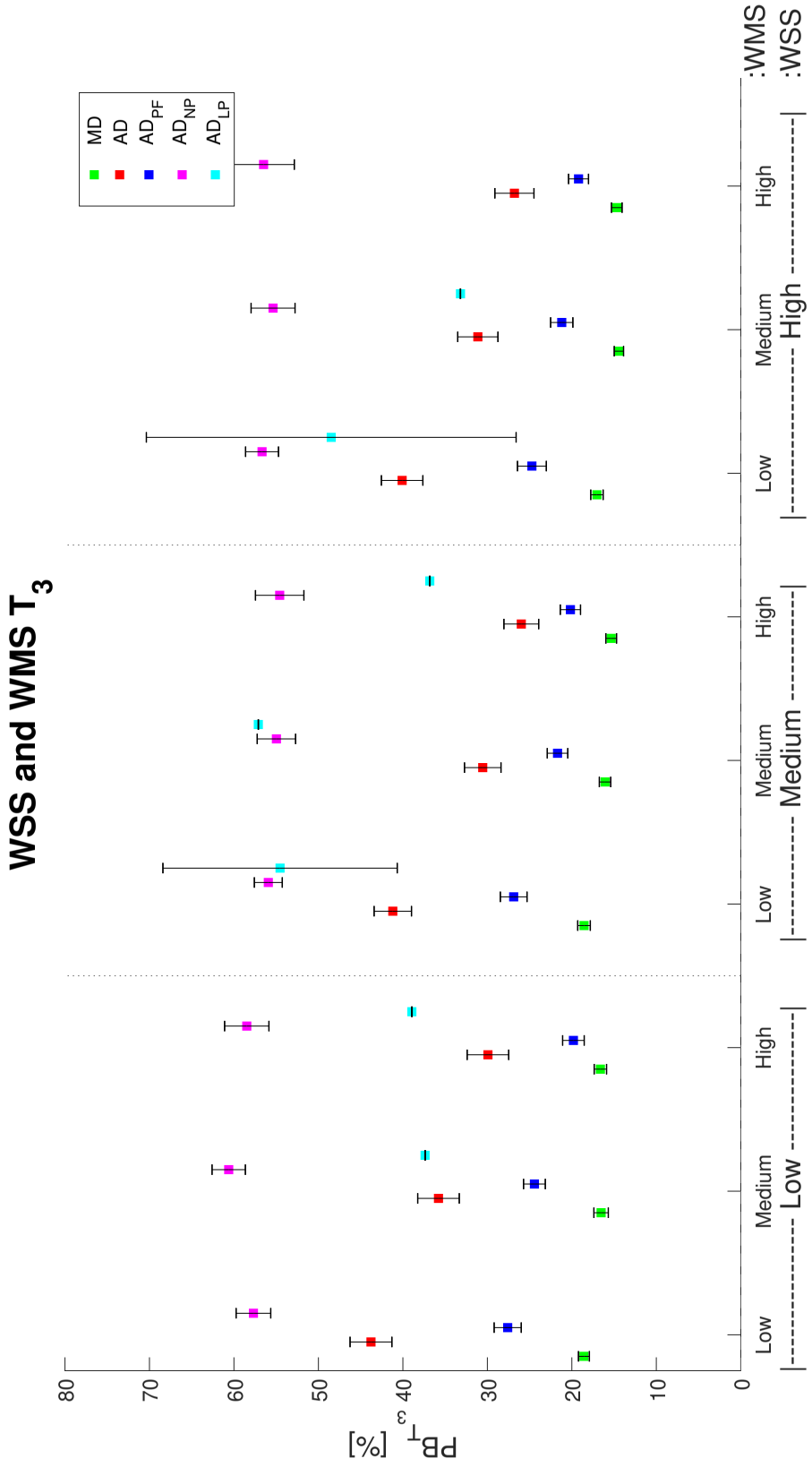

Figure 74: Plaque burden at T3 of all categorised sectors according to low, medium and high WSS and WMS. The 95% confidence interval is represented by vertical lines. MD: mildly-diseased; AD: advanced-diseased; PF: plaque-free; NP: plaque without lipid-pool; LP: plaque with lipid-pool.

E.2 Wall stresses and morphometrical change over time

E.2.1 Wall Shear Stress

Mildly-diseased pigs

PB change between baseline and T2 in MD pigs was greater in sectors exposed to low or medium WSS at T1 compared to sectors exposed to high WSS, observing a decrease of 0.04% in PB in sectors exposed to high WSS (Figure 75). On the contrary, sectors undergoing medium WSS at T2 experienced a bigger increase in PB at T3 (Figure 76). In any circumstance, the PB variation for MD pigs, both at initiation (T1-T2) and progression (T2-T3), was almost none.

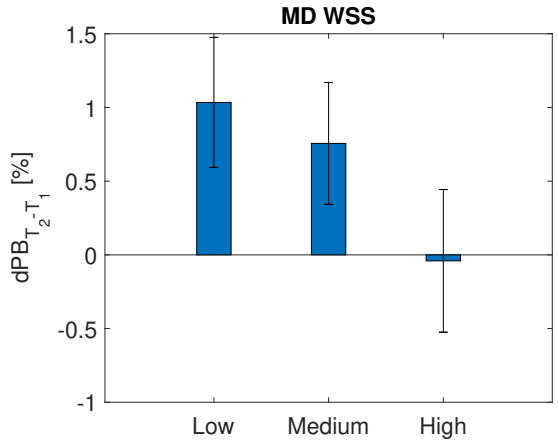

Figure 75: Plaque burden change between T1 to T2 of MD pigs according to low, medium and high WSS at T1. The 95% confidence interval is represented by vertical lines.

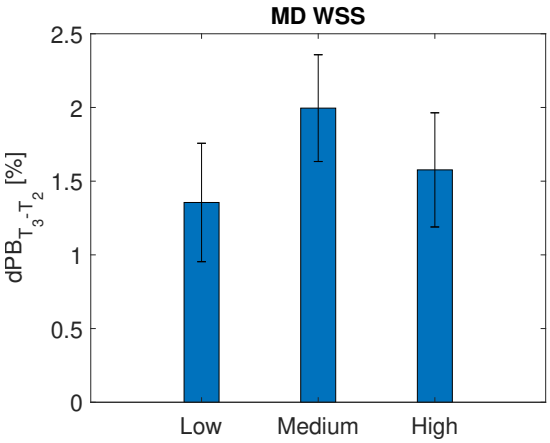

Figure 76: Plaque burden change between T2 to T3 of MD pigs according to low, medium and high WSS at T2. The 95% confidence interval is represented by vertical lines.

Advanced-diseased pigs

The interaction between WSS and PB change at plaque initiation and plaque progression for AD pigs are observed in Figure 77 and Figure 78 respectively. PB growth decreased as WSS increased both at initiation and progression; experiencing the highest growth of 12.89% at low WSS from T1 to T2, and the lowest growth of 3.32% at high WSS from T2 to T3.

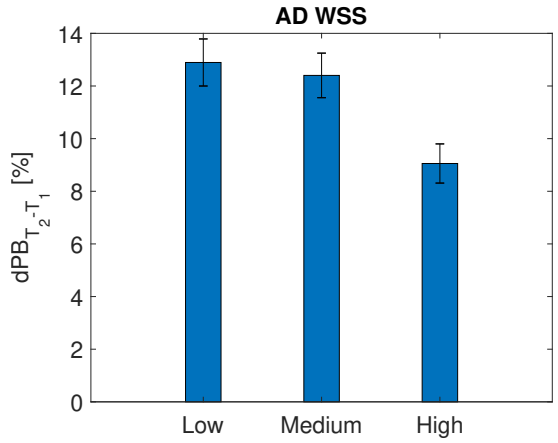

Figure 77: Plaque burden change between T1 to T2 of AD pigs according to low, medium and high WSS at T1. The 95% confidence interval is represented by vertical lines.

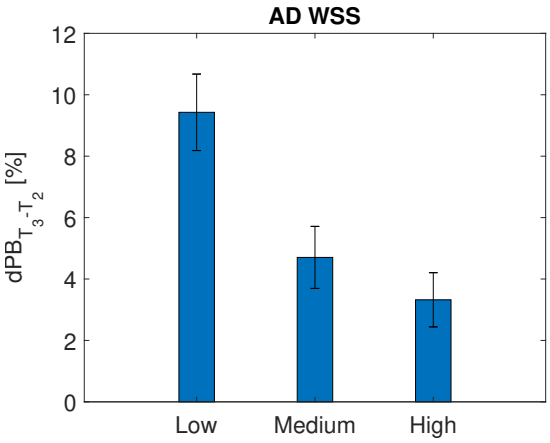

Figure 78: Plaque burden change between T2 to T3 of AD pigs according to low, medium and high WSS at T2. The 95% confidence interval is represented by vertical lines.

In regards to plaque-free sectors from AD pigs, at both plaque initiation and progression, an increase in WSS was observed with a gradual reduction in PB growth, with the most significant

decrease occurring between T2 and T3 (see Figure 79 and Figure 80). The highest growth of 12.87% was witness by sectors exposed to low WSS at T1 whereas the lowest growth of 3.93% was experienced by sectors exposed to high WSS at T2.

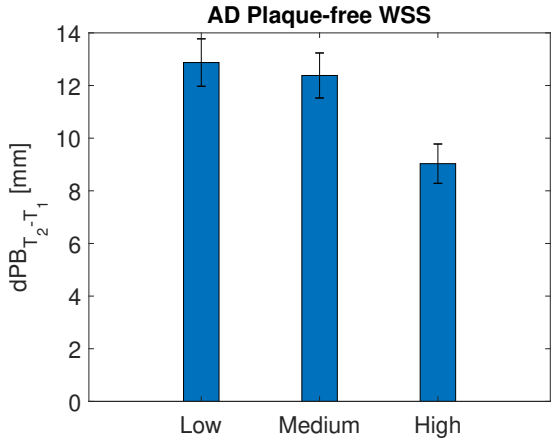

Figure 79: Plaque burden change between T1 to T2 of plaque-free sectors from AD pigs according to low, medium and high WSS at T1. The 95% confidence interval is represented by vertical lines.

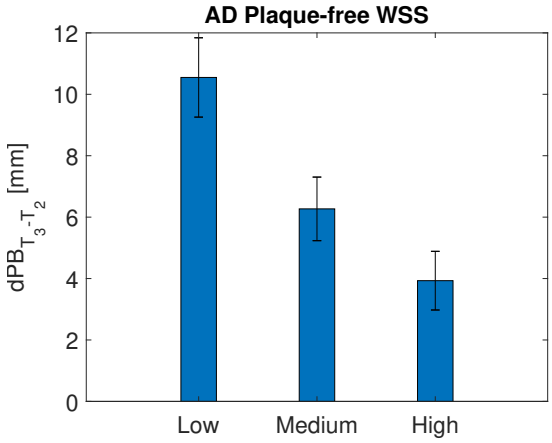

Figure 80: Plaque burden change between T2 to T3 of plaque-free sectors from AD pigs according to low, medium and high WSS at T2. The 95% confidence interval is represented by vertical lines.

In Figure 81 and Figure 82 the interaction between WSS and PB change at plaque initiation and progression for sectors with plaque but no LP from AD pigs are depicted. At plaque initiation, as WSS increased, there was a decrease in PB growth. At plaque progression, on the contrary, sectors under low or high WSS experienced 1.7% of PB growth while PB of sectors under mid WSS decreased in 1.25%.

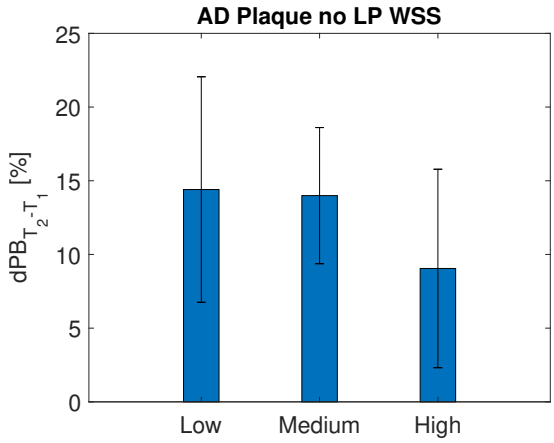

Figure 81: Plaque burden change between T1 to T2 of sectors with plaque but no lipid-pool from AD pigs according to low, medium and high WSS at T1. The 95% confidence interval is represented by vertical lines.

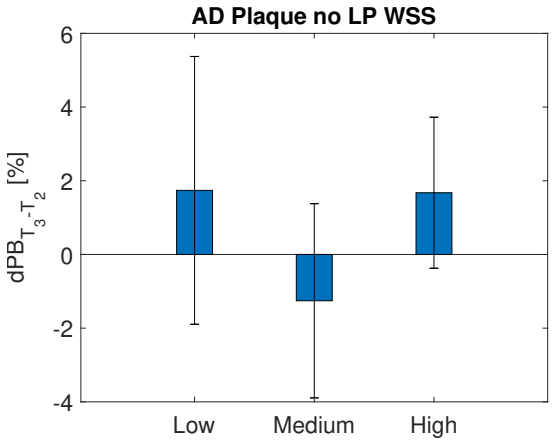

Figure 82: Plaque burden change between T2 to T3 of sectors with plaque but no lipid-pool from AD pigs according to low, medium and high WSS at T2. The 95% confidence interval is represented by vertical lines.

At T1, insufficient sectors with LP were present and the majority of sectors that developed LP belonged to AD pigs that died after T2 so little information could be obtained on the PB change over time for this group. However, in Figure 83 a reduction on PB growth at plaque progression could be observed as WSS level increased.

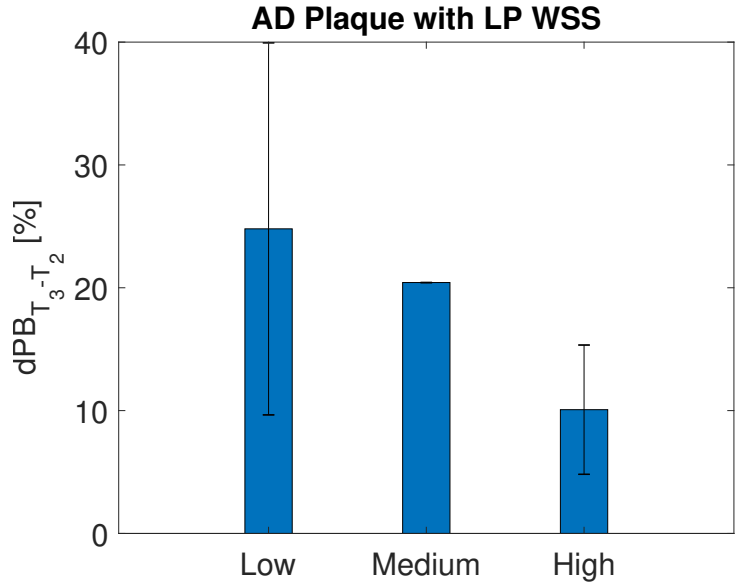

Figure 83: Plaque burden change between T2 to T3 of sectors with lipid-pool from AD pigs according to low, medium and high WSS at T2. The 95% confidence interval is represented by vertical lines.

E.2.2 Wall Mechanical Stress

Mildly-diseased pigs

Regarding PB growth over time, MD sectors exposed to low WMS experienced the lowest PB growth at T1 and at T2 (0.7% and 1.34% respectively) (see Figure 84 and Figure 85). However, the highest growth was observed in sectors undergoing high WMS at T1 and sectors undergoing medium WMS at T2 (1.4% and 1.8% respectively). Nevertheless, PB change was minimal in both cases.

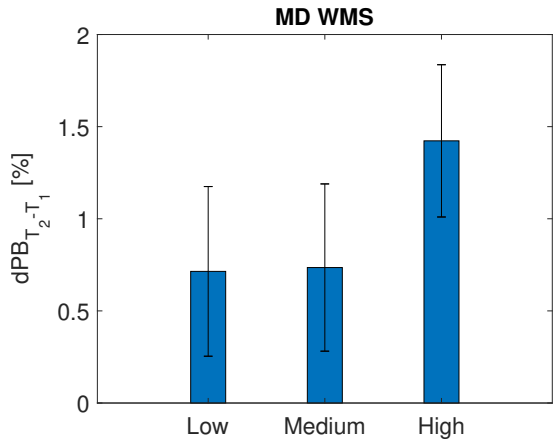

Figure 84: Plaque burden change between T1 to T2 of MD pigs according to low, medium and high WMS at T1. The 95% confidence interval is represented by vertical lines.

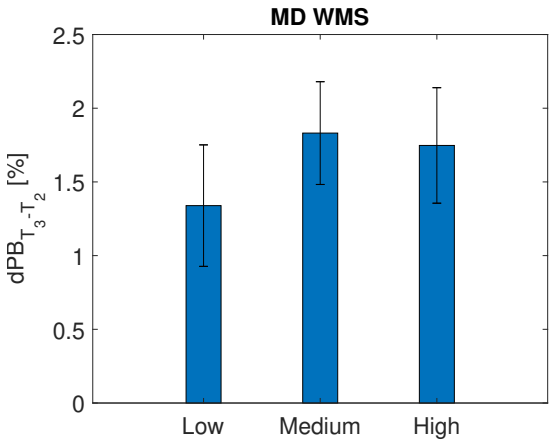

Figure 85: Plaque burden change between T2 to T3 of MD pigs according to low, medium and high WMS at T2. The 95% confidence interval is represented by vertical lines.

Advanced-diseased pigs

In Figure 86 and Figure 87, the PB change over time can be seen. An increase of 11% in PB was observed at plaque initiation independently of WMS levels. At plaque progression, a slight increase in PB was observed as WMS level increased; 4.6%, 5.5% and 7.2% at low, medium and high WMS respectively.

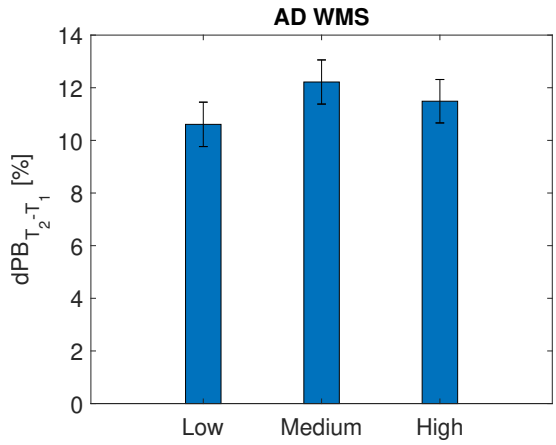

Figure 86: Plaque burden change between T1 to T2 of AD pigs according to low, medium and high WMS at T1. The 95% confidence interval is represented by vertical lines.

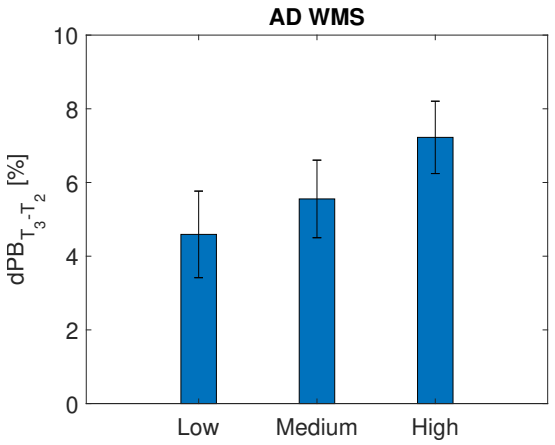

Figure 87: Plaque burden change between T2 to T3 of AD pigs according to low, medium and high WMS at T2. The 95% confidence interval is represented by vertical lines.

Regarding plaque-free sectors from AD pigs, at plaque initiation, an average increase of 11% in PB was observed independently of WMS levels (Figure 88). In contrast, at plaque progression, sectors undergoing low WMS witnessed a 8% growth in PB whereas sectors under medium or high WMS experienced an increase of 6% (Figure 89).

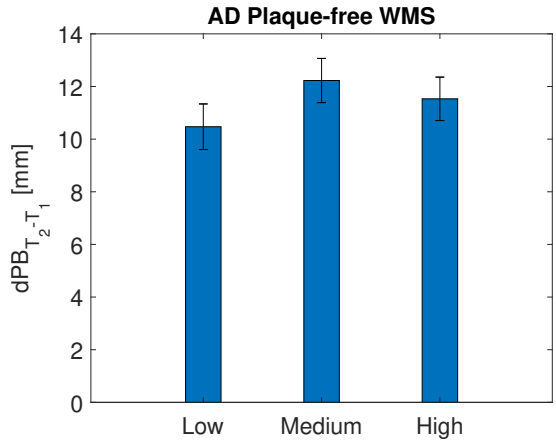

Figure 88: Plaque burden change between T1 to T2 of plaque-free sectors from AD pigs according to low, medium and high WMS at T1. The 95% confidence interval is represented by vertical lines.

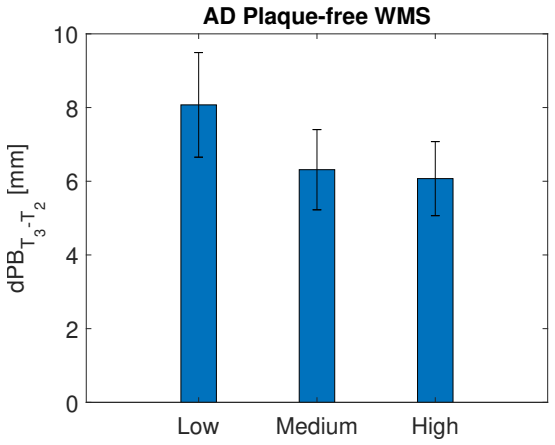

Figure 89: Plaque burden change between T2 to T3 of plaque-free sectors from AD pigs according to low, medium and high WMS at T2. The 95% confidence interval is represented by vertical lines.

On the other hand, when looking only at sectors with plaque but no LP belonging to AD pigs, increase in PB was observed as WMS levels increased (see Figure 90 and Figure 91). This behaviour was observed at plaque initiation as well as at plaque progression, being the later a more noticeable difference between low or medium and high WMS levels despite of having an overall smaller increase.

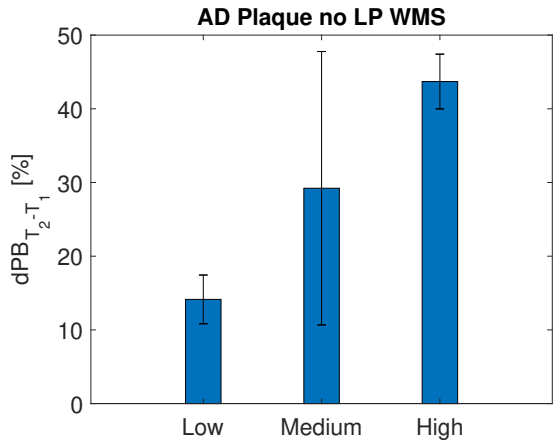

Figure 90: Plaque burden change between T1 to T2 of sectors with plaque but no lipid-pool from AD pigs according to low, medium and high WMS at T1. The 95% confidence interval is represented by vertical lines.

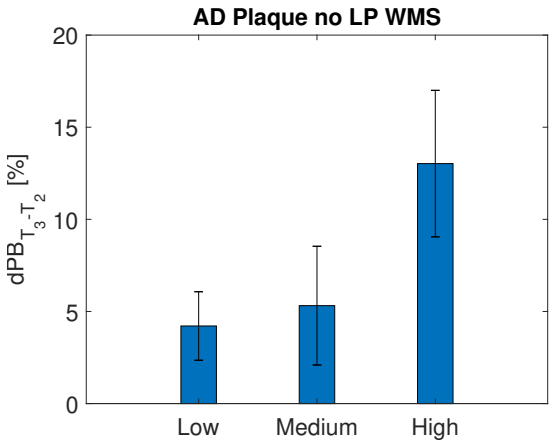

Figure 91: Plaque burden change between T2 to T3 of sectors with plaque but no lipid-pool from AD pigs according to low, medium and high WMS at T2. The 95% confidence interval is represented by vertical lines.

Due to insufficient amount of sectors with LP present at T1 and the subsequent death of 2 AD pigs containing the majority of sectors with LP, little information could be retrieved on the PB change over time. In spite of it, the relationship between PB difference and WMS levels between T2 and T3 is visualised in Figure 92. Following the same pattern previously described, sectors exposed to higher WMS at T2 experienced a higher increase in PB than sectors exposed to low WMS (42.69% vs. 7.21%).

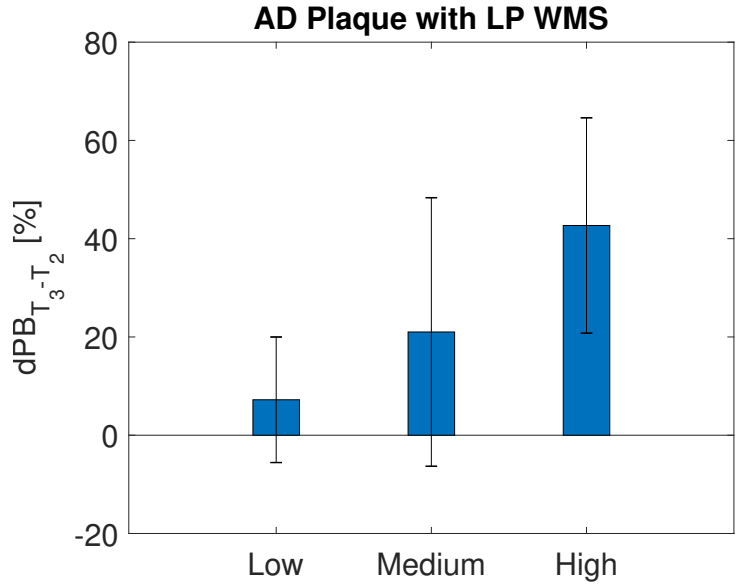

Figure 92: Plaque burden change between T2 to T3 of sectors with lipid-pool from AD pigs according to low, medium and high WMS at T2. The 95% confidence interval is represented by vertical lines.

E.2.3 Combination of WSS and WMS

The effect of WSS and WMS on PB change over time can be seen in Figure 93 and Figure 94.

Mildly-diseased pigs

Regarding sectors from MD pigs, both from T1 to T2 and from T2 to T3, PB change stayed stable at an increase of 3%, observing the highest change in sector exposed to high WSS and WMS, with an increase of 3.9%.

Advanced-diseased pigs

Regarding sectors belonging to AD pigs, at plaque initiation, PB change stayed stable around 13%, decreasing to 8% when WSS was high. At plaque progression, on the other hands, as WSS increased, PB change decreased. The highest PB change was noted in regions with low WSS and WMS and the lowest was seen in areas with high WSS and low WMS (13.26% vs. 2.5%). As for plaque-free sectors belonging to AD group, similarly to the previous category, plaque-free sectors from AD pigs had a stable change in PB at plaque initiation, and a slight reduction of its growth at plaque progression when WSS increased. In addition, a small increase was observed from T2 to T3 when WMS increased at high WSS level. When looking at sectors with plaque which do not contain LP, at initiation stage, not many sectors had developed plaque and, therefore, there was a lack of information about the combination of low or medium WSS with high WMS. Nevertheless, an increase in PB growth was noted as WMS increased, both at plaque initiation and progression. In contrast, from T1 to T2, as WSS increased, PB growth was reduced. As previously mentioned, not enough sectors with LP were present at T1 so no information could be retrieved for that time point. Despite the fact that at T2 there was not either a large number of sectors with plaque, it was witnessed that the arterial wall of sectors with higher WMS experienced a greater increase in PB (21% vs. 51.6% at low WSS and mid and high WMS respectively; 20.7% vs. 35.82% at high WSS and low and high WMS respectively) . In contrast, as WSS increased, PB increase got reduced, achieving the lowest increase of 20.7% when WSS was high and WMS low.

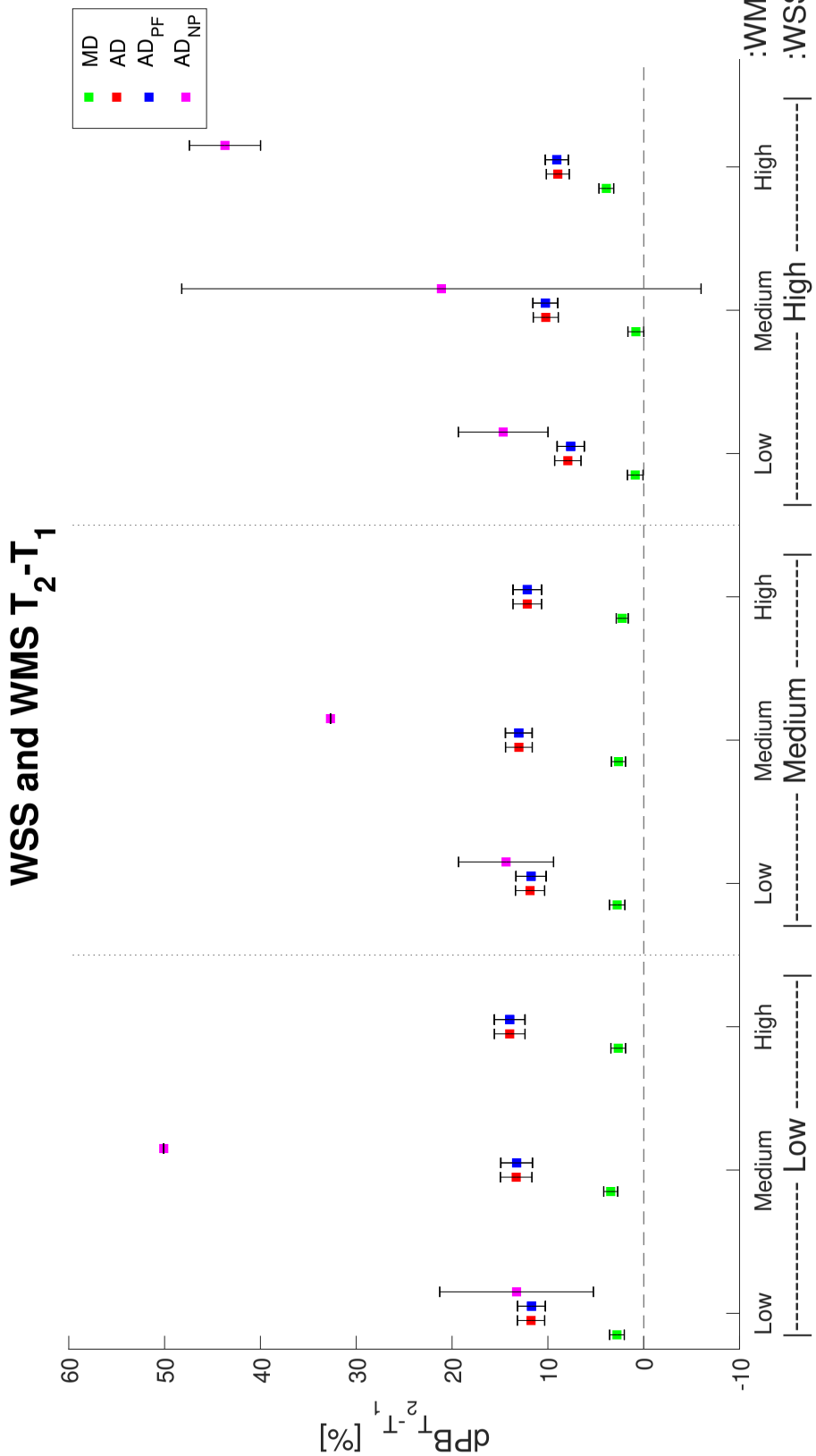

Figure 93: Plaque burden change between T1 to T2 of all categorised sectors according to low, medium and high WSS and WMS at T1. The 95% confidence interval is represented by vertical lines. MD: mildly-diseased; AD: advanced-diseased; PF: plaque-free; NP: plaque without lipid-pool.

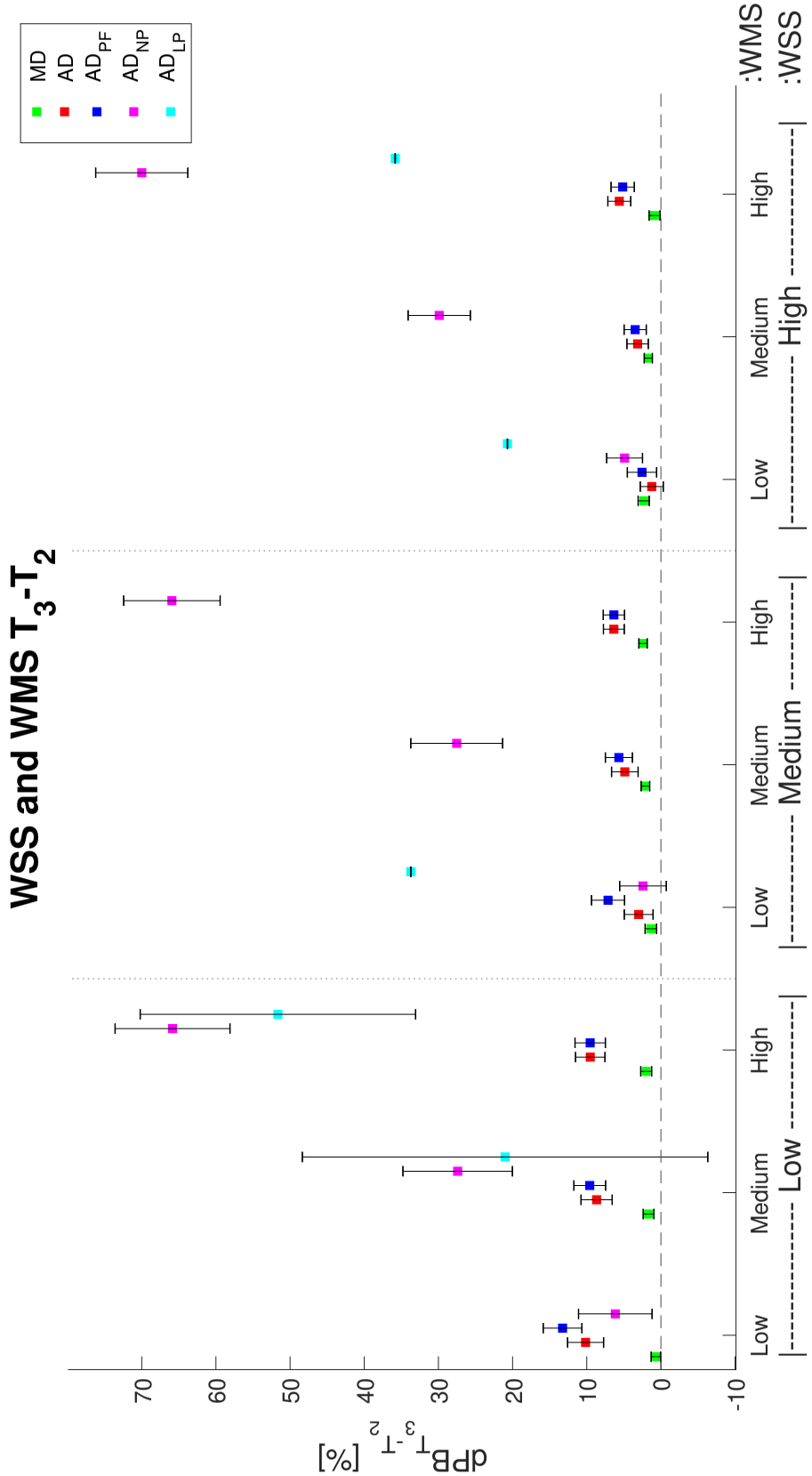

Figure 94: Plaque burden change between T2 to T3 of all categorised sectors according to low, medium and high WSS and WMS at T2. The 95% confidence interval is represented by vertical lines. MD: mildly-diseased; AD: advanced-diseased; PF: plaque-free; NP: plaque without lipid-pool; LP: plaque with lipid-pool.

References

[1] A. C. Akyildiz, L. Speelman, H. van Brummelen, M. A. Gutiérrez, A. Virmani, Renu van der Lugt, A. F. W. van der Steen, J. J. Wentzel, and F. J. H. Gijsen, "Effects of intima stiffness and plaque morphology on peak cap stress," *BioMedical Engineering OnLine*, vol. 10, no. 25, 2011.

[2] S. Mahmood, *Integrating Cardiology for Nuclear Medicine Physicians*, Nov 2008, pp. 23–28.

[3] W. Herrington, B. Lacey, P. Sherliker, J. Armitage, and S. Lewington, "Epidemiology of atherosclerosis and the potential to reduce the global burden of atherothrombotic disease," *Circulation Research*, vol. 118, no. 4, pp. 535–546, 2016.

[4] E. S. of Cardiology, "About cardiovascular disease in esc member countries," Available at https://www.escardio.org/The-ESC/Press-Office/Fact-sheets (2023/02/14).

[5] I. J. Kullo and C. M. Ballantyne, "Conditional risk factors for atherosclerosis," *Mayo Clinic Proceedings*, vol. 80, no. 2, pp. 219–230, 2005.

[6] S. Mahmood, *Integrating Cardiology for Nuclear Medicine Physicians*, Nov 2008, pp. 31–43.

[7] A. C. Akyildiz, L. Speelman, B. van Velzen, R. R. F. Stevens, A. F. W. van der Steen, W. Huberts, and F. J. H. Gijsen, "Intima heterogeneity in stress assessment of atherosclerotic plaques," *Interface Focus*, vol. 8, no. 1, p. 20170008, 2018.

[8] G. K. Hansson, "Inflammation, atherosclerosis, and coronary artery disease," *New England Journal of Medicine*, vol. 352, no. 16, pp. 1685–1695, 2005.

[9] K. Sakakura, M. Nakano, F. Otsuka, E. Ladich, F. D. Kolodgie, and R. Virmani, "Pathophysiology of atherosclerosis plaque progression," *Heart, Lung and Circulation*, vol. 22, no. 6, pp. 399–411, 2013.

[10] "Atherosclerosis," Available at https://en.wikipedia.org/wiki/Atherosclerosis#/media/File:Late_complications_of_atherosclerosis.PNG (2023/02/14).

[11] Z. Brown, Adam J. Teng, "Role of biomechanical forces in the natural history of coronary atherosclerosis," *Nature Reviews Cardiology*, vol. 13, 2016.

[12] P. Puylaert, M. Zurek, K. J. Rayner, G. R. D. Meyer, and W. Martinet, "Regulated necrosis in atherosclerosis," *Arteriosclerosis, Thrombosis, and Vascular Biology*, vol. 42, no. 11, pp. 1283–1306, 2022.

[13] H. C. Stary, A. B. Chandler, R. E. Dinsmore, V. Fuster, S. Glagov, W. Insull, M. E. Rosenfeld, C. J. Schwartz, W. D. Wagner, and R. W. Wissler, "A definition of advanced types of atherosclerotic lesions and a histological classification of atherosclerosis," *Circulation*, vol. 92, no. 5, pp. 1355–1374, 1995.

[14] C. Costopoulos, L. H. Timmins, Y. Huang, O. Y. Hung, D. S. Molony, A. J. Brown, E. L. Davis, Z. Teng, J. H. Gillard, H. Samady, and M. R. Bennett, "Impact of combined plaque structural stress and wall shear stress on coronary plaque progression, regression, and changes in composition," *European Heart Journal*, vol. 40, no. 18, pp. 1411–1422, 03 2019.

[15] A. J. Brown, Z. Teng, P. A. Calvert, N. K. Rajani, O. Hennessy, N. Nerlekar, D. R. Obaid, C. Costopoulos, Y. Huang, S. P. Hoole, M. Goddard, N. E. West, J. H. Gillard, and M. R. Bennett, "Plaque structural stress estimations improve prediction of future major adverse

cardiovascular events after intracoronary imaging," *Circulation: Cardiovascular Imaging*, vol. 9, no. 6, p. e004172, 2016.

[16] S. Z. Gu and M. R. Bennett, "Plaque structural stress: detection, determinants and role in atherosclerotic plaque rupture and progression," *Frontiers in Cardiovascular Medicine*, vol. 9, no. 6, 2022.

[17] J. N. Cameron, O. H. Mehta, M. Michail, J. Chan, S. J. Nicholls, M. R. Bennett, and A. J. Brown, "Exploring the relationship between biomechanical stresses and coronary atherosclerosis," *Atherosclerosis*, vol. 302, pp. 43–51, 2020.

[18] D. Shav, R. Gotlieb, U. Zaretsky, D. Elad, and S. Einav, "Wall shear stress effects on endothelial-endothelial and endothelial-smooth muscle cell interactions in tissue engineered models of the vascular wall," *PLOS ONE*, vol. 9, no. 2, pp. 1–13, 02 2014. [Online]. Available: 10.1371/journal.pone.0088304

[19] M. Zhou, Y. Yu, R. Chen, X. Liu, Y. Hu, Z. Ma, L. Gao, W. Jian, and L. Wang, "Wall shear stress and its role in atherosclerosis," *Frontiers in Cardiovascular Medicine*, vol. 10, 2023.

[20] D. Han, A. Starikov, B. Hartaigh, H. Gransar, K. K. Kolli, J. H. Lee, A. Rizvi, L. Baskaran, J. Schulman-Marcus, F. Y. Lin, and J. K. Min, "Relationship between endothelial wall shear stress and high-risk atherosclerotic plaque characteristics for identification of coronary lesions that cause ischemia: A direct comparison with fractional flow reserve," *Journal of the American Heart Association*, vol. 5, no. 12, p. e004186, 2016.

[21] J. H. Haga, Y.-S. J. Li, and S. Chien, "Molecular basis of the effects of mechanical stretch on vascular smooth muscle cells," *Journal of Biomechanics*, vol. 40, no. 5, pp. 947–960, 2007.

[22] H. Nieuwstadt, A. Akyildiz, L. Speelman, R. Virmani, A. van der Lugt, A. van der Steen, J. Wentzel, and F. Gijsen, "The influence of axial image resolution on atherosclerotic plaque stress computations," *Journal of Biomechanics*, vol. 46, no. 4, pp. 689–695, 2013.

[23] A. Hoogendoorn, A. M. Kok, E. M. J. Hartman, G. de Nisco, L. Casadonte, C. Chiastra, A. Coenen, S.-A. Korteland, K. Van der Heiden, F. J. H. Gijsen, D. J. Duncker, A. F. W. van der Steen, and J. J. Wentzel, "Multidirectional wall shear stress promotes advanced coronary plaque development: comparing five shear stress metrics," *Cardiovascular Research*, vol. 116, no. 6, pp. 1136–1146, 08 2019.

[24] Z. Teng, A. J. Brown, P. A. Calvert, R. A. Parker, D. R. Obaid, Y. Huang, S. P. Hoole, N. E. West, J. H. Gillard, and M. R. Bennett, "Coronary plaque structural stress is associated with plaque composition and subtype and higher in acute coronary syndrome," *Circulation: Cardiovascular Imaging*, vol. 7, no. 3, pp. 461–470, 2014.

[25] F. to Advance Vascular Cure, "Atherosclerosis," Available at https://www.vascularcures.org/atherosclerosis (2023/10/13).

[26] A. Hoogendoorn, S. den Hoedt, E. M. Hartman, I. Krabbendam-Peters, M. te Lintel Hekkert, L. van der Zee, K. van Gaalen, K. T. Witberg, K. Dorst, J. M. Ligthart, L. Drouet, K. V. der Heiden, J. R. van Lennep, A. F. van der Steen, D. J. Duncker, M. T. Mulder, and J. J. Wentzel, "Variation in coronary atherosclerosis severity related to a distinct ldl (low-density lipoprotein) profile," *Arteriosclerosis, Thrombosis, and Vascular Biology*, vol. 39, no. 11, pp. 2338–2352, 2019.

[27] J. Waggoner and M. D. Feldman, "How do oct and ivus differ?" May 2011.

[28] A. M. Kok, L. Speelman, R. Virmani, A. F. W. van der Steen, F. J. Gijsen, and J. J. Wentzel, "Peak cap stress calculations in coronary atherosclerotic plaques with an incomplete necrotic core geometry," *BioMedical Engineering OnLine*, vol. 15, no. 48, 2016.

[29] A. C. Akyildiz, L. Speelman, H. A. Nieuwstadt, H. van Brummelen, R. Virmani, A. van der Lugt, A. F. van der Steen, J. J. Wentzel, and F. J. Gijsen, "The effects of plaque morphology and material properties on peak cap stress in human coronary arteries," *Computer Methods in Biomechanics and Biomedical Engineering*, vol. 19, no. 7, pp. 771–779, 2016.

[30] V. Ayyalasomayajula, B. Pierrat, and P. Badel, "A computational model for understanding the micro-mechanics of collagen fiber network in the tunica adventitia," *Biomech Model Mechanobiol*, vol. 18, pp. 1507–1528, 2019.

[31] H. Chen, X. Guo, T. Luo, and G. S. Kassab, "A validated 3d microstructure-based constitutive model of coronary artery adventitia," *Journal of Applied Physiology*, vol. 121, no. 1, pp. 333–342, 2016.

[32] A. J. Brown, Z. Teng, P. A. Calvert, N. K. Rajani, O. Hennessy, N. Nerlekar, D. R. Obaid, C. Costopoulos, Y. Huang, S. P. Hoole, M. Goddard, N. E. West, J. H. Gillard, and M. R. Bennett, "Plaque structural stress estimations improve prediction of future major adverse cardiovascular events after intracoronary imaging," *Circulation: Cardiovascular Imaging*, vol. 9, no. 6, p. e004172, 2016.

[33] F. Dernoncourt, "Beatdb : an end-to-end approach to unveil saliencies from massive signal data sets," 06 2015.

[34] D. Sadhukhan and M. Mitra, "R-peak detection algorithm for ecg using double difference and rr interval processing," *Procedia Technology*, vol. 4, pp. 873–877, 2012.

[35] L. Speelman, E. Bosboom, G. Schurink, J. Buth, M. Breeuwer, M. Jacobs, and F. van de Vosse, "Initial stress and nonlinear material behavior in patient-specific aaa wall stress analysis," *Journal of Biomechanics*, vol. 42, no. 11, pp. 1713–1719, 2009.

[36] L. Speelman, A. Akyildiz, B. den Adel, J. Wentzel, A. van der Steen, R. Virmani, L. van der Weerd, J. Jukema, R. Poelmann, E. van Brummelen, and F. Gijsen, "Initial stress in biomechanical models of atherosclerotic plaques," *Journal of Biomechanics*, vol. 44, no. 13, pp. 2376–2382, 2011.

[37] S. de Putter, B. Wolters, M. Rutten, M. Breeuwer, F. Gerritsen, and F. van de Vosse, "Patient-specific initial wall stress in abdominal aortic aneurysms with a backward incremental method," *Journal of Biomechanics*, vol. 40, no. 5, pp. 1081–1090, 2007.

[38] P. K. Cheruvu, A. V. Finn, C. Gardner, J. Caplan, J. Goldstein, G. W. Stone, R. Virmani, and J. E. Muller, "Frequency and distribution of thin-cap fibroatheroma and ruptured plaques in human coronary arteries: A pathologic study," *Journal of the American College of Cardiology*, vol. 50, no. 10, pp. 940–949, 2007.

[39] K. C. Koskinas, C. L. Feldman, Y. S. Chatzizisis, A. U. Coskun, M. Jonas, C. Maynard, A. B. Baker, M. I. Papafaklis, E. R. Edelman, and P. H. Stone, "Natural history of experimental coronary atherosclerosis and vascular remodeling in relation to endothelial shear stress," *Circulation*, vol. 121, no. 19, pp. 2092–2101, 2010.

[40] E. Yamamoto, G. Siasos, M. Zaromytidou, A. U. Coskun, L. Xing, K. Bryniarski, T. Zanchin, T. Sugiyama, H. Lee, P. H. Stone, and I.-K. Jang, "Low endothelial shear stress predicts evolution to high-risk coronary plaque phenotype in the future," *Circulation: Cardiovascular Interventions*, vol. 10, no. 8, p. e005455, 2017.

[41] K. C. Koskinas, R. Maldonado, H. M. Garcia-Garcia, K. Yamaji, M. Taniwaki, Y. Ueki, T. Otsuka, C. Zanchin, A. Karagiannis, M. D. Radu Juul Jensen, S. Losdat, S. Zaugg, S. Windecker, and L. Räber, "Relationship between arterial remodelling and serial changes in coronary atherosclerosis by intravascular ultrasound: an analysis of the IBIS-4 study," *European Heart Journal - Cardiovascular Imaging*, vol. 22, no. 9, pp. 1054–1062, 09 2020.

[42] P. H. Stone, S. Saito, S. Takahashi, Y. Makita, S. Nakamura, T. Kawasaki, A. Takahashi, T. Katsuki, S. Nakamura, A. Namiki, A. Hirohata, T. Matsumura, S. Yamazaki, H. Yokoi, S. Tanaka, S. Otsuji, F. Yoshimachi, J. Honye, D. Harwood, M. Reitman, A. U. Coskun, M. I. Papafaklis, and C. L. Feldman, "Prediction of progression of coronary artery disease and clinical outcomes using vascular profiling of endothelial shear stress and arterial plaque characteristics," *Circulation*, vol. 126, no. 2, pp. 172–181, 2012.

[43] E. M. J. Hartman, G. D. Nisco, F. J. H. Gijsen, S.-A. Korteland, A. F. W. van der Steen, J. Daemen, and J. J. Wentzel, "The definitioin of low wall shear stress and its effect on plaque progression estimation in human coronary arteries," *Scientific reports*, vol. 11, 2021.

[44] E. S. Kröner, J. E. van Velzen, M. J. Boogers, H.-M. J. Siebelink, M. J. Schalij, L. J. Kroft, A. de Roos, E. E. van der Wall, J. W. Jukema, J. H. Reiber, J. D. Schuijf, and J. J. Bax, "Positive remodeling on coronary computed tomography as a marker for plaque vulnerability on virtual histology intravascular ultrasound," *The American Journal of Cardiology*, vol. 107, no. 12, pp. 1725–1729, 2011.

[45] L. Calleja, M. A. París, A. Paul, E. Vilella, J. Joven, A. Jiménez, G. Beltrán, M. Uceda, N. Maeda, and J. Osada, "Low-cholesterol and high-fat diets reduce atherosclerotic lesion development in apoe-knockout mice," *Arteriosclerosis, Thrombosis, and Vascular Biology*, vol. 19, no. 10, pp. 2368–2375, 1999.

[46] A. B. Waqar, T. Koike, Y. Yu, T. Inoue, T. Aoki, E. Liu, and J. Fan, "High-fat diet without excess calories induces metabolic disorders and enhances atherosclerosis in rabbits," *Atherosclerosis*, vol. 213, no. 1, pp. 148–155, 2010.

[47] S. Xi, W. Yin, Z. Wang, M. Kusunoki, X. Lian, T. Koike, J. Fan, and Q. Zhang, "A minipig model of high-fat/high-sucrose diet-induced diabetes and atherosclerosis," *International Journal of Experimental Pathology*, vol. 85, no. 4, pp. 223–231, 2004.

[48] X. Liu, G. Wu, C. Xu, Y. He, L. Shu, Y. Liu, N. Zhang, and C. Lin, "Quantitative evaluation of coronary plaque progression by computed tomographic angiography," *The Texas Heart Institute Journal*, vol. 44, no. 5, pp. 312–319, 2017.

[49] V. Subban and O. C. Raffel, "Optical coherence tomography: fundamentals and clinical utility," *Cardiovascular Diagnosis and Therapy*, vol. 10, no. 5, 2020.

[50] S. Kiechl and J. Willeit, "The natural course of atherosclerosis," *Arteriosclerosis, Thrombosis, and Vascular Biology*, vol. 19, no. 6, pp. 1484–1490, 1999.

[51] D. Wang, X. Xu, M. Zhao, and X. Wang, "Accelerated miniature swine models of advanced atherosclerosis: A review based on morphology," *Cardiovascular Pathology*, vol. 49, p. 107241, 2020.

[52] P. H. Stone, C. Michael Gibson, R. C. Pasternak, K. McManus, L. Diaz, T. Boucher, R. Spears, T. Sandor, B. Rosner, and F. M. Sacks, "Natural history of coronary atherosclerosis using quantitative angiography in men, and implications for clinical trials of coronary regression," *The American Journal of Cardiology*, vol. 71, no. 10, pp. 766–772, 1993.

[53] S. E. Margitić, M. G. Bond, J. R. Crouse, C. D. Furberg, and J. L. Probstfield, "Progression and regression of carotid atherosclerosis in clinical trials." *Arteriosclerosis and Thrombosis: A Journal of Vascular Biology*, vol. 11, no. 2, pp. 443–451, 1991.

[54] R. Virmani, F. D. Kolodgie, A. P. Burke, A. Farb, and S. M. Schwartz, "Lessons from sudden coronary death," *Arteriosclerosis, Thrombosis, and Vascular Biology*, vol. 20, no. 5, pp. 1262–1275, 2000.

[55] H. C. Stary, "Composition and classification of human atherosclerotic lesions," *Virchows Archiv*, vol. 421, pp. 277–290, 1992.

[56] S. S. Dhawan, R. P. A. Nanjundappa, J. R. Branch, W. R. Taylor, A. A. Quyyumi, H. Jo, M. C. McDaniel, J. Suo, D. Giddens, and H. Samady, "Shear stress and plaque development," *Expert Review of Cardiovascular Therapy*, vol. 8, no. 4, pp. 545–556, 2010.

[57] M. Cibis, W. V. Potters, M. Selwaness, F. J. Gijsen, O. H. Franco, A. M. A. Lorza, M. de Bruijne, A. Hofman, A. van der Lugt, A. J. Nederveen, and J. J. Wentzel, "Relation between wall shear stress and carotid artery wall thickening mri versus cfd," *Journal of Biomechanics*, vol. 49, no. 5, pp. 735–741, 2016.

[58] C. Costopoulos, A. Maehara, Y. Huang, A. J. Brown, J. H. Gillard, Z. Teng, G. W. Stone, and M. R. Bennett, "Heterogeneity of plaque structural stress is increased in plaques leading to mace: Insights from the prospect study," *JACC: Cardiovascular Imaging*, vol. 13, no. 5, pp. 1206–1218, 2020.

[59] D. N. Ku, D. P. Giddens, C. K. Zarins, and S. Glagov, "Pulsatile flow and atherosclerosis in the human carotid bifurcation. positive correlation between plaque location and low oscillating shear stress." *Arteriosclerosis: An Official Journal of the American Heart Association, Inc.*, vol. 5, no. 3, pp. 293–302, 1985.

[60] P. H. Stone, A. U. Coskun, S. Kinlay, M. E. Clark, M. Sonka, A. Wahle, O. J. Ilegbusi, Y. Yeghiazarians, J. J. Popma, J. Orav, R. E. Kuntz, and C. L. Feldman, "Effect of endothelial shear stress on the progression of coronary artery disease, vascular remodeling, and in-stent restenosis in humans: In vivo 6-month follow-up study," *Circulation*, vol. 108, no. 4, p. 438 – 444, 2003.

[61] X. Liu, G. Wu, C. Xu, Y. He, L. Shu, Y. Liu, N. Zhang, and C. Lin, "Prediction of coronary plaque progression using biomechanical factors and vascular characteristics based on computed tomography angiography," *Computer Assisted Surgery*, vol. 22, no. sup1, pp. 286–294, 2017.

[62] T. Hoshino, L. A. Chow, J. J. Hsu, A. A. Perlowski, M. Abedin, J. Tobis, Y. Tintut, A. K. Mal, W. S. Klug, and L. L. Demer, "Mechanical stress analysis of a rigid inclusion in distensible material: a model of atherosclerotic calcification and plaque vulnerability," *American Journal of Physiology-Heart and Circulatory Physiology*, vol. 297, no. 2, pp. H802–H810, 2009.

[63] H. M. Loree, B. J. Tobias, L. J. Gibson, R. D. Kamm, D. M. Small, and R. T. Lee, "Mechanical properties of model atherosclerotic lesion lipid pools." *Arteriosclerosis and Thrombosis: A Journal of Vascular Biology*, vol. 14, no. 2, pp. 230–234, 1994.

[64] K. Nakagawa, M. Tanaka, T.-H. Hahm, H.-N. Nguyen, T. Matsui, Y.-X. Chen, and Y. Nakashima, "Accumulation of plasma-derived lipids in the lipid core and necrotic core of human atheroma: Imaging mass spectrometry and histopathological analyses," *Arteriosclerosis, Thrombosis, and Vascular Biology*, vol. 41, no. 11, pp. e498–e511, 2021.

[65] U. Paslawska, A. Noszczyk-Nowak, R. Paslawski, A. Janiszewski, L. Kiczak, D. Zysko, J. Nicpon, E. A. Jankowska, A. Szuba, and P. Ponikowski, "Normal electrocardiographic and echocardiographic (m-mode and two-dimensional) values in polish landrace pigs," *Acta Vet Scand*, vol. 56, 2014.